

Settling Behavior in the Dewatering Process for Bitumen Froth with Different Qualities

By

Runzhi Xu

A thesis submitted in partial fulfillment of the requirements for the degree of

Master of Science

in

Chemical Engineering

Department of Chemical and Materials Engineering

University of Alberta

© Runzhi Xu, 2018

# Abstract

The formation of extremely fine water drops ( $<10\mu\text{m}$ ) during bitumen extraction causes trouble in downstream processing since chlorides in the water form hypo-chloric acids in the hydrogenation process, which corrodes equipment and leads to extensive maintenance costs. Hence, bitumen must be treated with demulsifier to improve settling by helping coalescence and flocculation. The effect of mixing on demulsifier performance has been studied on diluted bitumen and bitumen froth for many years, where mixing conditions during the addition of demulsifier have been shown to influence the settling of water and solids and affect the performance of the demulsifier.

Bitumen froth of varying qualities was initially treated as the same substance, adding the same amount of demulsifier and operating under the same mixing conditions. However, the settling behavior of water and solids in different qualities of froths can be different. This project sets out to compare the settling behavior of water and solids in bitumen froths of average and poor qualities, including average-quality, high-water and high-solids froth. In previous thesis projects, standardized experiments were performed using the Confined Impeller Stirred Tank (CIST) to study mixing effects on demulsifier performance in average-quality and high-water froth. Most of the water and solids in average-quality froth finishes settling within the first 10 minutes once the impellers are turned off. By contrast, high-water froth shows an induction time, which can be up to 40 minutes. In this thesis project, high-solids froth was added to the data set. High-solids froth can also show an induction time which is somewhat shorter: up to 25 minutes. If the settling behavior of average-quality froth is set as a benchmark, both high-water and high-

solids concentrations can lead to an induction time during separation. However, high-water concentration leads to a longer induction time than high-solids concentration. Although there is no measurable water settling during the induction time, coalescence and flocculation can still occur. In the last part of this work, microscope images are analyzed to determine the types of structures present in the froth. Under the microscope, irregularly-shaped large free water is dominant for high-water froth, but many spherical water drops are observed for high-solids froth. The identification and characterization of induction time in froth settling can be used to improve both the design of equipment and operating conditions. The most important lesson of this work is that froths with different qualities should be treated differently in order to obtain better dewatering efficiency.

# Acknowledgement

I would like to thank Dr. Suzanne Kresta for believing in me to complete the thesis. She is very patient and strategic to respond various problems, particularly towards the end of my program. I not only acquired technical knowledge but also obtained valuable lifetime lessons.

I sincerely appreciate the help from Colin Saraka and Marcio Machado. They both offered me hands-on help and shared great ideas and insights to help me expand my knowledge. Colin Saraka always explained patiently when I had problems. Other mixing team members including Nitin Arora and Khilesh Jairamdas also supported me in my project.

I also want to thank Samson Ng and Sujit Bhattacharya who are our industry sponsors. Their great enthusiasm in research shows me how research looks like in reality.

I really thank my parents for supporting me. Particularly, my father always encouraged me even in his most difficult time. Also, I thank my friends for cheering me up in the last few months.

Last but not least, I would like to thank Junkai (Karry) Wang. Your great persistence in pursuing your dream really makes me ashamed and inspired. I sincerely wish you a bright future!

# Table of Contents

<b>Chapter 1 Oil Sands Processing and Mixing</b> .....	1
1.1 Emulsified Water and Bitumen Froth Treatment .....	2
1.2 Mixing in Bitumen Froth Treatment .....	5
1.3 The Confined Impeller Stirred Tank (CIST).....	8
1.4 Surfactant-Mediated Tip Streaming .....	11
1.5 Research Objective .....	14
<b>Chapter 2: Procedures of Mixing Experiments with the FBRM Probe for Bitumen Froth</b> .....	15
2.1 The Confined Impeller Stirred Tank (CIST) Assembly.....	16
2.2 Sample Storage .....	19
2.3 Pre-Mixing.....	19
2.4 Naphtha Blending .....	20
2.5 Demulsifier Dispersion .....	21
2.6 Settling .....	22
2.7 Microscope Slides .....	25
2.8 Karl Fischer.....	25
2.9 Dean Stark.....	26
2.10 Focused-Beam Reflectance Measurements .....	26
<b>Chapter 3: The Design of Research Campaigns and Their Objectives</b> .....	28
3.1 Simulating High-Water Froth Settling Behavior.....	28
3.2 Determining the Sufficient Bulk Concentration of Demulsifier in High-Solids Froth for the Study of Mixing Effects .....	29
3.3 Mixing Effects on High-Solids Froth Settling Behavior.....	29
<b>Chapter 4 High-Solids Froth Mixing Experiments</b> .....	30
4.1 Simulating High-Water Froth Settling Behavior.....	31
4.1.1 Experimental Method .....	31
4.1.2 Results for simulated high-water froth.....	32
4.2 Determining Sufficient Bulk Concentration of Demulsifier .....	37
4.2.1 Experimental Method .....	38
4.2.2 Bulk Concentration vs. Final Water Content.....	39
4.3 Factorial Design.....	45
4.3.1 Experiment Method.....	45

4.3.2	Water Content at Height Z1 .....	47
4.3.3	Water Content at Height Z2 .....	52
4.3.4	Water Content at Height Z3 .....	55
4.3.5	Water Content at Height Z4 .....	58
4.3.6	Effect of Bulk Concentration vs. Mixing Energy at Height Z1 .....	63
4.3.7	Effect of Bulk Concentration vs. Mixing Energy at Height Z2 .....	68
4.3.8	Effect of Bulk Concentration vs. Mixing Energy at Height Z3 .....	71
4.3.9	Effect of Bulk Concentration vs. Mixing Energy at Height Z4 .....	73
4.4	Dean Stark OWS .....	76
<b>Chapter 5: The FBRM Data: Chord Length Distributions of High-solids Froth Settling Experiments .....</b>		<b>79</b>
5.1	Data Analysis Method .....	79
5.2	Low Bulk Concentration and Low Mixing Energy .....	81
5.3	High Bulk Concentration and High Mixing Energy .....	84
5.4	High Bulk Concentration and Low Mixing Energy .....	86
5.5	Low Bulk Concentration and High Mixing Energy .....	88
5.6	Square Weighted Data: Comparison at Different Stages .....	90
<b>Chapter 6: Analysis of Microscope Images of Bitumen Froth with Different Qualities Using a Mixed Approach: Qualitative and Quantitative Methods .....</b>		<b>94</b>
6.1	Capturing Microscope Images for High-Water Froth Settling .....	94
6.2	Mixed Approach to Analyze 10x Microscope Images .....	95
6.3	Microscope Analysis of High-Water and Average-Quality Froth .....	97
6.4	Method Improvement and Analysis on High-Solids Froth .....	115
<b>Chapter 7: Formation of Small Water Drops during Turbulent Mixing and Future Research .....</b>		<b>124</b>
<b>Chapter 8: Conclusion .....</b>		<b>127</b>
<b>References .....</b>		<b>130</b>
Appendix A: Standardized Operational Procedures (SOP) for High-Solids Froth Mixing Experiments		132
A.1	Experimental Procedures for High-solids Froth Mixing Experiments .....	132
A.2	Receiving Test Material from Syncrude .....	137
A.3	Unisol Preparation .....	139
A.4	Sending End-of-Run Samples to Syncrude .....	141
Appendix B: Experimental Data .....		143
B.1	Karl Fischer Data of Two Simulating Experiments Using High-Solids Froth with Additional Process Water .....	143

B.2 Karl Fischer Data for High-Solids Froth to Determine the Appropriate Bulk Concentration of Demulsifier to Study Mixing Effects.....	143
B.3 Karl Fischer Data for High-Solids Froth Mixing Experiments .....	144
B.4 OWS Data for High-Solids Froth Settling Experiments .....	145

# List of Tables

Table 2-1: The geometry of the froth can and the parameters of pre-mixing (Saraka, 2017).....	20
Table 2-2: The mixing geometry and parameters of naphtha blending (Saraka, 2017).....	21
Table 2-3: Sampling schedule of high-solids froth settling experiment based on the sampling schedule of high-water froth. Table reproduced with permission (Saraka, 2017).....	24
Table 4-1: The composition of high-water froth and the composition of high-solids froth before adding process water from OWS analysis (Syncrude) and the target composition of simulated high-water froth.....	33
Table 4-2: The water content of high-solids froth samples, measured using Karl Fischer titration, before and after adding process water prior to starting experiments, compared to the original water content of high-solid as provided by industry.....	34
Table 4-3: The operating conditions and water contents at height Z1 after 60 and 120 minutes of settling for each experiment to determine the sufficient bulk concentration of demulsifier in high-solids froth.....	39
Table 4-4: The composition of each froth as provided by industry partner.....	44
Table 4-5: The level of each variable for factorial design.....	45
Table 4-6: The level of each factor for each high-solids froth experiment.....	46
Table 4-7: Water content (wt %) difference at height Z1 of two replicates at each sampling time for different operating conditions including low J and low BC (HA), high J and high BC (HB), high J and low BC (HC) and low J and high BC (HD).....	48
Table 4-8: Water content difference (wt%) at height Z2 of two replicates at each sampling time for different operating situations including low J and low BC (HA), high J and high BC (HB), high J and low BC (HC) and low J and high BC (HD).....	53
Table 4-9: Water content difference (wt%) at height Z3 of two replicates at each sampling time for different operating situations including low J and low BC (HA), high J and high BC (HB), high J and low BC (HC) and low J and high BC (HD). Outliers are removed.....	56



Table 4-10: Water content difference (wt%) at height Z4 of two replicates at each sampling time for different operating situations including low J and low BC (HA), high J and high BC (HB), high J and low BC (HC) and low J and high BC (HD). Outliers are removed.....	59
Table 4-11: Water content difference (wt%) at all heights of two replicates during settling for different operating situations including low J and low BC (HA), high J and high BC (HB), high J and low BC (HC) and low J and high BC (HD). Outliers are removed.....	60
Table 4-12: The multivariate analysis for the water content at $h/H = 0.1$ .....	77
Table 4-13: The multivariate analysis for the solid content at $h/H = 0.1$ .....	77
Table 5-1: Chord length data selection for each high-solids froth settling experiment.....	80
Table 5-2: The operating condition, fouling index and data usability of the FBRM data for each high-solids froth experiment. ....	81
Table 6-1: Possible water structures observed on the 10x microscope images of average-quality and high-water froth during settling. ....	98
Table 6-2: Representative 10x microscope images of average-quality froth experiments with operating conditions: low mixing energy (-) and low injection rate (-). ....	99
Table 6-3: Representative 10x microscope images of average-quality froth experiments with operating conditions: high mixing energy (+) and low injection rate (-). ....	100
Table 6-4: Representative 10x microscope images of average-quality froth experiments with operating conditions: low mixing energy (-) and high injection rate (+). ....	102
Table 6-5: Representative 10x microscope images of average-quality froth experiments with operating conditions: high mixing energy (+) and high injection rate (+). ....	103
Table 6-6: Representative 10x microscope images of high-water froth experiments with operating conditions: low mixing energy (-) and low injection rate (-). ....	105
Table 6-7: Representative 10x microscope images of high-water froth experiments with less optimal mixing conditions: high mixing energy (+) and low injection rate (-).....	107
Table 6-8: Representative 10x microscope images of high-water froth experiments with less optimal mixing conditions: low mixing energy (-) and high injection rate (+).....	110
Table 6-9: Representative 10x microscope images of high-water froth experiments with the best mixing conditions: high mixing energy (+) and high injection rate (+).....	112

Table 6-10: Representative 10x microscope images of high-solids froth experiments with operating mixing conditions: low bulk concentration (-) and low mixing energy (-).....116

Table 6-11: Representative 10x microscope images of high-solids froth experiments with operating conditions: high bulk concentration (+) and low mixing energy (-).....118

Table 6-12: Representative 10x microscope images of high-solids froth experiments with optimal mixing conditions: low bulk concentration (-) and high mixing energy (+).....120

Table 6-13: Representative 10x microscope images of high-solids froth experiments with optimal mixing conditions: high bulk concentration (+) and high mixing energy (+).....122

# List of Figures

Figure 1-1: Comparison of different scales of segregation at same intensity of segregation ( $C_0V$ ). Figure used with permission (Kukukova et al., 2009)..... 6

Figure 1-2: Mechanism of surfactant-mediated tip streaming. Left-hand side shows an underformed water drop with surfactant molecules evenly distributed on the surface which is under external fluid force. Right-hand side shows that after the external force is applied, the surfactant molecules migrate from the equator to the pole of the drop and small drops have to be excluded as a reduction of surface tension on the pole. Figure used with permission (Sonthalia et al., 2016).....13

Figure 2-1: Schematic of experimental procedure. Four steps are included: pre-mixing, naphtha blending, demulsifier dispersion, and water and solids settling (Saraka, 2017).....16

Figure 2-2: Experimental setup for tests of demulsifier performance in bitumen froth. The confined impeller stirred tank (CIST) has 4 side sampling ports and a Teflon lid with two access ports for demulsifier injection (left) and the FBRM probe (right).....17

Figure 2-3: Comparison of geometry details of a Side Sampling CIST and a Top Sampling CIST (Arora, 2016). The four sampling heights are the same in both vessels: height Z1 is located at 77mm from the top; height Z2 is located at 44mm from height Z1; height Z3 is located at 44mm from height Z2; height Z4 located is at 44mm from height Z3 and 56mm from the bottom.....18

Figure 2-4: The relative location of the FRBM probe, the feed tube of demulsifier and the upper impeller on the shaft inside the CIST (Saraka, 2017).....19

Figure 2-5: Schematic demonstration of the FBRM probe operating principle: the probe emits a laser and receives the backscattered light as signal when the laser passes through an object; the chord length of an object is obtained through the multiplication of time interval where signal changes with laser velocity (Mettler Toledo, 2011).....27

Figure 4-1: Water content at height Z1 (wt%) vs. time (min) for average-quality froth, high-solids froth and high-water froth. Data reproduced with permission (Arora, 2016; Saraka, 2017).....31

Figure 4-2: Water content (wt%) at Z1 vs. time (min) for high-water froth and simulated high-water froth at similar dosages of demulsifier under good mixing conditions (high J and low IC): (a) high-water froth

at 25ppm vs. simulated high-water froth at 35ppm; (b) high-water froth at 196ppm vs. simulated high-water froth at 200ppm. High water froth data is reproduced with permission (Saraka, 2017).....36

Figure 4-3: 10x microscope images of froth at height Z1 after 25 minutes of settling: (a) high-water froth and (b) simulated high-water froth.....37

Figure 4-4: Effect of the demulsifier dosage on the water removal on high-solids froth. Results are shown in terms of water content at height Z1 (wt%) vs. time (min). All experiments were carried out at N:B ratio of close to 0.7 under good mixing conditions (high J and low IC). A demulsifier dosage of 100 ppm was set as the sufficient BC, which was required to obtain a final water content of lower than 1 wt% after 60 minutes of settling. Some obvious outliers (maximum of 2 per curve) were removed from data.....40

Figure 4-5: Effect of the demulsifier dosage on the water removal on high-water froth. Results are shown in terms of water content at height Z1 (wt%) vs. time (min). All experiments were carried out at N:B ratio of close to 0.7 under good mixing conditions (high J and low IC). A demulsifier dosage of 196 ppm, rounded up to 200 ppm, was set as the minimum BC – just sufficient to obtain a final water content of lower than 1 wt% after 120 minutes of settling (Saraka, 2017).....41

Figure 4.6: Final water content at Z1 (wt%) after 60 minutes of settling vs. various demulsifier bulk concentrations (ppm). A linear trend was observed in high-water froth. A clear trend was hard to distinguish in high-solids froth. Data reproduced with permission (Saraka, 2017).....42

Figure 4-7: Comparison of settling profiles for high-water froth, high-solids froth and average-quality froth. The high-water froth experiment was run at BC = 196 ppm. The high-solids froth experiment was run at BC = 150 ppm. The average-quality froth was run at BC = 150 ppm. Experiments were run under good mixing conditions (high J and low IC). Three settling stages were observed in both the settling process of high-water and high-solids froth: induction time, fast settling and slow settling. Water settling was considerably faster in average-quality froth since most of the separation finishes within the first 10 minutes. Data reproduced with permission (Arora, 2016; Saraka, 2017).....43

Figure 4-8: Comparison of two replicates run at low BC (35 ppm) and low J (425 J/kg) in terms of water content (wt%) at height Z1 vs. settling time (min). Experiments were run with high-solids (HS) froth at the fixed IC = 12 wt%.....47

Figure 4-9: Comparison of four operating conditions including low BC and low J, low BC and high J, high BC and low J and high BC and high J in terms of averaged water content (wt%) at height Z1 vs. time (min). Experiments were run with high-solids froth at the fixed IC = 12wt%.....49

Figure 4-10: Comparison of four mixing conditions including low J and low IC, low J and high IC, high J and low IC and high J and high IC in terms of averaged water content (wt%) at height Z1 vs. settling time (min). Experiments were run with high-water froth (HW) at the sufficient BC = 200 ppm. Data reproduced with permission (Saraka, 2017).....50

Figure 4-11: Comparison of four mixing conditions including low J and low IC, low J and high IC, high J and low IC and high J and high IC in terms of averaged water content (wt%) at height Z1 vs. time (min). Experiments were run with average-quality (AQ) froth at the sufficient BC = 150 ppm. Data reproduced with permission (Arora, 2016).....51

Figure 4-12: Comparison of four operating conditions including low BC and low J, low BC and high J, high BC and low J and high BC and high J in terms of averaged water content (wt%) at height Z2 vs. time (min). Experiments were run with high-solids froth at IC = 12 wt%.....52

Figure 4-13: Comparison of four mixing conditions including low J and low IC, low J and high IC, high J and low IC and high J and high IC in terms of averaged water content (wt%) at height Z2 vs. time (min). Experiments were run with high-water froth (HW) at sufficient BC = 200 ppm. Data reproduced with permission (Saraka, 2017).....54

Figure 4-14: Comparison of four mixing conditions including low J and low IC, low J and high IC, high J and low IC and high J and high IC in terms of averaged water content (wt%) at height Z2 vs. time (min). Experiments were run with average-quality froth (AQ) at the sufficient BC = 150 ppm. Data reproduced with permission (Arora, 2016).....54

Figure 4-15: Comparison of four operating conditions including low BC and low J, low BC and high J, high BC and low J and high BC and high J in terms of averaged water content (wt%) at height Z3 vs. time (min). Experiments were run with high-solids froth at the fixed IC = 12wt%. Averaged water content at height Z3 (wt%) vs. time (min) for high-solids froth experiments at different operating conditions without the centrepont.....55

Figure 4-16: Comparison of four mixing conditions including low J and low IC, low J and high IC, high J and low IC and high J and high IC in terms of averaged water content (wt%) at height Z3 vs. time (min).

Experiments were run with high-water froth (HW) at the sufficient BC = 200 ppm. Data reproduced with permission (Saraka, 2017).....57

Figure 4-17: Comparison of four mixing conditions including low J and low IC, low J and high IC, high J and low IC and high J and high IC in terms of averaged water content (wt%) at height Z3 vs. time (min). Experiments were run with average-quality froth (AQ) at the sufficient BC = 150 ppm. Data reproduced with permission (Arora, 2016).....57

Figure 4-18: Comparison of four operating conditions including low BC and low J, low BC and high J, high BC and low J and high BC and high J in terms of averaged water content (wt%) at height Z4 vs. time (min). Experiments were run with high-solids froth at the fixed IC = 12wt%.....58

Figure 4-19: Comparison of four mixing conditions including low J and low IC, low J and high IC, high J and low IC and high J and high IC in terms of averaged water content (wt%) at height Z4 vs. time (min). Experiments were run with high-water froth (HW) at the sufficient BC = 200 ppm. Data reproduced with permission (Saraka, 2017).....61

Figure 4-20: Comparison of four mixing conditions including low J and low IC, low J and high IC, high J and low IC and high J and high IC in terms of averaged water content (wt%) at height Z4 vs. time (min). Experiments were run with average-quality froth (AQ) at the sufficient BC = 150 ppm. Data reproduced with permission (Arora, 2016).....62

Figure 4-21: Effect of BC over settling time of height Z1 at IC = 12 wt% for high-solids froth.....63

Figure 4-22: Effect of J over settling time at height Z1 at IC = 12 wt% for high-solids froth.....64

Figure 4-23: Effect of BC\*J over settling time of height Z1 at IC = 12wt% for high-solids froth.....65

Figure 4-24: Effect of variables over settling time of height Z1 at BC = 200 ppm for high-water froth (Saraka, 2017).....66

Figure 4-25: Effect of variables over settling time of height Z1 at BC = 150 ppm for average-quality froth (Arora, 2016).....67

Figure 4-26: Effect of BC over settling time of height Z2 at IC = 12wt% for high-solids froth.....68

Figure 4-27: Effect of J over settling time of height Z2 at IC = 12wt% for high-solids froth.....68

Figure 4-28: Effect of BC\*J over settling time of height Z2 at IC = 12wt% for high-solids froth.....69

Figure 4-29: Effect of variables over settling time of height Z2 at BC = 150 ppm for average-quality froth (Saraka, 2017).....70

Figure 4-30: Effect of BC over settling time of height Z3 at IC = 12wt% for high-solids froth.....71

Figure 4-31: Effect of J over settling time of height Z3 at IC = 12wt% for high-solids froth.....71

Figure 4-32: Effect of BC\*J over settling time of height Z3 at IC = 12wt% for high-solids froth.....72

Figure 4-33: Effect of variables over settling time of height Z3 at BC = 150 ppm for average-quality froth (Saraka, 2017).....72

Figure 4-34: Effect of BC over settling time of height Z4 at IC = 12wt% for high-solids froth.....73

Figure 4-35: Effect of J over settling time of height Z4 at IC = 12wt% for high-solids froth.....74

Figure 4-36: Effect of BC\*J over settling time of height Z4 at IC = 12wt% for high-solids froth.....74

Figure 4-37: Effect of variables over settling time of height Z4 at BC = 150 ppm for average-quality froth (Saraka, 2017).....75

Figure 4-38 Water and solids content for several operating conditions with high-solids froth. Samples collected at the top height of the CIST ( $h/H=0.1$ ).....76

Figure 4-39 Water and solids content for several operating conditions with high-water froth. Samples collected at the top height of the CIST ( $h/H=0.1$ ) (Saraka, 2017).....77

Figure 5-1: Square weighted and unweighted chord length distribution at the beginning and the end of naphtha blending for low BC and low J operating conditions for high-solids froth settling experiment.102

Figure 5-2: Square weighted and unweighted chord length distribution at the beginning and the end of demulsifier dispersion for low BC and low J operating conditions for high-solids froth settling experiment.....83

Figure 5-3: Square weighted and unweighted chord length distribution over settling for low BC and low J operating conditions for high-solids froth settling experiment.....83

Figure 5-4: Square weighted and unweighted chord length distribution at the beginning and the end naphtha blending for high BC and high J operating conditions for high-solids froth settling experiment .....84

Figure 5-5: Square weighted and unweighted chord length distribution at the beginning and the end of demulsifier dispersion for high BC and high J operating conditions for high-solids froth settling experiment.....85

Figure 5-6: Square weighted and unweighted chord length distribution over settling for high BC and high J operating conditions for high-solids froth settling experiment.....86

Figure 5-7: Square weighted and unweighted chord length distribution at the beginning and the end of naphtha blending for high BC and low J operating conditions for high-solids froth settling experiment106

Figure 5-8: Square weighted and unweighted chord length distribution at the beginning and the end of demulsifier dispersion for high BC and low J operating conditions for high-solids froth settling experiment.....87

Figure 5-9: Square weighted and unweighted chord length distribution over settling for high BC and low J operating conditions for high-solids froth settling experiment.....88

Figure 5-10: Square weighted and unweighted chord length distribution at the beginning and the end of naphtha blending for low BC and high J operating conditions for high-solids froth settling experiment..88

Figure 5-11: Square weighted and unweighted chord length distribution at the beginning and the end of demulsifier dispersion for low BC and high J operating conditions for high-solids froth settling experiment.....89

Figure 5-12: Square weighted and unweighted chord length distribution over settling for low BC and high J operating conditions for high-solids froth settling experiment.....90

Figure 5-13: Square weighted chord length distributions at the beginning and the end of naphtha blending for four different operating conditions of high-solids froth settling experiment.....90

Figure 5-14: Square weighted chord length distributions at the beginning and the end of demulsifier dispersion for four different operating conditions of high-solids froth settling experiment.....91



Figure 5-15: Square weighted chord length distributions over settling for four different operating conditions of high-solids froth settling experiment.....92

Figure 6-1: Estimation of the size of a single small free water drop observed on the 10x microscope image for the high-water froth. Experiment was run at good mixing conditions (high J and low IC) at BC = 200 ppm.....95

Figure 6-2: Estimation of the size of a single spherical water drop observed on the 40x microscope image for the high-water froth. Experiment was run at good mixing conditions (high J and low IC) at BC = 200 ppm.....96

Figure 6-3: Graphic demonstration of the proposed settling mechanism of free water in high-water froth experiments (a) at the beginning of settling, naturally present free-water are evenly distributed in each height zone (b) during the induction time, flocculation-induced coalescence happen in the bottom height zones, free space is squeezed, and some naturally present free-water flow to the empty space (c) at the end of settling, the bottom height zones are packed and top height zone is quite empty.....115

Figure 7-1: Formation of small water drops at the interface of a fluid system which contains 10wt% of water in canola oil at the bench-scale of turbulent mixing in the CIST with a set of Rushton impellers at 655rpm: (a) oil-water interface before the impellers were turned on (b) t = 4 s when a stretched water drop with a long tail is observed (c) and t = 10 s when smaller drops are excluded from the stretched water drops. ....126

# List of Symbols

BC	Bulk Concentration
CHWE	Clark Hot Water Extraction
CIST	Confined Impeller Stirred Tank
CLD	Chord Length Distribution
CP	Centrepoint
D	Impeller Diameter
FBRM	Focused Beam Reflectance Measurement
HA	High-solids froth mixing experiments: factorial run A, low BC and low J
HB	High-solids froth mixing experiments: factorial run B, high BC and high J
HC	High-solids froth mixing experiments: factorial run C, high BC and low J
HD	High-solids froth mixing experiments factorial run D, low BC and high J
IC	Injection Concentration
J	Mixing Energy
KF	Karl Fischer Water Titration
N	Rotational Speed
NaOH	Sodium Hydroxide
NAs	Naphthenic Acids
NaHs	Sodium Naphthenates
N:B	Naphtha to Bitumen Ratio
$N_p$	Power Number of Impeller
OWS	Oil, Water, and Solids as detected by Dean Stark Extraction
P	Power Required by the Impellers
PSV	Primary Separation Vessel
Re	Reynolds Number
S	Impeller Submergence
SAGD	Steam Assisted Gravity Drainage
$t_{mix}$	Mixing Time

$V_{IMP}$	Impeller Swept Volume
$V$	CIST Volume
$\beta$	Regression Coefficient
$\epsilon$	Energy Dissipation
$\mu$	Dynamic Viscosity
$\nu$	Kinematic Viscosity
$\rho$	Density
$\sigma$	Interfacial Tension
$G$	Strain Rate
$C_a$	Capillary Number

# Chapter 1 Oil Sands Processing and Mixing

The oil sands of Alberta, sometimes also known as tar sands, are the largest source of unconventional fuel in North America (Gray et al., 2009). The Alberta oil sands deposit has 9wt%-13wt% bitumen, 3wt%-7wt% water and 80wt%-85wt% mineral solids, where the bitumen that can be recovered by current and foreseeable technologies is estimated at 172 billion to 315 billion barrels compared to the estimated 264 billion barrels for the crude oil reserves in Saudi Arabia (Gray et al., 2009).

Currently, two technologies are used to extract bitumen from oil sands. If oil sands are rich and at a depth of more than about 40m, in-situ technology, such as the Steam Assisted Gravity Drainage (SAGD) , is applied (Gray et al., 2009). In this process, two L-shaped wells are drilled horizontally into deposits where superheated steam at approximately 250°C is injected to the top well to reduce the bitumen viscosity (Gray et al., 2009). The bottom well then collects mobilized bitumen, which is pumped upwards to the ground (Gray et al., 2009).

If oil sands are shallow and barren, the Clark Hot Water Extraction (CHWE) process, which was developed by Karl Clark of the Alberta Research Council and the University of Alberta in the 1920s, is applied (Rao and Liu, 2013). This extraction process was later modified and commercialized by many oil sands producers, such as Syncrude Canada Ltd., Suncor Energy Inc., and Albion Sands Energy Inc., etc. (Rao and Liu, 2013). In this process, oil sands ores are extracted by surface mining where overburdens are removed by massive trucks or shovels, ore is harvested, and landscapes are reclaimed to support vegetation and wildlife (Gray et al., 2009). After harvesting, the ores are crushed and mixed with hot water and sodium hydroxide (NaOH) to a prepare slurry at 75-80°C (Gray et al., 2009). The slurry is hydro-transported by pipeline for conditioning where air is introduced to liberate bitumen from water (Gray et al., 2009). The turbulence in the pipeline also breaks lumps into even smaller sizes (Gray et al., 2009). The slurry is sent to the Primary Separation Vessel (PSV) where most of the sands and water settle easily. The middling stream is further processed to recover any residual bitumen.

The aerated bitumen goes to the top and is skimmed off as bitumen froth, which is directed to the froth treatment plant to separate more water and solids from bitumen (Gray et al., 2009). The top stream has a typical composition of 60wt% bitumen, 30wt% water, and 10wt% solids (Gray et al., 2009). The composition of froth can vary depending on the quality of ores mined and conditions of processing. Bitumen froth can be sorted by different qualities based on its composition such as high-water and high-solids froth, where the amount of water and solids respectively are above the typical composition. The bottom stream, which mostly contains sands, clays, water and a small quantity of trapped bitumen, is then transferred to the tailing pond where sands settle rapidly and clays are suspended (Gray et al., 2009). The relatively clean water on the pond surface is recycled to the bitumen extraction process, but the solids suspended in water can form a loose network, which leads to an extremely slow settling due to the colloidal force formed between particles (BCG Engineering Inc., 2010; Gray et al., 2009). In this thesis project, all ore samples were extracted using surface mining and froth samples were generated in the industrial pilot plant.

## 1.1 Emulsified Water and Bitumen Froth Treatment

The bitumen froth recovered from either surface mining or SAGD technology is a mixture of bitumen, water, and solids, and must go through the froth treatment plant to reduce the water content to less than 1wt% of water and solids before upgrading (Rao and Liu, 2013). Any remaining water and solids are extremely detrimental to the downstream processing. Solids can foul equipment, such as centrifuges and contaminate catalysts (Rao and Liu, 2013). The emulsified water (<10  $\mu\text{m}$ ) can be accumulated through recycling and converted to hydrochloric acid by hydrogenation during upgrading, which causes serious corrosive problems and leads to a huge amount of maintenance cost in downstream processing (Rao and Liu, 2013). These emulsified water drops are easily stabilized by some natural surfactants, such as clays, asphaltenes and naphthenic acids. Process parameters, such as the temperature of aqueous phase and bitumen, can contribute to the formation of emulsified water drops (Gingras et al., 2005). Asphaltenes are also known to play an important role in stabilizing water drops. The

polycyclic part of asphaltenes contains aromatic and naphthenic molecules with aliphatic side chains, which can also be described as hydrocarbon tails (Rao and Liu, 2013). On the contrary, some metals and polar heteroatoms, such as nitrogen, oxygen and sulfur, can be considered as polar heads (Rao and Liu, 2013). Asphaltenes, together with some hydrophilic clay particles, can form a rigid barrier at the water-oil interface (Rocha et al., 2016). This prevents water drops from coalescing since the repulsive steric layer force overcomes the attractive van der Waals force (Rao and Liu, 2013). The resistance of the rigid film formed on the surface of water drops to prevent coalescence is equivalent to about 1000 G acceleration, which is difficult to overcome at full scale (Rao and Liu, 2013).

Although the amphipathic behavior of asphaltenes is often believed to contribute to the stabilization of emulsified water, there is a different view that asphaltenes stabilize water drops only due to their propensity to aggregate (Czarnecki et al., 2012). In this case, a thin layer of oil wraps the surface of a fine water drop, where a network structure of the fluid is formed within the film (Czarnecki et al., 2012). The rheology of the fluid within this thin layer becomes non-Newtonian with a small Bingham yield stress generated to prevent the film drainage and prevent water coalescence (Czarnecki et al., 2012). In terms of naphthenic acids (NAs), it is a complex mixture of cyclic carboxylic acids that may contain aliphatic side chains, which helps stabilize water drops (Gao et al., 2010). When NaOH is added during the bitumen extraction process, NAs are easily converted to sodium naphthenates (NaNs), which form mesomorphic phases with multilayered structure at the interface, and increase the stability of emulsion (Gao et al., 2010). NAs can also entrap solids, such as kaolinite, causing a segregation at the surface of a water drop and further which contributes to the emulsion stability (Quraishi et al., 2015).

These emulsified water drops cannot be removed easily through physical separations, such as the inclined plate separation (IPS) and centrifuges. Diluent and demulsifier must be added to help separation. There are two types of diluents: naphtha, used in most of the Athabasca oil sands projects, and paraffinic solvents, used in a few projects such as Kearl Lake (Rao and Liu, 2013). In naphthenic froth treatment (NFT), the solvent naphtha is added at the optimal

naphtha to bitumen (N:B) ratio 0.7 by mass to reduce the fluid viscosity and increase the density difference (Rao and Liu, 2013). Demulsifier, which is typically a proprietary formulation of polymers, is added to induce flocculation or coalescence of emulsified water drops. Generally speaking, demulsifier can be sorted into two types. Coalescence-inducing demulsifier migrates to the interface, breaks down the thin layer and decreases the surface tension to make drop coalescence easier. By contrast, flocculation-inducing demulsifier migrates on top of the thin layer, and attracts other water drops to form large aggregates. These aggregates settle very fast and act as a moving filter as they settle, capturing many remaining water drops and solids. This process is known as sweep flocculation, where fine solids are captured by settling water flocs. After NFT, the froth typically contains 1-2wt% water and 0.5wt% solids (Rao and Liu, 2013). The naphtha diluent in the diluted froth is then evaporated and recycled.

In paraffinic froth treatment (PFT), the paraffin, an aliphatic solvent, is added at a much higher paraffin to bitumen ratio ( $\geq 1.5$ ) by mass to precipitate asphaltenes (Rao and Liu, 2013). The large aggregates formed help capture any remaining water and solids during settling, which is the same settling mechanism as sweep flocculation. The settling rate of these aggregates is strongly influenced by operating temperature since high temperature helps form larger aggregates, resulting in a significant increase in settling rate (Long et al., 2004). The treated bitumen product from PFT has much lower amounts of water and solids, nearly zero, and only needs to go through several physical separations before refining (Rao and Liu, 2013).

Comparing these two froth treatments, the recovery from PFT is lower than NFT since most of the asphaltenes, which are also hydrocarbon fractions of crude oil, are lost in the precipitation (Rao and Liu, 2013).

## 1.2 Mixing in Bitumen Froth Treatment

Kukukova et al. (2009) proposed a definition of mixing which requires three separate dimensions of segregation, in order to characterize mixing problems more clearly and accurately.

The first dimension, the intensity of segregation, can be quantified by the normalized concentration variance ( $C_oV$ ) using Equation 1 (Kukukova et al., 2009).

$$C_oV = \sqrt{\frac{1}{N_t} \sum_{i=1}^{N_t} \left( \frac{C_i - C_{\text{mean}}}{C_{\text{mean}}} \right)^2} \quad (1)$$

Where  $N_t$  is the total number of sampling points,  $C_i$  is the concentration at sampling point  $i$ ;  $C_{\text{mean}}$  is the mean concentration.

The second dimension, the scale of segregation, refers to the instantaneous length scale of mixing, which can take on a distribution of values from the largest scale of segregation to the smallest scale of segregation (e.g. drop size distribution) (Kukukova et al., 2009). A small concentration variance does not necessarily mean a small segregation of segregation.

Figure 1-1 shows that two mixing fields can have the same normalized concentration variance, while one scale of segregation (left) is larger than the other (right). The intensity of segregation only quantifies how widely the concentration varies, but does not measure the arrangement of elements at the scale of segregation (Kukukova et al., 2009).



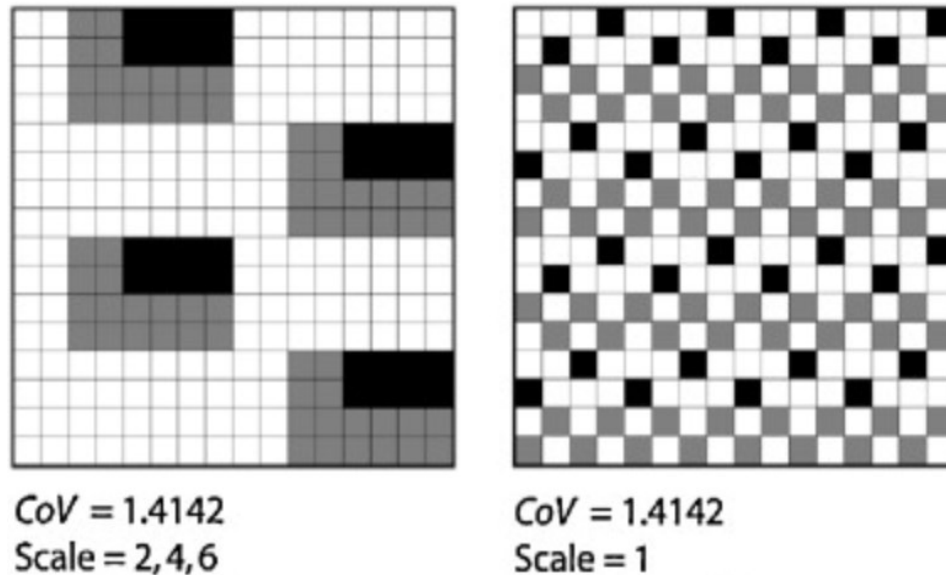


Figure 1-1: Comparison of different scales of segregation at same intensity of segregation ( $C_oV$ ).  
Figure used with permission (Kukukova et al., 2009).

For example, there are two fields mixing the same dye: the left field has not only some small dye aggregates but also some large aggregates; the right field has well-distributed equal-sized small dye aggregates. Although the normalized concentration variance is the same in each field, the largest segregation scale in the first field, which is equivalent to the size of the largest aggregate, is much bigger than the segregation scale in the second field, which is only equivalent to the size of small dye aggregates.

The third dimension of segregation, mixing time, is also an important process specification. If a process is limited by mass transfer and no reactions take place, mixing time is determined by mass transfer. For example, if there are only two components and no reactions occur, the overall processing time is dominated by the mass transfer rate, which relates to mixing conditions. On the contrary, if a slow reaction occurs, mixing time determines when these two components meet each other before the reaction takes place. In addition, optimal mixing conditions can shift the distribution of reaction rates by changing local concentrations, as well as increasing contacting areas for reaction. For example, in the research of mixing effects on the reactive precipitation of amine mono- and di-hydrochloride salts, mixing conditions, such as

mixing energy and mixing intensity, are proven to help prevent meso-mixing effects and affect the distribution of products (Maluta et al., 2017). Hence, when defining a mixing problem, all three dimensions of segregation should be reviewed.

Mixing effects on the settling of water and solids in diluted bitumen and froths at the bench-scale have been studied by the mixing group at the University of Alberta for many years. Initially, the relative effects of demulsifier dosage, local maximum energy dissipation, mixing time, and injection concentration of demulsifier on the water removal of diluted bitumen were studied in the Confined Impeller Stirred Tank (originally named the Shear and Sedimentation Test Cell (SSTC)), and the bulk concentration appeared to be the dominant variable (Laplante, 2011). When the experimental design was refined, (Chong, 2013; Laplante, 2011) two dominant mixing factors were identified: mixing energy, which was identified as the product of energy dissipation and mixing time, and injection concentration of demulsifier.

In order to better understand the settling mechanisms, an image analysis was developed to study mixing effects on demulsifier performance for diluted bitumen, where water drops were predominantly spherical, isolated drops. These drops could be captured using an image analysis algorithm based on the Hough Circle Detection algorithm (Leo, 2013). This image analysis was later adapted for average-quality froth, which is a much more complex mixture of water, solids, and aggregates, to determine the Cluster Size Distribution. In froth, flocculation of water drops and solids, and subsequent sweep flocculation of fine solids were found to be the dominant settling mechanisms (Arora, 2016).

However, neither the Hough circle algorithm nor the cluster analysis algorithm can be applied to high-water froth since irregularly-shaped large water drops (free water) are dominant. According to the water content analysis obtained using Karl Fischer titrations and OWS analysis, high-water froth shows an induction time, which is a delayed settling behavior of up to 40 minutes (Saraka, 2017). In this project, a third froth sample, high-solids froth, was studied and similar outcomes are observed. According to all previous mixing studies at the bench-scale, mixing conditions play an important role in the performance of demulsifier in froth treatment.

In general, good mixing conditions, which refer to high mixing energy and low injection concentration of demulsifier, can improve demulsifier performance. On the contrary, poor mixing conditions can reduce the effectiveness of the separation, even if more demulsifier is added.

### 1.3 The Confined Impeller Stirred Tank (CIST)

The confined impeller stirred tank is a customized mixing test vessel designed by the mixing group at the University of Alberta. The CIST is used to study mixing effects on the performance of demulsifier for diluted bitumen and froth. Local mixing conditions in industrial froth treatment are simulated in the CIST ( $T=0.076\text{m}$ ,  $H=3T$ ), which is filled with five or six impellers to produce a more uniform field of turbulence at the bench-scale (Machado and Kresta, 2013). The CIST used in this work is a 1L double-walled glass vessel with four side sampling ports and two access ports, one for demulsifier injection and the other one for the Focused Beam Reflectance Measurement (FRBM) probe, used to obtain the in-situ chord length distribution of fluid particles. The submergence of the upper impeller ( $S=D$ ) is selected to reduce air entrainment; the off-bottom clearance of the lowest impeller ( $C=D/3$ ) is selected to provide active circulation and achieve fully turbulent flow at the bottom of the tank. The remaining impellers are equally spaced on the shaft to provide uniform flow and energy dissipation (Komrakova et al., 2017)

The Reynolds number (Re) is used to characterize the mixing impeller, which can be expressed by Equation 2:

$$\text{Re} = \frac{\rho N D^2}{\mu} \quad (2)$$

Where  $\rho$  is the fluid density,  $N$  is the rotational speed of the impeller,  $D$  is the impeller diameter, and  $\mu$  is the fluid dynamic viscosity. Fully turbulent flow across the whole vessel is

always desirable to better disperse and dissolve demulsifier in bitumen froth treatment, which is an expensive chemical additive, and to ensure accurate data for scale-up.

The impellers are characterized by using the power number ( $N_p$ ), which can be calculated based on the balance of angular momentum around the impeller using Equation 3 (Machado and Kresta, 2013)

$$N_p = \frac{P}{\rho N^3 D^5} \quad (3)$$

Where  $P$  is the total power consumed by the impeller,  $\rho$  is the fluid density,  $N$  is rotational speed of the impeller and  $D$  is the impeller diameter. The  $N_p$  of different types of impellers, such as the Rushton, A310 and Intermig, can be obtained through placing impellers in a known fluid, varying the rotational speed and measuring the corresponding power consumed. A correlation of  $N_p$  and  $Re$  can be drawn, where a constant  $N_p$  is usually reached when  $Re$  is fully turbulent. When scaling up at constant power per unit mass, this equation shows that the rotating speed has to be reduced significantly as result of the increased impeller diameter.

When comparing the CIST to conventional stirred tanks used in many industrial applications and scale-down experiments, energy dissipation ( $\epsilon$ ) is often used to characterize the extent of mixing, but there are variations of this parameter. The average power dissipation ( $\epsilon_{ave}$ ) in the tank can be expressed by Equation 4 (Machado and Kresta, 2013):

$$\epsilon_{ave} = \frac{P}{\rho V_{tank}} \quad (4)$$

Where  $P$  is the power consumption, which can be calculated by the  $N_p$  equation above,  $\rho$  is the fluid density, and  $V_{tank}$  is the total volume of a stirred tank. When the swept volume of impellers ( $V_{impeller}$ ) is considered rather than  $V_{tank}$ ,  $\epsilon_{swept}$  can be calculated instead (Machado and Kresta, 2013).

The maximum energy dissipation ( $\epsilon_{\max}$ ), which considers only the most turbulent region of the stirred tank, the discharge stream leaving the impeller, can be expressed by Equation 5 (Komrakova et al., 2017):

$$\epsilon_{\max} = A \frac{u_{\max}^3}{L} \quad (5)$$

Where A is a constant,  $u_{\max}$  is the maximum velocity in the dominant flow direction, which can be measured, and L is the integral-length scale of turbulence, which is roughly equal to the size of the trailing vortices ( $L=D/10$ ) for the fluid volume in the impeller discharge stream.

When considering  $\epsilon_{\text{ave}}$  and  $\epsilon_{\max}$ , the minimum drop size correlates with  $\epsilon_{\max}$  rather than  $\epsilon_{\text{ave}}$  in a liquid-liquid dispersion, but  $\epsilon_{\max}$  is not often used since  $u_{\max}$  is hard to measure (Zhou and Kresta, 1998). Instead,  $\epsilon_{\text{swept}}$  is often used to scale the local turbulence since a significant fraction (about 30%) (Komrakova et al., 2017; Zhou and Kresta, 1996) of the energy is dissipated within the swept volume of impellers instead of the whole tank.

To summarize, in a mixing experiment, the power consumption of chosen impellers can be calculated using the  $N_p$  equation, specifying fluid density, impeller category, diameter, and rotating speed. The average energy dissipation can be calculated knowing the tank volume. If the maximum velocity in the dominant flow direction can be measured, the maximum energy dissipation can be calculated as well.

The CIST, which is used at the bench-scale to obtain reproducible and repeatable mixing data has been modeled using five flow zones: (1) the impeller swept volume, (2) the impeller discharge stream, (3) the wall jet, (4) the return stream, and (5) the surface. This model was based on measured mean and fluctuating velocities using Rushton impellers to understand the hydrodynamics and mixing in the CIST (Komrakova et al., 2017). Within these five zones, the discharge streams for all Rushton impellers was found to have similar behavior. The jet leaving

the impeller blade does not expand in the CIST (Komrakova et al., 2017), unlike the discharge stream in a conventional stirred tank.

Compared to the conventional stirred tank, the CIST can reach a fully turbulent flow regime with a much lower  $Re$  ( $\approx 3000$ ) rather than ( $\approx 20,000$ ) in a stirred tank for fully turbulent flow close to the impeller and ( $\approx 300,000$ ) to achieve fully turbulent flow in the top third of a tank (Komrakova et al., 2017). The bulk of the tank in a CIST is also turbulent with an inactive volume of only 3% in the CIST vs. 33% in a conventional stirred tank (Chong et al., 2016; Komrakova et al., 2017). Finally, only 1L of fluid is required when conducting experiments using CIST vs. 10L required by the conventional stirred tank (Chong et al., 2016). Hence, less waste is generated, and more experiments can be done. The CIST also allows for settling in place after demulsifier dispersion without fluid transfer (Chong et al., 2016).

#### 1.4 Surfactant-Mediated Tip Streaming

In recent studies of the formation of fine water drops, (Sonthalia et al., 2016) found that fine water drops was formed due to surfactant-mediated tip streaming, which can even happen at low shear force. When a water drop is suspended in a flowing fluid, it is stretched into a thread-like structure due to external fluid force and breaks into daughter drops due to capillary instability or end-pinching effects (Sonthalia et al., 2016). Capillary instability is characterized by the dimensionless capillary number, which describes the ratio of fluid viscous force required to break the drop vs. the interfacial tension force of the drop to restore the surface, by Equation 6 (Sonthalia et al., 2016)

$$C_a = \frac{\mu_c GR}{\sigma} \quad (6)$$

Where  $G$  is the strain rate (related to, but not the same as,  $\epsilon_{max}$ ),  $R$  is drop radius,  $\sigma$  is the interfacial tension, and  $\mu_c$  is the fluid viscosity. There is a critical value of capillary number to

reach for a drop breakup to happen: above this critical number, drop breakup happens; below this critical value, the drop stays deformed without fracture (Sonthalia et al., 2016).

There are three types of drop fractures: primary drop breakup, which results in daughter drops with diameter of the same order of magnitude as the parent drop; secondary drop breakup, which results in satellite daughter drops with diameters one or more orders of magnitudes smaller than the parent drop; and secondary drop breakup by surfactant-mediated tip streaming, which results in extremely fine water droplets that can be 100 times smaller than the parent drop (Sonthalia et al., 2016).

Since primary drop breakup requires an extremely high shear rate to achieve the finest drops observed in froth, on the order of  $10^6 \text{s}^{-1}$ , this is unlikely to occur in the froth treatment plant (Sonthalia et al., 2016) and fine water drops are unlikely to be generated by the primary drop breakup. Both satellite daughter drops and fine water drops via tip streaming are possible, but the tip streaming has been identified as the major breakup mechanism to form fine water drops in at least one fundamental study (Sonthalia et al., 2016). In this study, at the very fine scale of microfluidics, the volume loss of a water drop due to tip streaming was approximately 72%, compared to the only 0.1% volume loss due to the secondary breakup mechanism to form satellite drops (Sonthalia et al., 2016). The analysis of length scale ( $\sim 10\text{--}100\mu\text{m}$ ) and the time scale ( $\sim 1\text{--}10\text{ms}$ ) also shows that tip streaming can exist under the conditions observed in a froth treatment plant to produce fine water drops (Sonthalia et al., 2016).

The capillary number which has been discussed above for tip streaming ( $C_a \approx 0.5$ ) is only half of the capillary number ( $C_a \approx 1$ ) required for the formation of satellite drops, which also shows that tip streaming is more likely to happen even at a low shear force (Sonthalia, et al., 2016). When the capillary number is low ( $C_a \approx 0.1$ ), large drops ( $\approx 100\mu\text{m}$ ) are formed due to end-pinching effects, which are controlled by constriction. When the capillary number is high ( $C_a > 1$ ), dripping and jetting happen to form small water drops ( $\sim 20\text{--}60\mu\text{m}$ ) (Sonthalia et al., 2016).

Figure 1-2 shows the surfactant-mediated tip streaming where the adsorbed surfactants on the surface of water drops experience extensional force from the fluid, and are convected from the equator to the tip of the drop (Sonthalia et al., 2016). As a result, there is an accumulation of surfactants on the tip, which significantly reduces the interfacial tension (Sonthalia et al., 2016). The reduction of interfacial tension on the tip leads to an imbalance of force across the drop surface. Fine water drops have to be excluded from the drop tip to balance the force (Sonthalia et al., 2016).

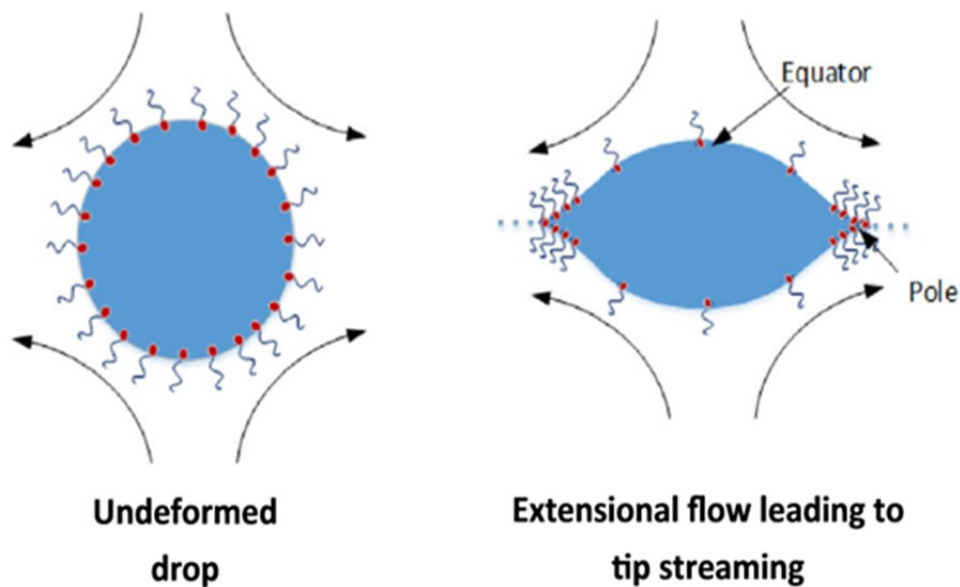


Figure 1-2: Mechanism of surfactant-mediated tip streaming. Left-hand side shows an undeformed water drop with surfactant molecules evenly distributed on the surface which is under external fluid force. Right-hand side shows that after the external force is applied, the surfactant molecules migrate from the equator to the pole of the drop and small droplets have to be excluded as a reduction of surface tension on the pole. Figure used with permission (Sonthalia et al., 2016).



## 1.5 Research Objective

The settling behavior of water and solids in average-quality and high-water froth has been studied using the CIST. Induction time, which is a delayed settling behavior, was observed in high-water froth compared to the fast settling observed in average-quality froth. In this thesis project, another quality of froth, high-solids froth, was studied following the same standardized procedures as the other two froths to understand mixing effects and settling mechanisms. In this work, the settling behavior of these three froths was compared using the water content reduction over time (Karl Fischer titrations), chord length distributions (FBRM measurements), and microscope images to better understand how mixing conditions affect settling in various extraction streams.

# **Chapter 2: Procedures of Mixing Experiments with the FBRM Probe for Bitumen Froth**

The procedures for mixing experiments for bitumen froth have been continuously developed by the mixing group but are modified for each research project, depending on the sample and the goals of the project (Arora, 2016; Saraka, 2017). The mixing experiments at the bench-scale are used to simulate the effect of mixing on the separation of water and solids from bitumen froth. The experiments and the mixing test vessel, the Confined Impeller Stirred Tank, have standard operating procedures, which can be found in Appendix A.1.

Figure 2-1 shows that there are four major steps of a full mixing experiment including pre-mixing, naphtha blending, demulsifier dispersion, and settling. Pre-mixing is where water and solids are resuspended homogeneously across the froth can. Naphtha blending is where naphtha is added to froth to reduce the overall fluid's viscosity and density. Demulsifier dispersion is where demulsifier is added and mixing energy is varied. Settling is where water and solids start to settle once impellers are shut off. All mixing experiments were performed using the CIST.

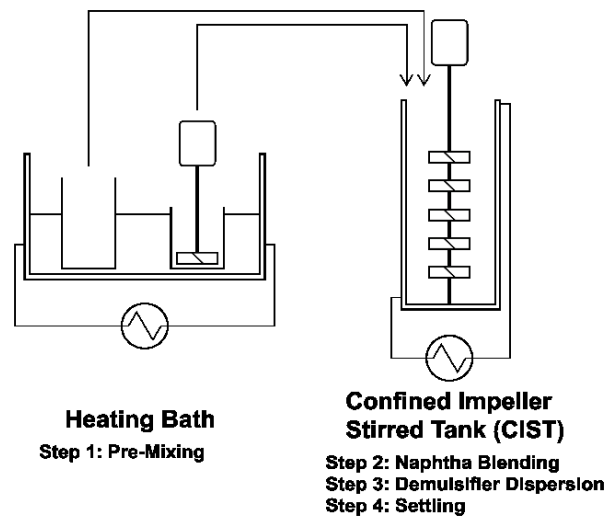


Figure 2-1: Schematic of experimental procedure. Four steps are included: pre-mixing, naphtha blending, demulsifier dispersion, and water and solids settling (Saraka, 2017).

## 2.1 The Confined Impeller Stirred Tank (CIST) Assembly

Figure 2-2 shows the mixing test vessel - or CIST - used at the bench-scale to study mixing effects in bitumen froth. The CIST is a double-walled glass vessel holding approximately 1L of fluid with ethylene glycol through a heating jacket to keep experiments at 80°C. Prior to performing each experiment, a septum, which can be punctured and self-heals, is put at the top of each Teflon plug, then capped and screwed to each sampling port. A Teflon spacer is then put at the bottom of the vessel to hold the shaft. Figure 2-3 shows the detailed dimensions of two vessels: side sampling (left) and top sampling (right). A shaft with either five Rushton impellers ( $D=T/2$ ) or six Intermig impellers ( $D=2T/3$ ) is seated on the spacer and secured to the motor on the top. An assembly of four baffles, which are equally spaced and perpendicular to the tank walls, converts tangential flow to axial circulation. In the end, a Teflon lid is covered at the top of the vessel, providing two ports for the FBRM probe and demulsifier injection respectively. The FBRM probe is located above the first impeller, beside the feed pipe of the

demulsifier. The relative locations of the FBRM probe, the feed pipe and the first impeller are shown in Figure 2-4.



Figure 2-2: Experimental setup for tests of demulsifier performance in bitumen froth. The confined impeller stirred tank (CIST) has 4 side sampling ports and a Teflon lid with two access ports for demulsifier injection (left) and the FBRM probe (right).

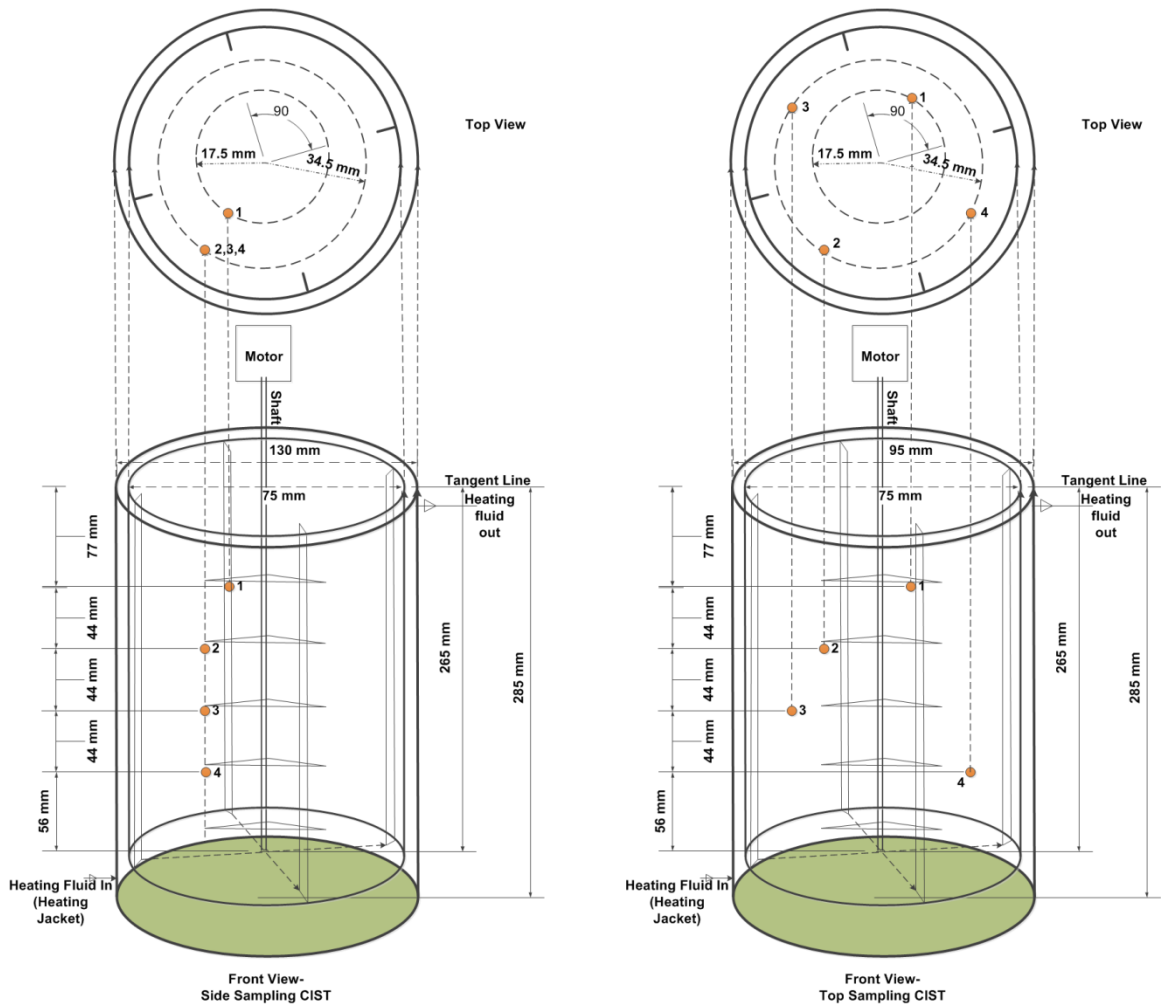


Figure 2-3: Comparison of geometry details of a Side Sampling CIST and a Top Sampling CIST (Arora, 2016). The four sampling heights are the same in both vessels: height Z1 is located at 77mm from the top; height Z2 is located at 44mm from height Z1; height Z3 is located at 44mm from height Z2; height Z4 located is at 44mm from height Z3 and 56mm from the bottom.

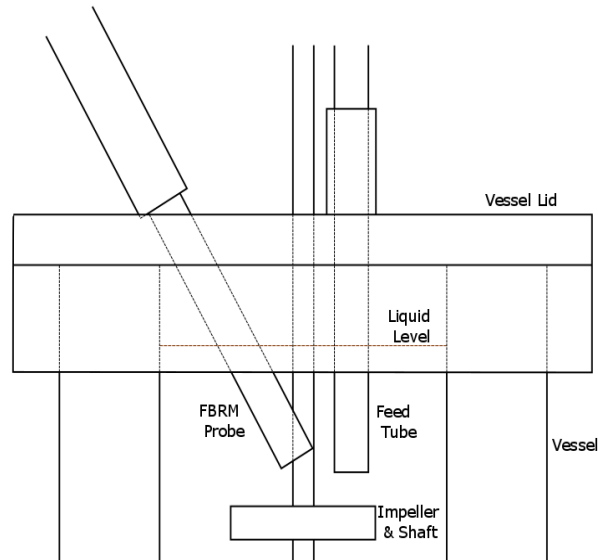


Figure 2-4: The relative location of the FBRM probe, the feed tube of demulsifier and the upper impeller on the shaft inside the CIST (Saraka, 2017).

## 2.2 Sample Storage

Each froth sample can arrives approximately 80% filled. Based on experience from previous projects, one and a half froth cans are needed for a full settling experiment. Before the experiment, froth cans are stored in the fridge to reduce aging effects, which can affect settling behavior. The cans are also put upside down to slowly displace water and solids from the bottom to the top of the can so that they can all be captured when the can is emptied. On the day of the experiment, two froth cans are taken out of the fridge and are placed on the bench, still upside down.

## 2.3 Pre-Mixing

The pre-mixing heating bath, which uses ethylene glycol, is heated for at least one hour prior to starting an experiment. Froth samples are heated to at least 70°C, which can take up to two hours, before pre-mixing starts. Pre-mixing then re-suspends and re-dispenses the water and

solids in the froth. By the end of pre-mixing, the solids and water contents are uniform across the froth can. Mixing is done using a 45° Pitched Blade (down-pumping) turbine impeller ( $D=T/2$ ) centered in the froth can at a clearance of ( $C=D/3$ ). A custom lid fitted with 2 baffles, which are set perpendicular to each other, is used to cover the can. The impeller speed is set at 1000rpm for 15 minutes. Table 2-1 shows the geometry of the froth can and the parameters for pre-mixing.

Table 2-1: The geometry of the froth can and the parameters of pre-mixing (Saraka, 2017).

Impeller	45° Pitched Blade (Down-Pumping)
Tank Diameter (m)	0.1
Impeller Diameter (m)	0.06
Off Bottom Clearance (m)	0.02
Impeller Speed (rpm)	1000
Reynolds Number	11 - 61
Mixing Time (min)	15

## 2.4 Naphtha Blending

Naphtha is used to dilute the froth, decreasing its viscosity and density. While the pre-mixing is running, a beaker filled with a fixed amount of naphtha is placed inside the same heating bath for approximately 30 minutes to reach 80°C, which is the temperature of the froth at the end of pre-mixing. The amount of naphtha added is based on the specified naphtha-to-bitumen (N:B) ratio of 0.7 by mass. The beaker is covered by duct tape during heating to minimize de-volatilization of naphtha. After pre-mixing, naphtha is poured into the CIST first to prevent froth from sticking to the wall, and froth is then poured until the fluid level reaches the 1L mark of the CIST. The FBRM probe is inserted before naphtha blending starts. The FBRM instrument is set to collect data when the impellers are turned on for naphtha blending and collects data

until the end of settling. The froth and naphtha are always blended for 2 minutes for different impellers. The speeds of impellers are varied to reach the same mixing energy, which means mixing effects are expected to be equivalent in this step. At the end of naphtha blending, a 1mL sample is taken at height Z1 to measure its water content by Karl Fischer titration. The mixing geometry and parameters of naphtha blending for different impellers are shown in Table 2-2.

Table 2-2: The mixing geometry and parameters of naphtha blending (Saraka, 2017).

Impeller	Intermig	Rushton
N (rpm)	1060	600
Re	7240	2367
Impeller swept volume (L)	0.168	0.0431
Single-impeller $N_p$	0.63	4.2
Power per mass (W/kg)	6.55	1.67
Power per mass in swept volume (W/kg)	38.8	38.6
Mixing time (min)	2	2
J (J/kg)	4652	4633

## 2.5 Demulsifier Dispersion

The demulsifier, which has 35wt% active ingredients in xylene, is called X-2105 as provided by Champion. The same demulsifier has been used when studied average and high-water froth (Arora, 2016; Saraka, 2017). Different types of demulsifier were used by our research group but no obvious difference was observed on dewatering efficiency. This demulsifier is further diluted with additional xylene to reach different concentrations: 12wt%, 16.5wt%, and 21wt% as required by the experimental design. Demulsifier is fed to the vessel either through a feed pipe by a syringe pump or injected manually using a glass syringe. Either the feed pipe or the glass syringe is inserted into the vessel through the Teflon lid until it reaches its marked insertion depth, which is 8.6cm. If the amount of demulsifier required is low, a glass syringe is used where demulsifier is injected slowly by hand. At the same time, the impellers are turned on to



minimize meso-mixing. A 1 mL sample is taken 30s before the end of demulsifier dispersion at height Z1 for Karl Fischer analysis. If the amount of demulsifier required is high, the syringe pump is used where demulsifier is fed at a certain injection rate, which is determined by local mixing conditions to avoid formation of a feed plume. The injection rate of demulsifier can be calculated using the Equation 7 based on the local turbulence field to minimize the meso-mixing effects (Chong, 2013):

$$Q_I = 0.54 \frac{v^{0.5} U_z d_{\text{pipe}}^{1.5}}{u'_z{}^{0.5}} \quad (7)$$

Where  $Q_I$  is the volumetric flowrate,  $v$  is the kinematic viscosity of the surrounding fluid, and  $d_{\text{pipe}}$  is the inner diameter of the feed pipe,  $U_z$  is the local mean velocity in the z-direction,  $u'_z$  is the root mean square velocities in the z-direction.  $U_z$  and  $u'_z$  can be obtained separately using laser Doppler anemometry (Komrakova et al., 2017). In the case of a froth system, the injection rate is 125 mL/hr at poor mixing conditions and 635 mL/hr at good mixing conditions (Arora, 2016; Saraka, 2017). The demulsifier dispersion step is where mixing parameters of mixing energy and injection concentration of demulsifier vary.

## 2.6 Settling

Once mixing stops, settling begins. The settling time of each experiment is usually 60 minutes to capture all settling behavior of water and solids but settling time can be extended to capture delayed settling behavior. According to previous projects, average-quality froth has a very different settling behavior compared to high-water froth. Most of the settling of water and solids in average-quality froth finishes within the first 10 minutes, so 60 minutes is enough for average-quality froth to finish settling. However, the settling of high-water froth can be delayed up to 40 minutes, so 120 minutes is required for high-water froth in order to capture all possible settling behavior. Since there are no previous experiments performed to study high-solids froth, a combined sampling schedule of average-quality and high-water froth is used for high-solids froth experiments. The sampling schedule for Karl Fischer, microscope, Dean Stark,

and the Focused Beam Reflectance Measurements (FBRM) is shown in Table 2-3. During settling, approximately 1mL fluid is taken at each height by inserting a needle attached to a pipette, which has been silanized by dichlorodimethylsilane, through the septum of each sampling port according to the sampling schedule. Each sample is stored in a 20ml glass vial sealed with a cap, which is covered by aluminum foil inside. These samples are used for both microscope and Karl Fischer analysis.

Table 2-3: Sampling schedule of high-solids froth settling experiment based on the sampling schedule of high-water froth. Table reproduced with permission (Saraka, 2017).

<b>Data Label</b>	<b>Description</b>	<b>Collection Method</b>	<b>Location</b>	<b>Analysis Techniques</b>	<b>Number of Samples</b>
<b>P</b>	End of pre-mixing	Small spoon	Just below the liquid	KF	1
<b>B</b>	End of naphtha blending	Needle tip and pipette	Z1	KF, Microscope	1
<b>D (0 minutes)</b>	30s before demulsifier dispersion ends	Needle tip and pipette	Z1	KF, Microscope	1
<b>5, 10, 15, 20, 25, 30, 40, 50, 60</b>	During settling	Needle tip and pipette	Z1, Z2 Z3, Z4	KF (all heights), Microscope (all heights)	36
<b>DS-1, DS-5, DS-9</b>	End of settling	100 mL syringe and plastic tubing	At z/H = 0.1, 0.5, 0.9	Dean Stark	3
<b>FBRM</b>	From naphtha blending to end	Probe	Below feed tube		1

## 2.7 Microscope Slides

Microscope slides are made first for all collected samples prior to starting any Karl Fischer tests. The glass sample vial is first tilted slightly and shaken by hand gently to help micro-mix the fluid inside. A plastic dropper is used to get around 0.5mL fluid. One or two drops are then deposited onto a silanized microscope slide, which is 75mm in length and 25mm in width. A cover slip, which is not silanized, is gently put onto the fluid. This microscope slide is then put under the microscope to capture images at different locations by sweeping the microscope evenly across the slide. More images are taken at locations when targeted water structures are observed, such as water flocs. For each microscope slide, there are approximately 15 images taken for 10x, which gives an overview of the slide, and 50 images taken for 40x, which gives more detail in specific locations.

## 2.8 Karl Fischer

The Karl Fischer equipment in the lab can detect a small amount of water in samples with high accuracy. In order to obtain high accuracy for samples containing a great amount of water, all samples are first diluted with unisol, which consists of high-grade toluene and isopropanol with a 3:1 ratio by volume. Every sample is titrated three times by the equipment if a small standard deviation (<10%) of back-calculated water contents for the fluid sample is calculated. If a high Karl Fischer value of greater than 800 is returned, the sample should be further diluted by unisol until a Karl Fischer value is smaller than 500. The detail of procedures for unisol preparation and Karl Fischer titration can be found in Appendix B.3.

## 2.9 Dean Stark

Plastic tubes are cut at three different lengths: 58mm, 150mm and 242mm, and are attached to three 100mL glass syringes by duct tape. At the end of settling, a 100mL sample is collected at relative heights of 0.1, 0.5 and 0.9 based on the top of liquid for each corresponding glass syringe with plastic tube attached. Samples are refrigerated to prevent aging effects and sent for analysis using the Dean Stark method of extraction to determine the levels of oil, water, and solids (OWS) of the fluid across the vessel after settling.

## 2.10 Focused-Beam Reflectance Measurements

The focused-beam reflectance measurement (FBRM) probe is inserted into the vessel to track the chord length of a particle, a drop, or an aggregate of an in-situ and dynamic system. The FBRM probe emits a laser beam, passing through particles, receiving backscattered lights and interpreting as the chord length distribution vs. time (Mettler Toledo, 2011a).

Figure 2-5 shows that different shapes of particles, drops and aggregates result in different amounts of backscattered light. These signals are then interpreted by the FBRM software as Chord Length Distribution by the multiplication of the beam circulating velocity at 2m/s, and the time interval over which the backscattered light is elevated (Mettler Toledo, 2011a).

Objects such as particles, drops and aggregates with any shape or size can be detected if they have a different refractive index than the continuous phase (Mettler Toledo, 2011a).

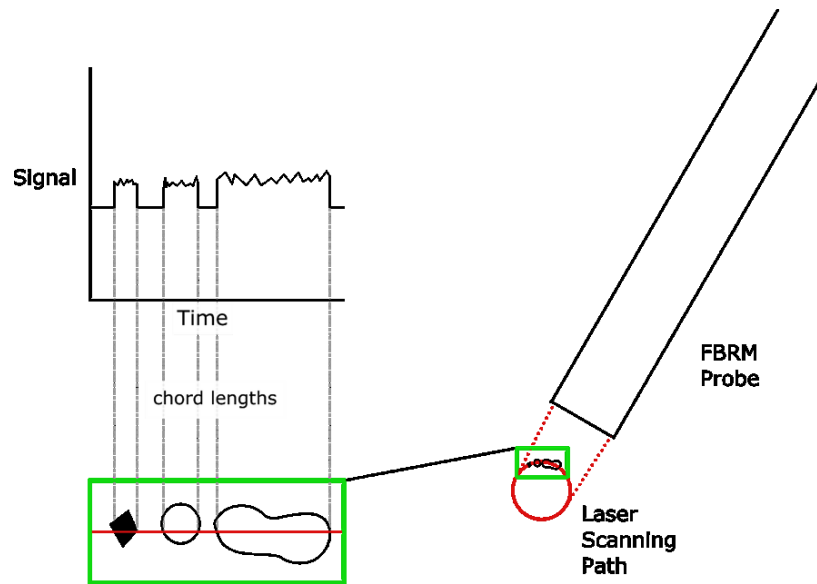


Figure 2-5: Schematic demonstration of the FBRM probe operating principle: the probe emits a laser and receives the backscattered light as signal when the laser passes through an object; the chord length of an object is obtained through the multiplication of time interval where signal changes with laser velocity (Mettler Toledo, 2011b).

# Chapter 3: The Design of Research Campaigns and Their Objectives

There are three research campaigns in this thesis project. The first campaign investigated whether the settling behavior of high-water froth could be simulated using high-solids froth with additional process water, which was collected in the pilot plant. The second campaign was to find the sufficient bulk concentration of demulsifier to add to high-solids froth for the study of mixing effects. In the third campaign, a full factorial design of experiments was performed to understand the settling behavior of high-solids froth at the sufficient bulk concentration of demulsifier. In the end, the settling behavior was compared through Karl Fischer titrations, Dean Stark analysis, microscope images and chord length distributions to further understand mixing effects on each froth. The Karl Fischer data for all three campaigns is summarized in Chapter 4. The chord length distribution of the third campaign is discussed in Chapter 5. Finally, microscope images of all three froths were compared using qualitative and quantitative methods in Chapter 6.

## 3.1 Simulating High-Water Froth Settling Behavior

The observation of induction time in high-water froth in a previous research project (Saraka, 2017) is of great interest for further study since it affects equipment design and operating conditions. For this project, high-solids froth was obtained from the industry partner. The first goal of this campaign was to evaluate whether the settling behavior of high-water froth could be simulated using high-solids samples by simply adding process water to change the composition of the froth. The settling behavior of this simulated high-water froth was compared with high-water froth at the same bulk concentration of demulsifier using water contents (Karl Fischer titrations) measured at height Z1 during settling. The major observation, which is discussed in Chapter 4.1, is that the settling behavior of high-water froth could not be simulated using high-solids froth diluted with process water. At this point, the focus of this

thesis project shifted to study the settling behavior of high-solids froth as an independent type of froth.

### 3.2 Determining the Sufficient Bulk Concentration of Demulsifier in High-Solids Froth for the Study of Mixing Effects

The goal of the second research campaign was to determine the sufficient bulk concentration of demulsifier in high-solids froth. The sufficient bulk concentration was chosen through comparing the final water contents at height Z1 (the product layer) at varying bulk concentrations of demulsifier. There were two major observations: 60 minutes was enough to perform experiments to study mixing effects; and 100 ppm was set as the sufficient bulk concentration. In addition, the effect of increasing bulk concentration was not significant when the concentration increased beyond the sufficient concentration. Based on these observations, which are discussed in more detail in Chapter 4.2, the factorial design in the third campaign of the project shifted to focus on the effect of bulk concentration at the lower end: a low concentration of 35 ppm (a typical plant scale concentration) was contrasted with 100 ppm, the sufficient concentration measured in the lab.

### 3.3 Mixing Effects on High-Solids Froth Settling Behavior

The goal of this campaign was to investigate the relative effects of mixing energy and the bulk concentration of demulsifier on the removal of water in high-solids froth through a two-factor, two-level factorial design of experiments. The two factors studied include the bulk concentration of demulsifier at the lower end and mixing energy. The effect of injection concentration was proven to enhance demulsifier function by preventing a formation of feed plume in previous studies (Arora, 2016; Chong, 2013; Saraka, 2017), so it was not investigated in this work. The Karl Fischer data of height Z1 to Z4 is discussed in Chapter 4.3. The chord length distribution of each experiment in this campaign is discussed in Chapter 5. The microscopic images are discussed in Chapter 6.



# Chapter 4 High-Solids Froth Mixing Experiments

This chapter discusses the results of experiments which were performed to study the behavior of water and solids in high-solids froth. These experiments include attempts to simulate high-water froth using high-solids froth and process water, to determine a sufficient bulk concentration of demulsifier (BC), and to study the effect of mixing and bulk concentration on separation. It is shown that high-solids froth is different than average-quality and high-water froth and that froths with different qualities separate differently.

Figure 4-1 summarizes one of the key results and shows that high-water froth has the longest induction time (up to 40 minutes). High-solids froth has a shorter induction time (up to 25 minutes), and rapid settling within the first 10 minutes can be achieved in average-quality froth when mixing conditions are favorable. These differences in separation behavior have implications for processing strategies in the froth treatment plant.

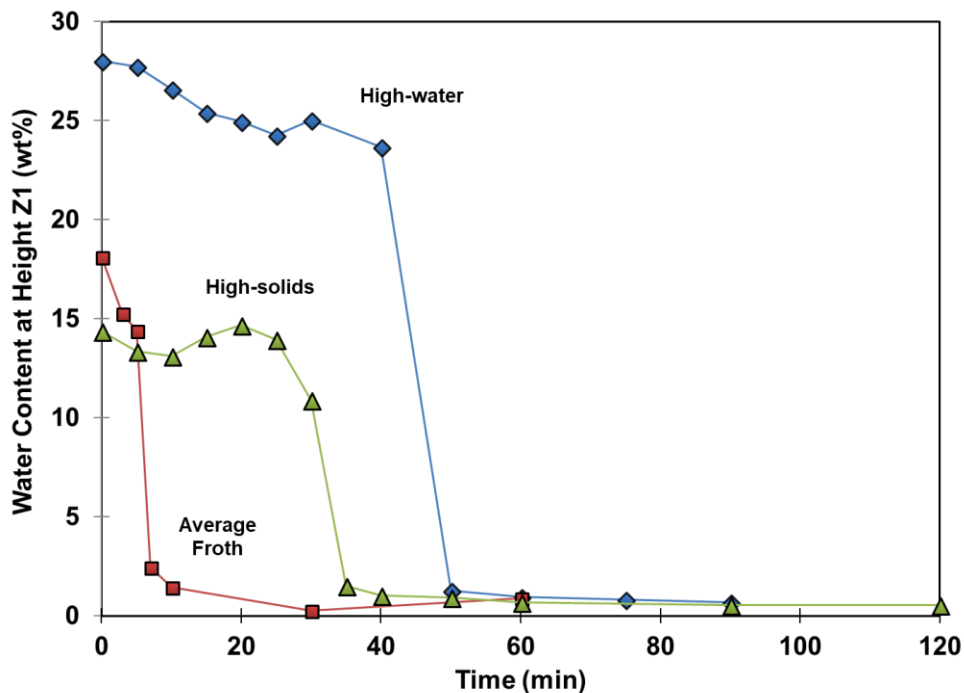


Figure 4-1: Water content at height Z1 (wt%) vs. time (min) for average-quality froth, high-solids froth and high-water froth. Data reproduced with permission (Arora, 2016; Saraka, 2017).

## 4.1 Simulating High-Water Froth Settling Behavior

High-water froth does occur only occasionally in plant operations and was not available at the time of this study, so an attempt was made to simulate it. The simulated high-water froth was made by vigorously mixing high-solids froth with process water.

### 4.1.1 Experimental Method

Process water, which was collected from the pilot plant, and was expected to have the same composition as the water in high-solids froth, was added to high-solids froth during premixing to reach a water content similar to high-water froth. The method used to add process water during premixing was as follows:

- A high-solids froth can was put into the heating bath for at least 2 hours to reach approximately 70°C before premixing started.
- Premixing, as described in Chapter 2.3, was then conducted. After pre-mixing, two froth samples were taken for Karl Fischer titrations: one just below the froth surface and the other one in the middle of the can.
- Process water was slowly added through a funnel beside the shaft.
- Premixing was repeated. Three froth samples were taken for Karl Fischer titrations: one just below the froth surface, one in the middle and the remaining one at the bottom of the can.

The separation behavior of simulated high-solids froth was tested at 200 ppm, the BC which was sufficient to achieve good separation in high-water froth. All experiments were performed

under good mixing conditions: high mixing energy (22778 J/kg) and low injection concentration (12 wt%) of demulsifier in xylene. Samples were taken only at height Z1 for Karl Fischer titrations. The settling time for each experiment was 120 minutes since it was hypothesized that this simulated high-water froth would have the same induction time as high-water froth.

Some initial experiments were performed using the top-sampling vessel. There were many difficulties when using this vessel. Getting samples from the top by hand was not as easy as getting samples from the side, since hands were easily touching the rotating motor on the top and sampling tips could not easily go straight down to the sampling point. The experience of using top sampling vessel reinforced our earlier conclusion (Arora, 2016; Arora et al., 2015) that the side-sampled CIST is easier to use and supports the goal of obtaining repeatable and reproducible mixing data.

#### 4.1.2 Results for simulated high-water froth

Table 4-1 shows the composition of high-water froth from OWS analysis, the original composition of high-solids froth (before adding process water) also from OWS analysis, and the target composition of simulated high-water froth after adding process water (based on a mass balance).

Table 4-1: The composition of high-water froth and the composition of high-solids froth before adding process water from OWS analysis (Syncrude) and the target composition of simulated high-water froth.

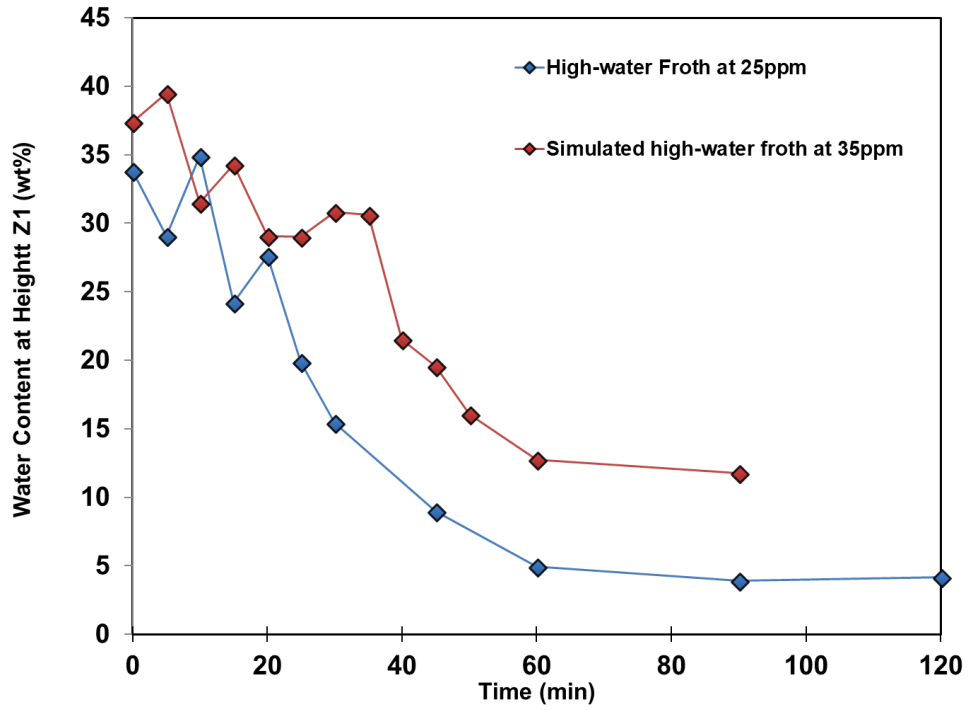
<b>Composition</b>	<b>High-water froth composition from OWS analysis (wt%)</b>	<b>High-solids froth composition from OWS analysis (wt%)</b>	<b>Target composition of Simulated High-Water froth (wt%)</b>
<b>Bitumen</b>	50	54	46.3
<b>Water</b>	37	27	37.3
<b>Solids</b>	13	19	16.3

Table 4-2 shows Karl Fischer data for the same high-solids froth. Since Karl Fischer equipment is more accurate for measuring water content at low concentrations of water, froth samples were diluted with unisol at a mass ratio of unisol to froth of 25 to 30 before measurements were taken. The water contents of both froth samples before adding process water were consistent between the top and middle of the can at 18.5-20.5 wt%. This is significantly lower than the value of 27 wt% obtained from OWS analysis and reported in Table 4-1. We were unable to resolve this discrepancy, even after repeating both the OWS analysis (Syncrude) and the Karl-Fisher titration. As a result of this discrepancy, discovered after the first set of experiments were complete, the actual water content in the simulated high-water froth was quite a bit lower than the target concentration of 37 wt%. After water addition, the water contents are consistent across the can and increase to a range of 26.9-29.6 wt%, excluding an outlier of 20.4 wt%.

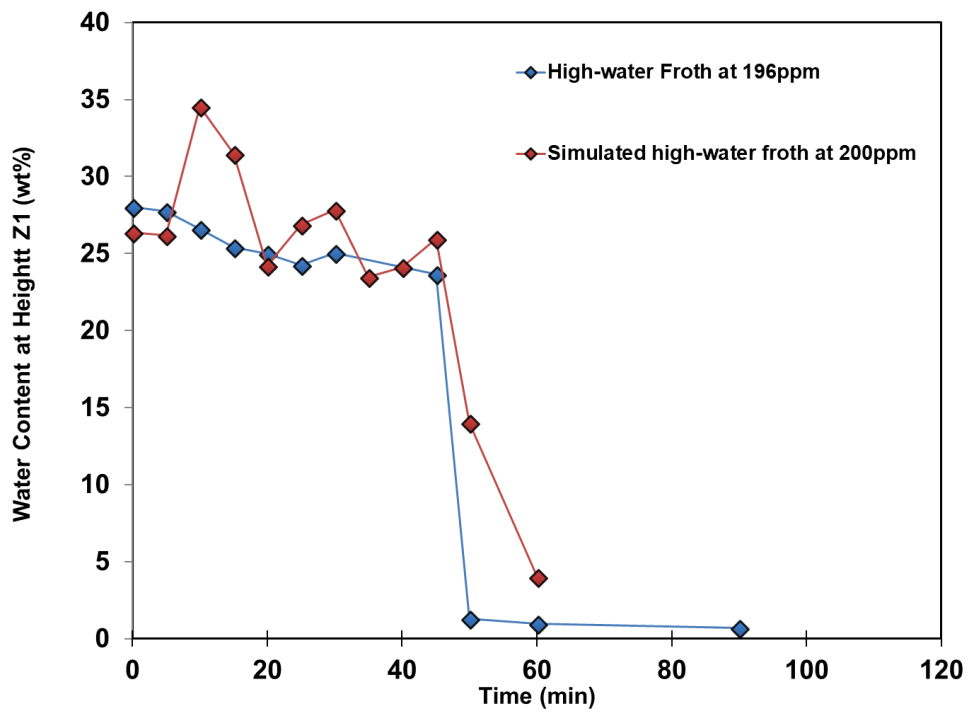
Table 4-2: The water content of high-solids froth samples, measured using Karl Fischer titration, before and after adding process water prior to starting experiments, compared to the original water content of high-solid as provided by industry.

Water Content		KF (wt%) Sample 1 (35ppm)	KF (wt%) Sample 2 (200ppm)	Expected water content (wt%)
<b>Before adding water</b>	Top	18.52	17.52	Measured by Syn crude
	Middle	18.49	20.49	
	Average	18.51	19.01	27 wt%
<b>After adding water</b>	Top	28.17	29.64	Target water content
	Middle	29.47	20.40	
	Bottom	28.85	26.85	
	Average	28.83	25.63	30 wt%

Figure 4-2 compares the drop in water content vs. time in the simulated and original high-water froth. Figure 4-2a shows the results for 35 ppm demulsifier. Figure 4-2b the results at 200 ppm demulsifier. Both samples follow a similar trend, with the expected higher water content in the high-water froth. The 200 ppm case has an induction time of approximately 40 minutes, mimicking the high-water froth. Based in this first test, the simulated high-solids froth was successful. The full Karl Fischer data set is given in Appendix B.1.



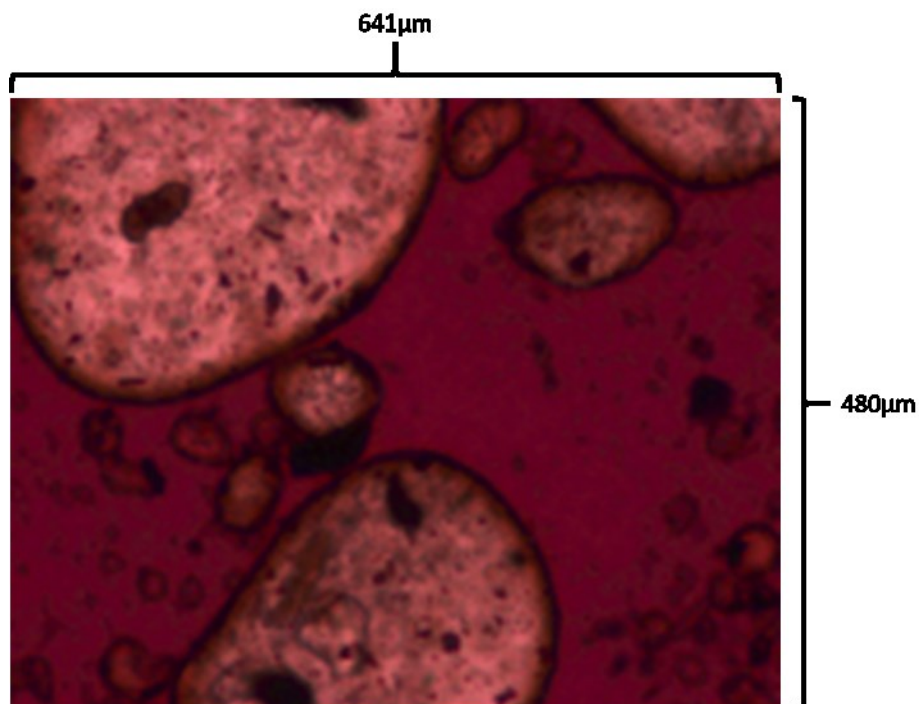
(a)



(b)

Figure 4-2: Water content (wt%) at Z1 vs. time (min) for high-water froth and simulated high-water froth at similar dosages of demulsifier under good mixing conditions (high J and low IC): (a) high-water froth at 25ppm vs. simulated high-water froth at 35ppm; (b) high-water froth at 196ppm vs. simulated high-water froth at 200ppm. High water froth data is reproduced with permission (Saraka, 2017).

In a second test, the water structures in the simulated froth were compared to the original high-water froth. Figure 4-3 compares microscope images of the high-water and simulated high-water froth. Figure 4-3a shows that large, irregularly shaped free water drops are present in the high-water froth. By contrast, Figure 4-3b shows only small spherical water drops in the simulated high-water froth. Although similar induction times and dewatering curves were observed in both high-water and simulated high-water froth at similarly doses of demulsifier, the resulting water structures were quite different. Since part of the goal of this project is to observe the structures in the froth as separation proceeds, the attempt to simulate high-water froth was deemed to be a failure and the research shifted to a new direction. High-solids froth is now identified as another type of poor quality froth, and the focus of the project was altered to a more direct comparison of the two types of froth.



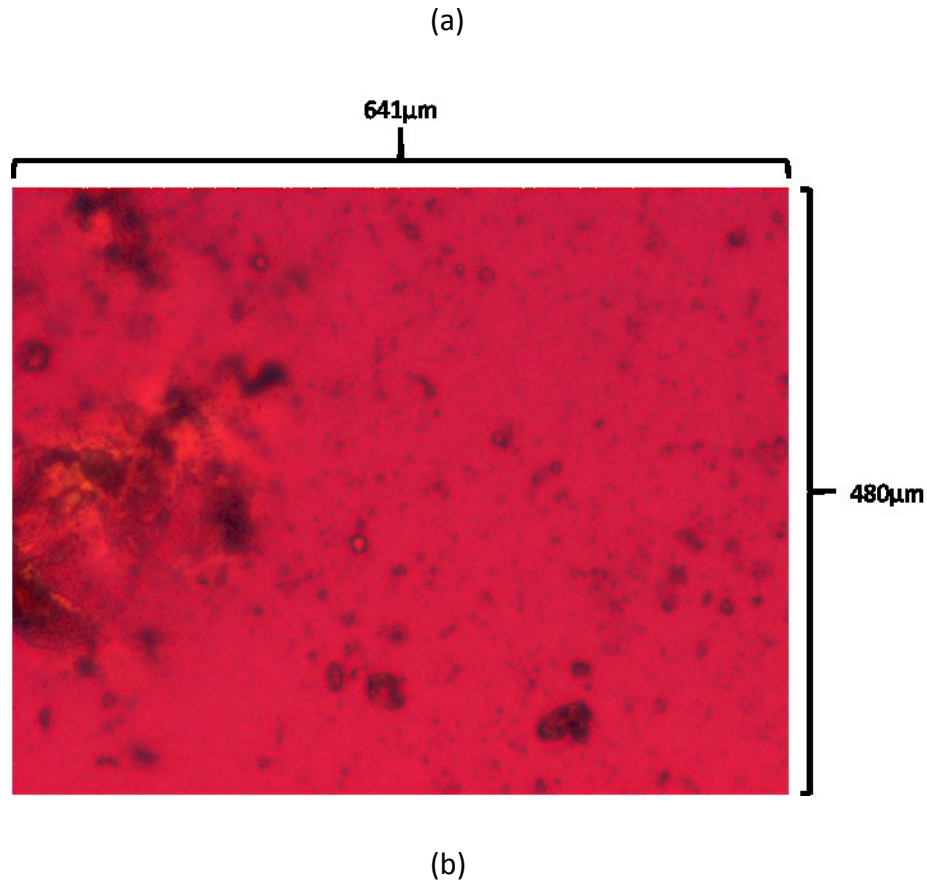


Figure 4-3: 10x microscope images of froth at height Z1 after 25 minutes of settling: (a) high-water froth and (b) simulated high-water froth.

## 4.2 Determining Sufficient Bulk Concentration of Demulsifier

When studying a new type of froth, the sufficient bulk concentration (BC) of demulsifier, which is the minimal acceptable dosage of demulsifier which leads to good dewatering performance under good mixing conditions, has to be first determined. The concentration of demulsifier has to be well below the overdosing limit, and also below the point where the demulsifier concentration overwhelms all other effects. The minimum dose which gives good separation gives the point at or below which mixing effects should be evident.



### 4.2.1 Experimental Method

Since high-solids froth was identified as a new type of poor quality froth, no information is available to set the starting point to determine the sufficient BC. In previous studies, average-quality froth had a sufficient BC of 150 ppm (Arora, 2016), and high-water froth had a sufficient BC of 200 ppm (Saraka, 2017). The high-solids froth was initially expected to require the lowest BC because it had the lowest amount of water present among three froths. However, since the presence of additional solids can also affect settling efficiency, 175 ppm was set as the starting point in this campaign.

The sufficient BC was tested from 175 ppm, and through 150 ppm, 125 ppm, 100 ppm, 75 ppm reducing the level by 25 ppm at each step. 35 ppm was also added as a lower limit. All bulk concentrations are the weight percent: the active ingredient in the demulsifier as a percentage of the total weight of naphtha and froth. Under this definition, 35 ppm is equivalent to 50 ppm of demulsifier based on the froth weight alone. Both definitions are used in the literature, so it is important to carefully define the basis for the concentration.

All experiments were performed under good mixing conditions: high mixing energy (22778 J/kg) and low injection concentration (12 wt%) of demulsifier. In the experiments used to determine the sufficient concentration, no experiments were performed under poor mixing conditions. The N:B ratio was kept at 0.7 mass/mass as in previous studies (Arora, 2016; Chong, 2013; Saraka, 2017). However, this ratio is known to contain small errors due to the difficulty of transferring hot bitumen and hot naphtha, completely emptying froth cans, small spill losses of bitumen and naphtha during operations, the difficulty of precisely controlling the fill height in the CIST, and the different amounts of froths initially contained in froth cans. The N:B ratio values are measured directly and reported with the experimental results.

The settling time of each experiment was 120 minutes in order to fully capture the settling behavior in high-solids froth. The water content at height Z1 during settling for each

experiment was measured by Karl Fischer titrations. An separation of 1 wt % of water content after 60 minutes of settling is set as acceptable performance.

#### 4.2.2 Bulk Concentration vs. Final Water Content

Table 4-3 summarizes the operating conditions and water content at height Z1 after 60 and 120 minutes of settling. The complete Karl Fischer data is given in Appendix B.2. Experiments with an N:B ratio higher than 0.7 were excluded since additional naphtha leads to a lower density and viscosity and more liberated hydrocarbon components of bitumen, resulting in a better separation. The water content after 60 minutes of settling at 125 ppm also seems to be an outlier since all other experiments above 35 ppm show adequate settling with a final water content lower than 1 wt%.

Table 4-3: The operating conditions and water contents at height Z1 after 60 and 120 minutes of settling for each experiment to determine the sufficient bulk concentration of demulsifier in high-solids froth.

<b>BC</b>	<b>N:B ratio</b>	<b>Demulsifier (mL)</b>	<b>60 minutes (wt%)</b>	<b>120 minutes (wt%)</b>
<b>0 ppm</b>	0.78	0	19.11	12.29
<b>35 ppm</b>	0.69	0.4	2.69	1.71
<b>75 ppm</b>	0.76	0.8	0.85	0.69
<b>100 pm</b>	0.70	1.0	0.38	0.54
<b>125 ppm</b>	0.73	1.3	1.56	0.58
<b>150 ppm</b>	0.67	1.6	0.68	0.54
<b>175 ppm</b>	0.72	1.8	0.39	0.21

The following discussion follows the water content at height Z1 over settling for each BC experiment plotted in Figure 4-4. Time 0 is the baseline of water content, determined using the sample taken at 30 s before the end of demulsifier addition.

Figure 4-4 shows that a small amount of demulsifier (35 ppm) reduces water content significantly, and the desired threshold of <1 wt% final water is first achieved at 75 ppm. In addition, water content at BCs of 75 ppm, 100 ppm, 125 ppm, 150 ppm, and 175 ppm show little difference during settling, particularly between 40 minutes and 120 minutes. This suggests that the effect of bulk concentration at higher end is not very significant. Although the BC of 75 ppm contributes to the highest final water content, which is still below 1 wt%, the N:B ratio for this run is slightly higher than 0.7. Hence, a BC of 100 ppm with the optimal N:B ratio of 0.70 was set as the sufficient BC in high-solids froth.

60 minutes is also enough for high-solids froth to finish settling since little difference is observed in water content after 60 minutes of settling compared to 120 minutes of settling.

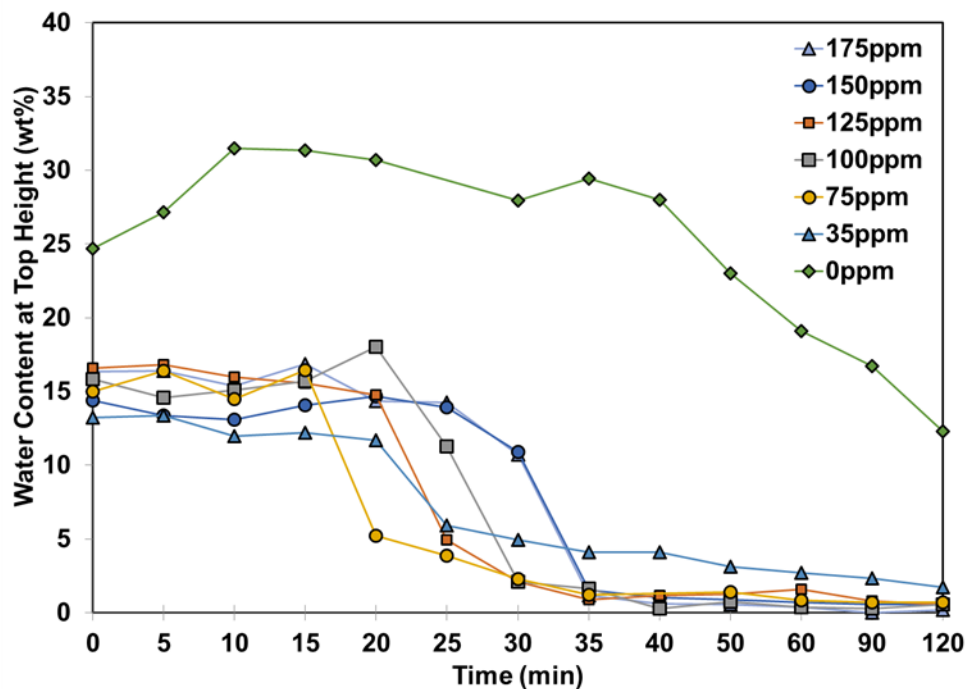


Figure 4-4: Effect of the demulsifier dosage on the water removal on high-solids froth. Results are shown in terms of water content at height Z1 (wt%) vs. time (min). All experiments were carried out at N:B ratio of close to 0.7 under good mixing conditions (high J and low IC). A demulsifier dosage of 100 ppm was set as the sufficient BC, which was

required to obtain a final water content of lower than 1 wt% after 60 minutes of settling. Some obvious outliers (maximum of 2 per curve) were removed from data.

Figure 4-5 shows the water content (wt%) at height Z1 during settling for each BC experiment with high-water froth for comparison. The sufficient BC in high-water froth was 196 ppm and rounded up to 200 ppm, and 120 minutes was required for settling (Saraka, 2017). Compared to high-solids froth, there was a significant difference in water content at different BC levels between 40 minutes and 120 minutes. This suggests that the effect of bulk concentration at the higher end is significant for high-water froth, which is the opposite to what was observed in high-solids froth.

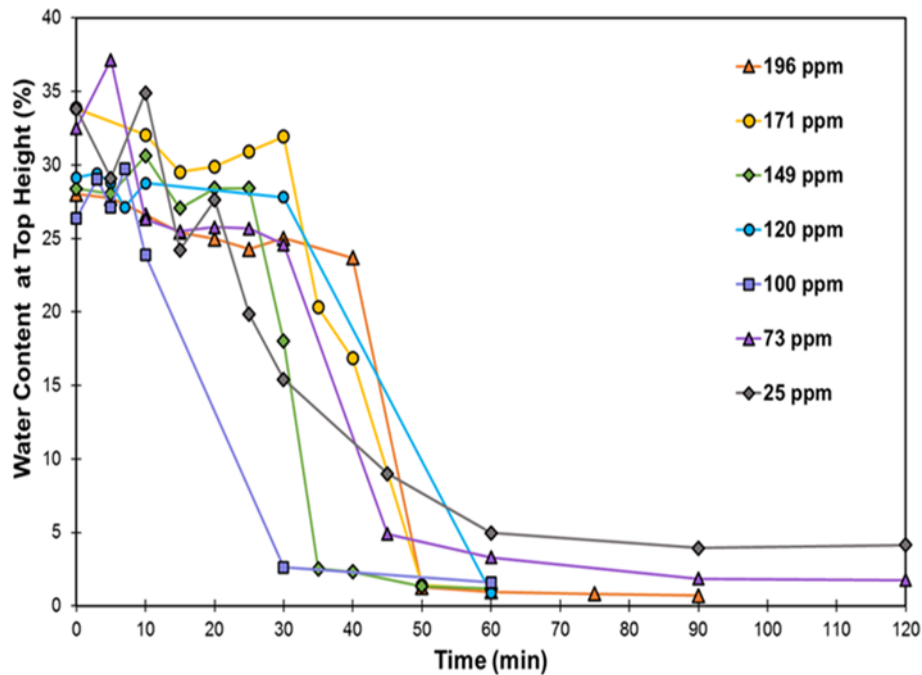


Figure 4-5: Effect of the demulsifier dosage on the water removal on high-water froth. Results are shown in terms of water content at height Z1 (wt%) vs. time (min). All experiments were carried out at N:B ratio of close to 0.7 under good mixing conditions (high J and low IC). A demulsifier dosage of 196 ppm, rounded up to 200 ppm, was set as the minimum BC – just sufficient to obtain a final water content of lower than 1 wt% after 120 minutes of settling (Saraka, 2017).

In Figure 4-6 the final water content (wt%) at Z1 after 60 minutes of settling is plotted against the corresponding bulk concentration for both high-water and high-solids froth. In this figure, a linear trend was observed in high-water froth (Saraka, 2017). By contrast, a trend was hard to distinguish in high-solids froth. Overall, the effect of BC on final water contents varies in different froths.

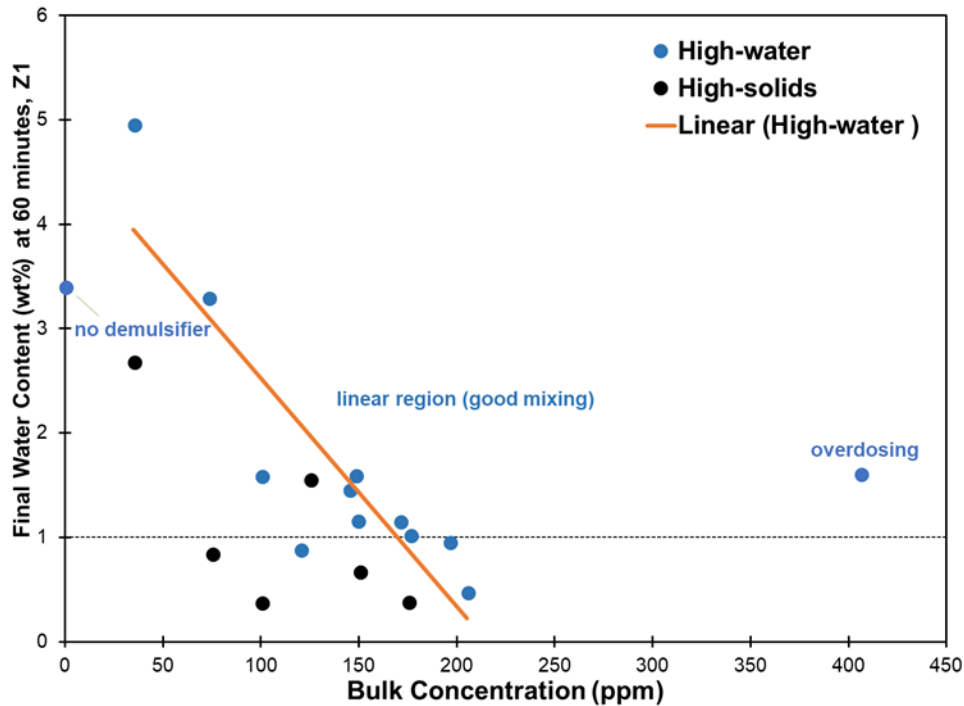


Figure 4-6: Final water content at Z1 (wt%) after 60 minutes of settling vs. various demulsifier bulk concentrations (ppm). A linear trend was observed in high-water froth. A clear trend was hard to distinguish in high-solids froth. Data reproduced with permission (Saraka, 2017).

Through comparing the settling behavior in high-water and high-solids froth based on Figure 4-4 and 4-5, it seems that high-solids froth has similar settling behavior to high-water froth. Figure 4-7 directly compares the settling curves of high-water, high-solids and average-quality froth. In this figure, high-water and high-solids froth have a very different settling behavior compared to average-quality froth. In a previous study of high-water froth, three stages of settling were identified including induction time (up to 40 minutes) where no or slow settling

occurs, fast settling where a rapid settling occurs after induction time and slow settling where water content goes to the lowest level (Saraka, 2017). In this campaign, the settling of water in high-solids froth has the same three stages but with a shorter induction time (up to 25 minutes). By contrast, most of the settling finishes within the first 10 minutes in average-quality froth (Arora, 2016; Saraka, 2017).

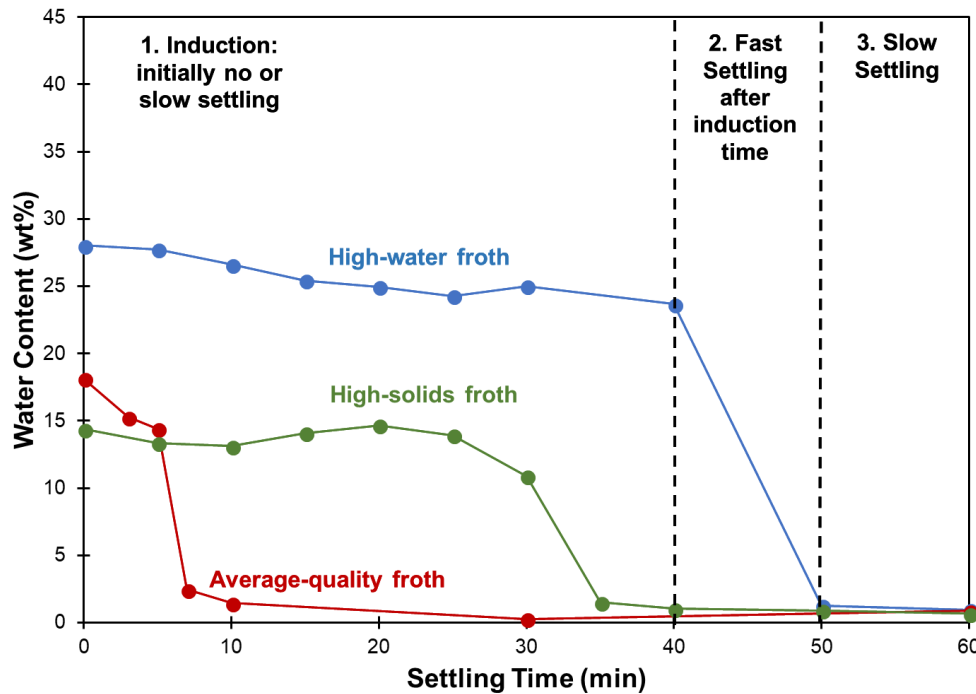


Figure 4-7: Comparison of settling profiles for high-water froth, high-solids froth and average-quality froth. The high-water froth experiment was run at BC = 196 ppm. The high-solids froth experiment was run at BC = 150 ppm. The average-quality froth was run at BC = 150 ppm. Experiments were run under good mixing conditions (high J and low IC). Three settling stages were observed in both the settling process of high-water and high-solids froth: induction time, fast settling and slow settling. Water settling was considerably faster in average-quality froth since most of the separation finishes within the first 10 minutes. Data reproduced with permission (Arora, 2016; Saraka, 2017).

The induction time observed for both the high-water and high-solids froth is undesirable, and it is hypothesized that the presence of induction time can be attributed to the composition of each froth.

Table 4-4 summarizes the composition of each froth, which helps further analyze the settling behavior of each froth. If the composition and the settling behavior of average-quality froth is set as a benchmark, high-water froth has a higher amount of solids by 3 wt% and a higher amount of water by 7 wt%. This produces an induction time of up to 40 minutes. Compared to average-quality froth, high-solids froth has a lower amount of water by 3 wt% but a higher amount of solids by 9 wt% and an induction time of up to 25 minutes. Neglecting any effects due to the change of bitumen content, the effect of extra water on induction time is more significant than the effect of extra solids, since 7 wt% additional water leads to an induction time of up to 40 minutes vs. 9 wt% additional solids leads to an induction time of up to 25 minutes. In addition, the doubled settling time (120 minutes) required in high-water froth compared to the settling time (60 minutes) in high-solids froth reinforces that the effect of extra water is more profound than the effect of extra solids on froth settling.

Table 4-4: The composition of each froth as provided by OWS analysis (Syncrude).

Composition (wt%)	Average-quality froth	High-water froth	High-solids froth
Bitumen	60	50	54
Water	30	37	27
Froth	10	13	19

To summarize what was achieved in this campaign, 100 ppm was set as the sufficient BC in high-solids froth. An induction time of up to 25 minutes was observed during the settling of high-solids froth. However, since the effect of BC at higher end (>75 ppm) is not so significant, the focus of the experiments in the next campaign study the effect of mixing in high-solids froth when the BC is varied from 35 ppm and 100 ppm. Another reason for this change is that low IC has been proven in industry to help settling by preventing the formation of a feed plume when

demulsifier is added. The effect of IC was also well-established in previous studies on diluted bitumen, average-quality froth and high-water froth (Arora, 2016; Chong, 2013; Laplante, 2011; Saraka, 2017). Hence, IC is not studied again in the next campaign. Mixing energy (J) is still of great interest to study.

### 4.3 Factorial Design

The sufficient bulk concentration in high-solids froth was set at 100ppm. A factorial design, which is two-factor, two-level and two-replicate with one centerpoint (Montgomery and Runger, 2011), was designed to study the effect of bulk concentration and mixing energy on the settling behavior of water and solids in high-solids froth. All Karl Fischer data can be found in Appendix B.3.

#### 4.3.1 Experiment Method

Table 4-5 shows the level of each factor: mixing energy (J) and bulk concentration of demulsifier (BC). The injection concentration of demulsifier is 12wt% in xylene in all experiments. Each experiment is 60 minutes long.

Table 4-5: The level of each variable for factorial design.

Variable Level (X)	-1	0	1
J (J/kg)	425	11601	22778
BC (ppm)	35	67.5	100

The levels of these two factors,  $X_{BC}$  and  $X_J$ , can be related to the variables BC and J by Equation 8 and 9:

$$BC \approx 67\text{ppm} + X_{BC} \times 33\text{ppm} \quad (8)$$



$$J \approx 11602 \frac{J}{\text{kg}} + X_J \times 11176 \frac{J}{\text{kg}} \quad (9)$$

Table 4-6 shows that there were  $2 \times 2^2 + 1 = 9$  experiments performed (Montgomery and Runger, 2011). Experiments were randomised before starting as in previous study (Arora, 2016; Saraka, 2017). Experimental detail of each experiment can be found in Appendix A.1. Samples were taken for Karl Fischer titrations from height Z1 to Z4 according to the sampling schedule described in Chapter 2.8.

Table 4-6: The level of each factor for each high-solids froth experiment

Experiment Code	$X_{BC}$	$X_J$
HA-1	-	-
HC-1	+	-
HD-1	-	+
HB-1	+	+
CP-1	0	0
HD-2	-	+
HA-2	-	-
HB-2	+	+
HC-2	+	-

### 4.3.2 Water Content at Height Z1

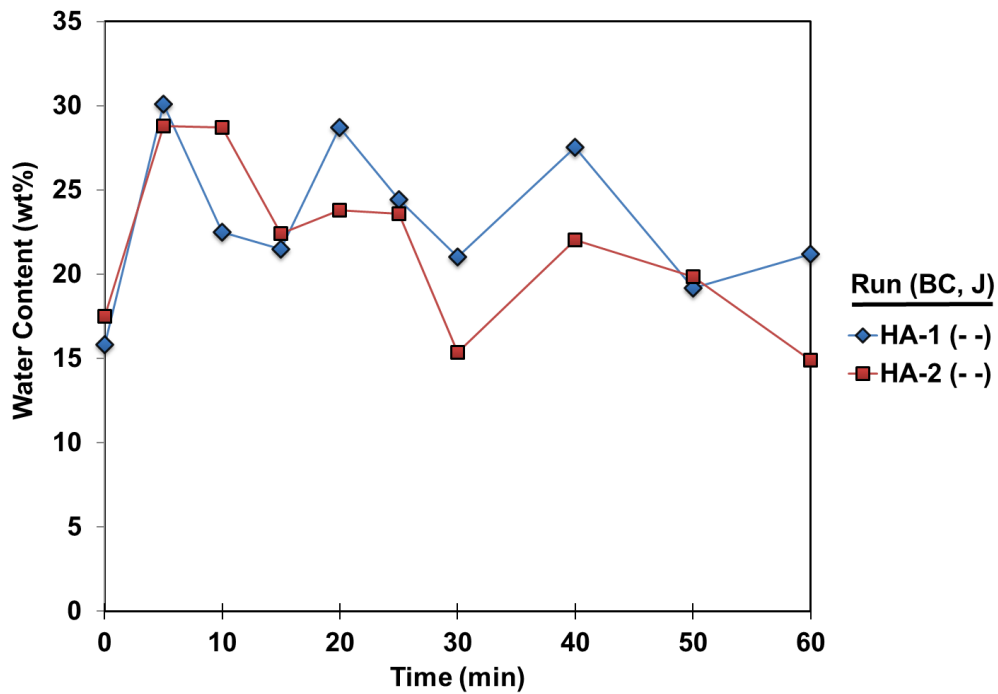


Figure 4-8: Comparison of two replicates run at low BC (35 ppm) and low J (425 J/kg) in terms of water content (wt%) at height Z1 vs. settling time (min). Experiments were run with high-solids (HS) froth at the fixed IC = 12 wt%.

Figure 4-8 shows that water contents at height Z1 vs. time follow a similar trend in two replicates of experiments under low BC and low J operating conditions. Since the other operating conditions showed similar behavior, the averaged water contents of two replicates are used for the following analysis.

Table 4-7: Water content (wt %) difference at height Z1 of two replicates at each sampling time for different operating conditions including low J and low BC (HA), high J and high BC (HB), high J and low BC (HC) and low J and high BC (HD).

Operating Condition	Absolute Value of Water Content (wt %) Difference at Height Z1									
	0 min	5 min	10 min	15 min	20 min	25 min	30 min	40 min	50 min	60 min
Settling Time										
Delta (HA)	1.66	1.33	6.20	0.93	4.91	0.80	5.68	5.49	0.70	6.27
Delta (HB)	0.09	3.95	4.70	2.39	2.19	1.35	1.92	2.83	0.70	1.69
Delta (HC)	1.63	12.97	2.90	4.24	1.49	2.70	1.45	4.83	1.70	3.88
Delta (HD)	4.44	10.27	0.80	5.36	4.59	1.60	1.47	6.58	1.11	4.50
								Average	Variance	S.D.
								3.36	7.19	2.68

In order to further characterize the water content difference, the differences of two replicates during settling at each height are first calculated. The absolute values are used to calculate the average to eliminate the effect of minus sign. The standard deviation of the water content difference at height Z1 can be obtained using Equation 10.

$$\sigma = \sqrt{\frac{(x-\mu)^2}{N-1}} \quad (10)$$

where  $\sigma$  is the standard deviation, N is the number of data points and  $\mu$  is the average. Table 4-7 shows all the absolute value of water content difference at height Z1 and the standard deviation at the top height is 2.68. This standard deviation is bit high, but still acceptable. The same calculations are performed at other heights.

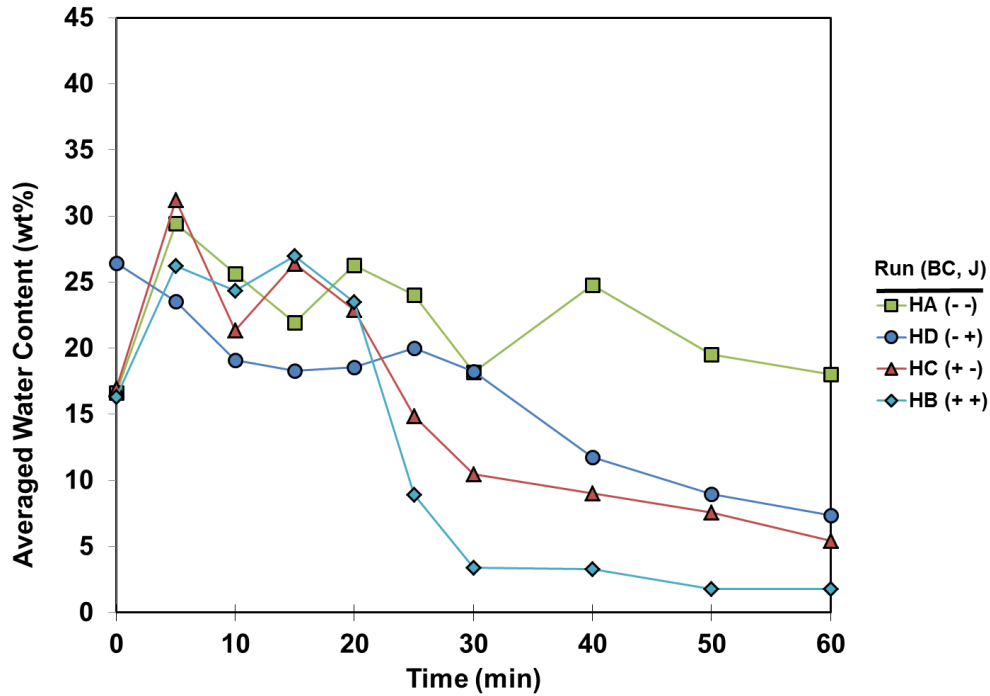


Figure 4-9: Comparison of four operating conditions including low BC and low J, low BC and high J, high BC and low J and high BC and high J in terms of averaged water content (wt%) at height Z1 vs. time (min). Experiments were run with high-solids froth at the fixed IC = 12wt%.

Figure 4-9 shows that the optimal operating condition of high BC and high J results in the lowest amount of water at height Z1, which is below 5wt%. By contrast, the worst operating condition of low BC and low J lead to the highest amount of water at height Z1, which is above 15wt%. In addition, little difference in final water content is observed between high BC and low J, and low BC and high J, which means the effect of BC can be balanced by the effect of J to some extent. Overall, an induction time of up to 25 minutes at height Z1 is observed without considering the worst condition: low BC and low J.

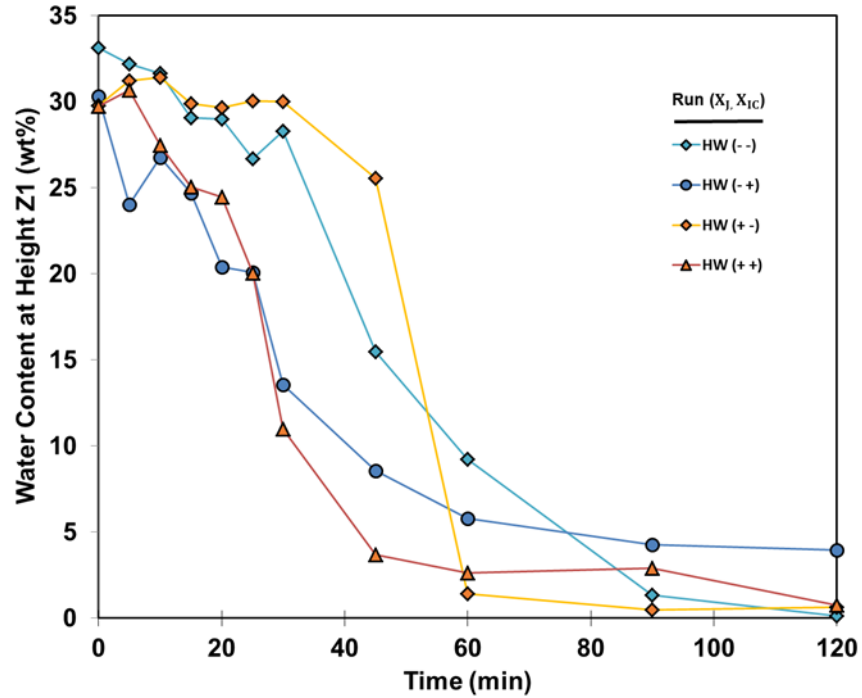


Figure 4-10: Comparison of four mixing conditions including low J and low IC, low J and high IC, high J and low IC and high J and high IC in terms of averaged water content (wt%) at height Z1 vs. settling time (min). Experiments were run with high-water froth (HW) at the sufficient BC = 200 ppm. Data reproduced with permission (Saraka, 2017).

Figure 4-10 shows that the induction time in high-water froth at height Z1 can be up to 40 minutes and that the effects of mixing follow a similar trend.

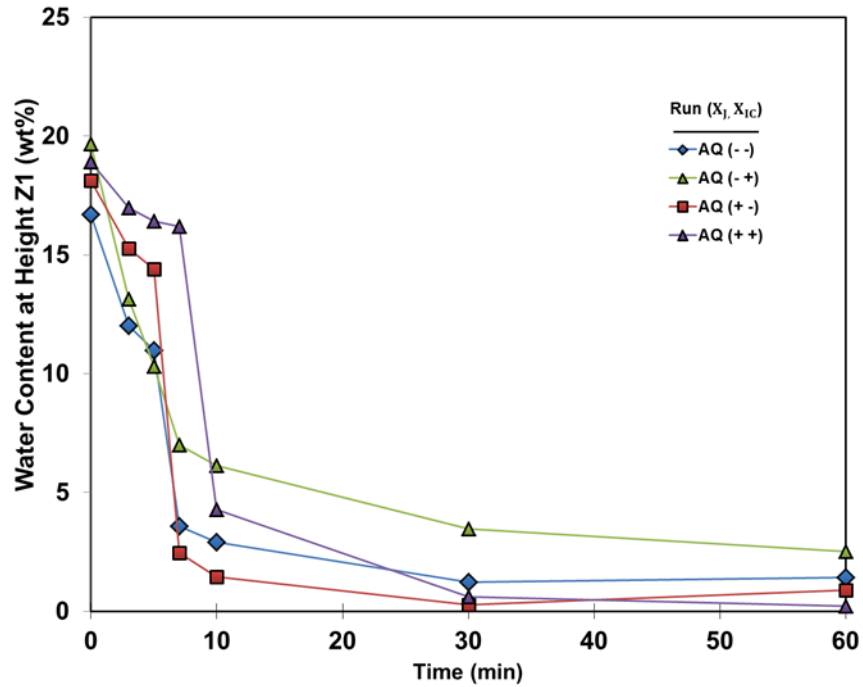


Figure 4-11: Comparison of four mixing conditions including low J and low IC, low J and high IC, high J and low IC and high J and high IC in terms of averaged water content (wt%) at height Z1 vs. time (min). Experiments were run with average-quality (AQ) froth at the sufficient BC = 150 ppm. Data reproduced with permission (Arora, 2016).

Figure 4-11 shows that most of the water and solids in average quality froth at height Z1 settle within the first 10 minutes with little or no induction time before dewatering starts.

### 4.3.3 Water Content at Height Z2

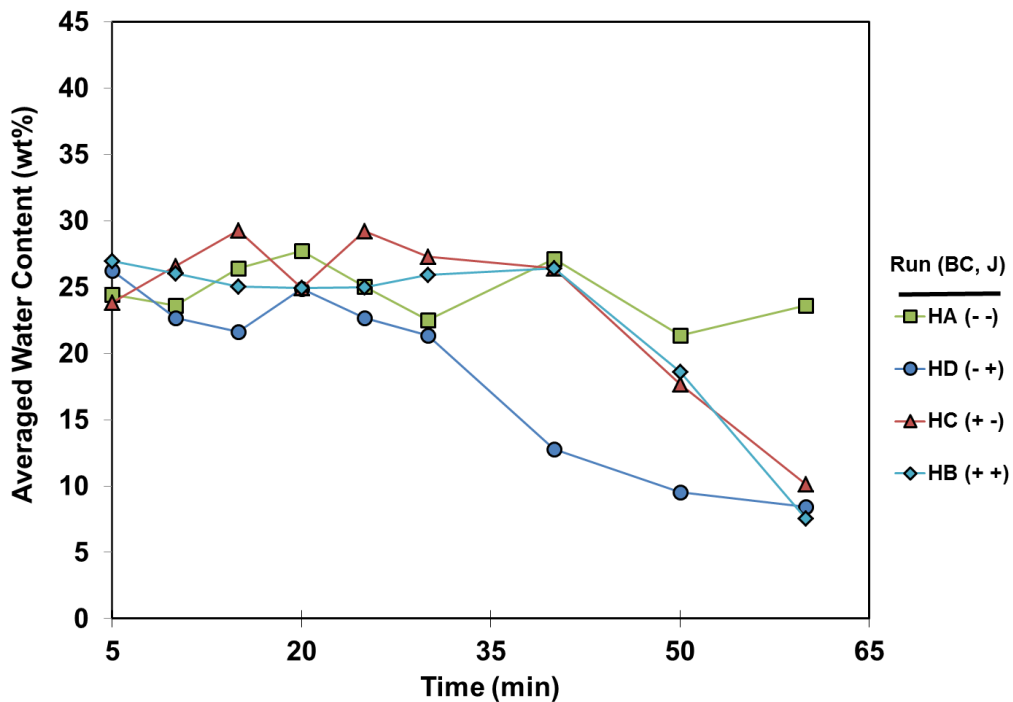


Figure 4-12: Comparison of four operating conditions including low BC and low J, low BC and high J, high BC and low J and high BC and high J in terms of averaged water content (wt%) at height Z2 vs. time (min). Experiments were run with high-solids froth at IC = 12 wt%.

Figure 4-12 shows that there is an induction time at height Z2, which can be up to 40 minutes without considering the condition of low BC and low J. By considering that the induction time at height Z1 can be up to 25 minutes, the extended induction time at height Z2 implies that water slowly settles from height Z1 to height Z2.

Table 4-8: Water content difference (wt%) at height Z2 of two replicates at each sampling time for different operating situations including low J and low BC (HA), high J and high BC (HB), high J and low BC (HC) and low J and high BC (HD).

Operating Conditions	Absolute Value of Water Content (wt %) Difference at Height Z2								
	5 min	10 min	15 min	20 min	25 min	30 min	40 min	50 min	60 min
Delta (HA)	0.44	1.40	4.43	9.30	1.60	6.40	7.92	3.58	4.84
Delta (HB)	2.03	1.90	3.47	0.05	0.60	2.73	3.24	5.83	3.62
Delta (HC)	6.94	1.80	2.92	3.79	1.10	2.51	1.30	8.50	11.97
Delta (HD)	3.35	3.60	1.19	3.07	4.80	5.56	0.49	5.50	6.77
							Average	Variance	S.D.
							3.85	7.63	2.76

Table 4-8 shows all the absolute value of water content difference at height Z2 and the standard deviation is 2.76, which is very close to height Z1.

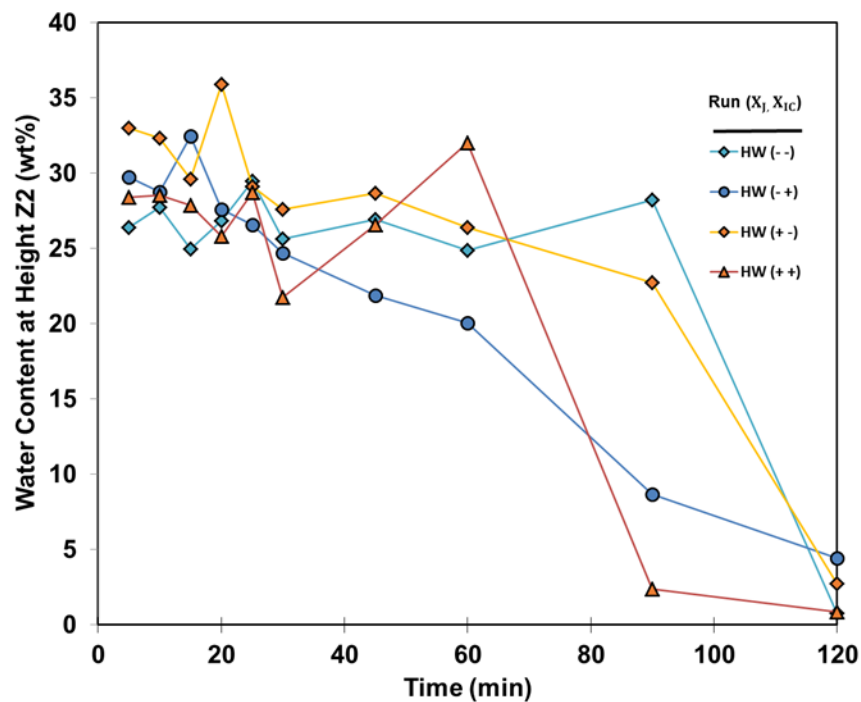




Figure 4-13: Comparison of four mixing conditions including low J and low IC, low J and high IC, high J and low IC and high J and high IC in terms of averaged water content (wt%) at height Z2 vs. time (min). Experiments were run with high-water froth (HW) at sufficient BC = 200 ppm. Data reproduced with permission (Saraka, 2017).

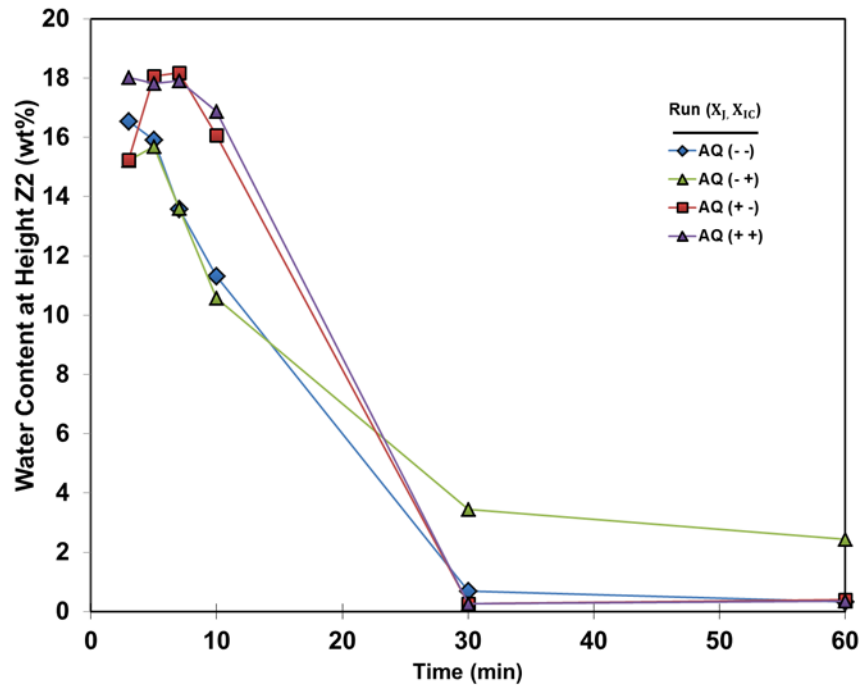


Figure 4-14: Comparison of four mixing conditions including low J and low IC, low J and high IC, high J and low IC and high J and high IC in terms of averaged water content (wt%) at height Z2 vs. time (min). Experiments were run with average-quality froth (AQ) at the sufficient BC = 150 ppm. Data reproduced with permission (Arora, 2016).

Figure 4-13 shows that the water content at height Z2 for high-water froth shows a longer induction time (Saraka, 2017). Figure 4-14 shows that no or a shorter induction time of approximately 5 minutes is observed at height Z2 in average-quality froth, but most of the settling happens within the first 30 minutes, particularly between 10 minutes and 30 minutes. Compared to height Z1, settling at height Z2 is a bit slower in average-quality froth. The induction time at height Z2 in high-water froth implies that water slowly settle from height Z1. The shorter induction time at height Z2 in average-quality froth also implies that water and solids settle out of zone Z1 and into zone Z2.

### 4.3.4 Water Content at Height Z3

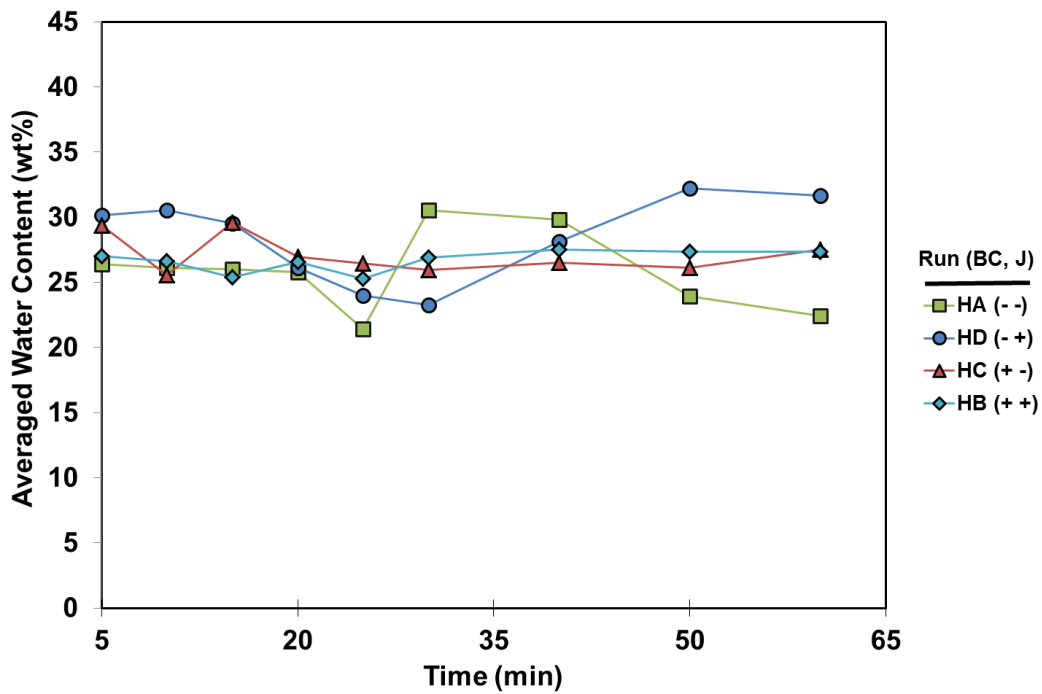


Figure 4-15: Comparison of four operating conditions including low BC and low J, low BC and high J, high BC and low J and high BC and high J in terms of averaged water content (wt%) at height Z3 vs. time (min). Experiments were run with high-solids froth at the fixed IC = 12wt%. Averaged water content at height Z3 (wt%) vs. time (min) for high-solids froth experiments at different operating conditions without the centrepont.

Figure 4-15 shows that there is no significant reduction of water content at height Z3 for any of the four different operating conditions, which means water flow in is equivalent to water flow out. The height Z3 is assumed to be at steady state during settling.

Table 4-9: Water content difference (wt%) at height Z3 of two replicates at each sampling time for different operating situations including low J and low BC (HA), high J and high BC (HB), high J and low BC (HC) and low J and high BC (HD). Outliers are removed.

Operating Conditions	Absolute Value of Water Content (wt %) Difference at Height Z3								
	5 min	10 min	15 min	20 min	25 min	30 min	40 min	50 min	60 min
Delta (HA)	1.92	1.20	2.02	1.01	2.00	NA	0.03	0.52	8.99
Delta (HB)	0.29	1.60	2.06	1.88	6.80	1.25	3.42	1.70	2.37
Delta (HC)	1.07	6.50	8.70	0.04	0.10	4.80	7.28	0.26	4.38
Delta (HD)	6.93	4.30	5.16	3.10	3.00	1.48	10.25	2.45	2.16
							Average	Variance	S.D.
							2.25	7.81	2.80

Table 4-9 shows all the absolute value of water content difference at height Z3 and the standard deviation is 2.80, which is very close to height Z1 and Z2.

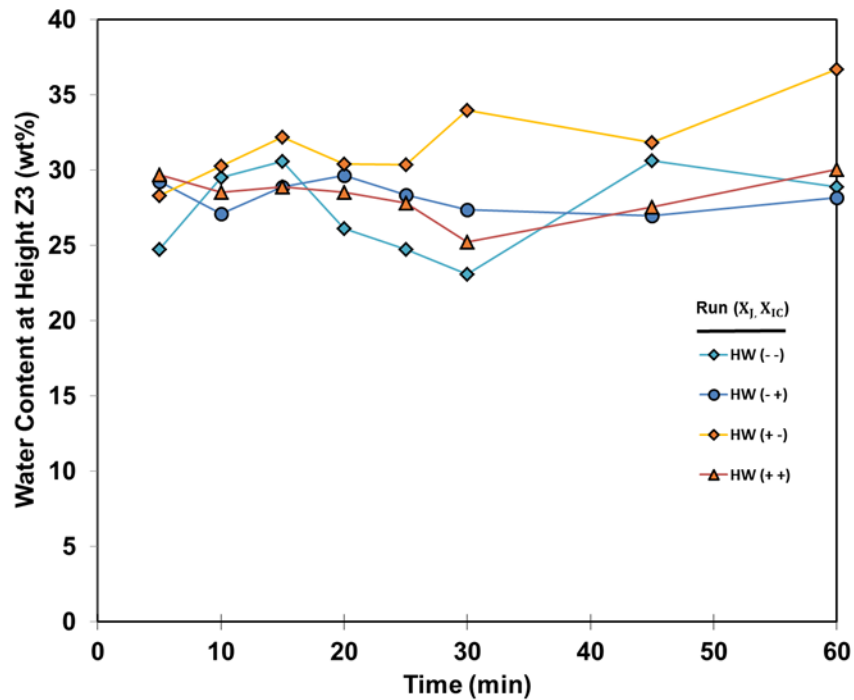


Figure 4-16: Comparison of four mixing conditions including low J and low IC, low J and high IC, high J and low IC and high J and high IC in terms of averaged water content (wt%) at height Z3 vs. time (min). Experiments were run with high-water froth (HW) at the sufficient BC = 200 ppm. Data reproduced with permission (Saraka, 2017).

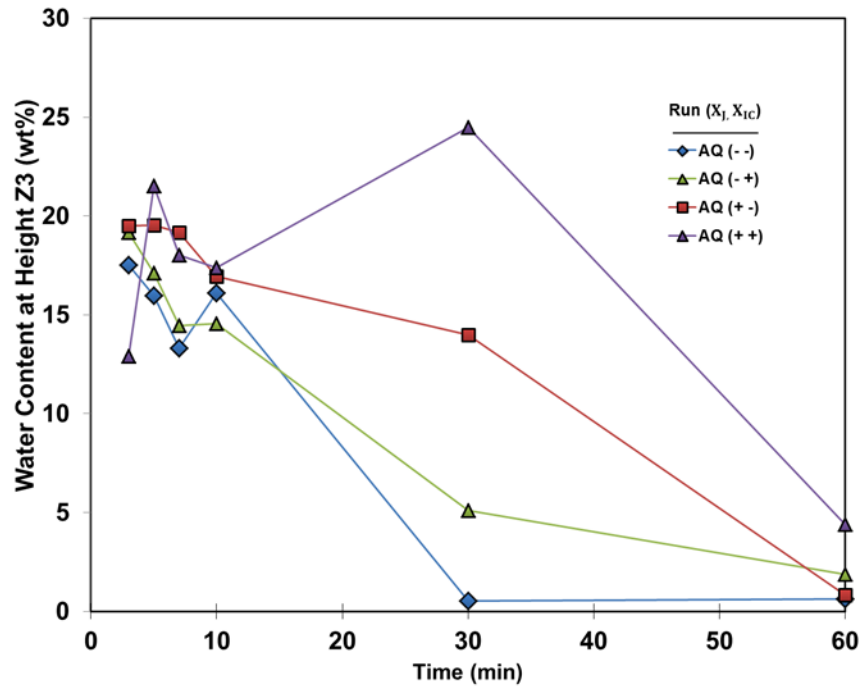


Figure 4-17: Comparison of four mixing conditions including low J and low IC, low J and high IC, high J and low IC and high J and high IC in terms of averaged water content (wt%) at height Z3 vs. time (min). Experiments were run with average-quality froth (AQ) at the sufficient BC = 150 ppm. Data reproduced with permission (Arora, 2016).

Figure 4-16 shows little reduction at height Z3 in water contents for high-water froth, which implies a steady state as well. By contrast, Figure 4-17 shows that the water content at height Z3 for average-quality froth looks very differently. Water content has a sharp reduction after approximately 10 minutes.

### 4.3.5 Water Content at Height Z4

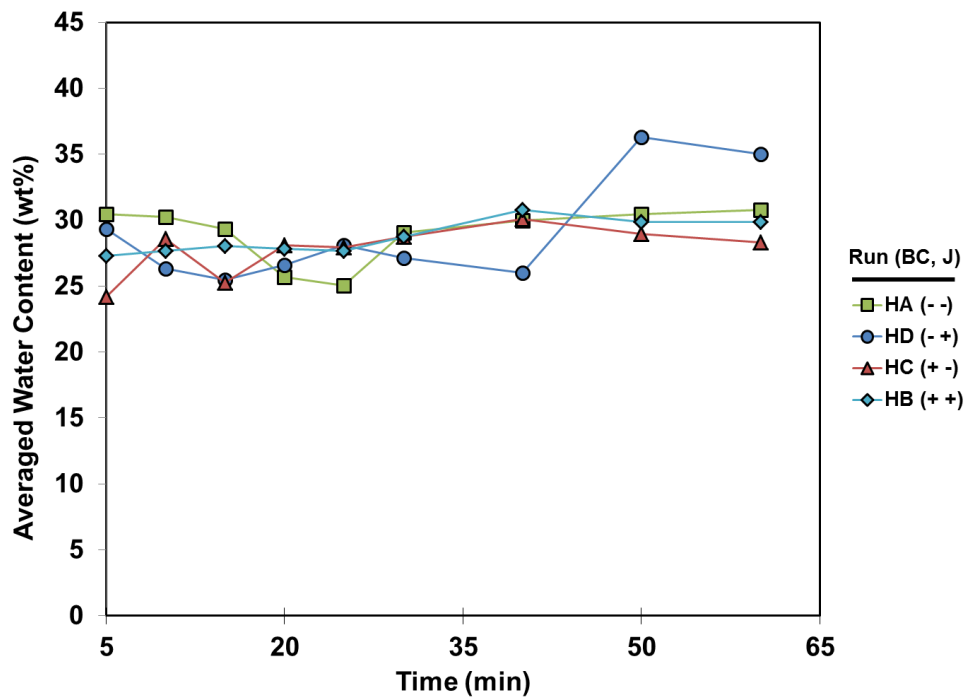


Figure 4-18: Comparison of four operating conditions including low BC and low J, low BC and high J, high BC and low J and high BC and high J in terms of averaged water content (wt%) at height Z4 vs. time (min). Experiments were run with high-solids froth at the fixed IC = 12wt%.

Figure 4-18 shows that there is a small increase in water amount after 60 minutes of settling, but the mass is not quite balanced if the water contents at four heights are combined. This observation can be explained by the fact that height Z4 is not at the bottom of the CIST. Water can settle below height Z4 where no samples are taken for Karl Fischer titrations.

Table 4-10: Water content difference (wt%) at height Z4 of two replicates at each sampling time for different operating situations including low J and low BC (HA), high J and high BC (HB), high J and low BC (HC) and low J and high BC (HD). Outliers are removed.

Operating Conditions	Absolute Value of Water Content (wt %) Difference at Height Z4								
	5 min	10 min	15 min	20 min	25 min	30 min	40 min	50 min	60 min
Delta (HA)	1.65	2.10	2.88	3.53	2.60	NA	NA	1.86	3.42
Delta (HB)	NA	1.90	1.42	0.87	0.70	2.75	3.04	1.39	0.10
Delta (HC)	0.53	4.80	3.85	1.92	4.70	8.67	4.08	9.00	0.98
Delta (HD)	6.36	9.70	0.43	3.33	1.60	7.15	5.83	9.48	6.44
							Average	Variance	S.D.
							3.61	7.76	2.79

Table 4-10 shows all the absolute value of water content difference at height Z3 and the standard deviation is 2.79, which is very close to above three heights. Therefore, all water content difference are summarized as below to calculate the overall average and standard deviation at all heights.

Table 4-11: Water content difference (wt%) at all heights of two replicates during settling for different operating situations including low J and low BC (HA), high J and high BC (HB), high J and low BC (HC) and low J and high BC (HD). Outliers are removed.

Height	Operating Conditions	Absolute Value of Water Content (wt %) Difference at Height Z4									
Height Z1	Delta (HA)	1.66	1.33	6.20	0.93	4.91	0.80	5.68	5.49	0.70	6.27
	Delta (HB)	0.09	3.95	4.70	2.39	2.19	1.35	1.92	2.83	0.70	1.69
	Delta (HC)	1.63	12.97	2.90	4.24	1.49	2.70	1.45	4.83	1.70	3.88
	Delta (HD)	4.44	10.27	0.80	5.36	4.59	1.60	1.47	6.58	1.11	4.50
Height Z2	Delta (HA)	0.44	1.40	4.43	9.30	1.60	6.40	7.92	3.58	4.84	
	Delta (HB)	2.03	1.90	3.47	0.05	0.60	2.73	3.24	5.83	3.62	
	Delta (HC)	6.94	1.80	2.92	3.79	1.10	2.51	1.30	8.50	11.97	
	Delta (HD)	3.35	3.60	1.19	3.07	4.80	5.56	0.49	5.50	6.77	
Height Z3	Delta (HA)	1.92	1.20	2.02	1.01	2.00	NA	0.03	0.52	8.99	
	Delta (HB)	0.29	1.60	2.06	1.88	6.80	1.25	3.42	1.70	2.37	
	Delta (HC)	1.07	6.50	8.70	0.04	0.10	4.80	7.28	0.26	4.38	
	Delta (HD)	6.93	4.30	5.16	3.10	3.00	1.48	10.25	2.45	2.16	
Height Z4	Delta (HA)	1.65	2.10	2.88	3.53	2.60	NA	NA	1.86	3.42	
	Delta (HB)	NA	1.90	1.42	0.87	0.70	2.75	3.04	1.39	0.10	
	Delta (HC)	0.53	4.80	3.85	1.92	4.70	8.67	4.08	9.00	0.98	
	Delta (HD)	6.36	9.70	0.43	3.33	1.60	7.15	5.83	9.48	6.44	
									Average	Variance	S.D.
									3.49	7.49	2.74

By looking through all tables, the average and standard deviation at all heights do not vary with height and it appears that as the sample size increase from 36 to 148, they also remain the same. Therefore, the population average difference between points at the same time in two runs can be reported as 3.49 with a standard deviation of 2.74 and N = 148.

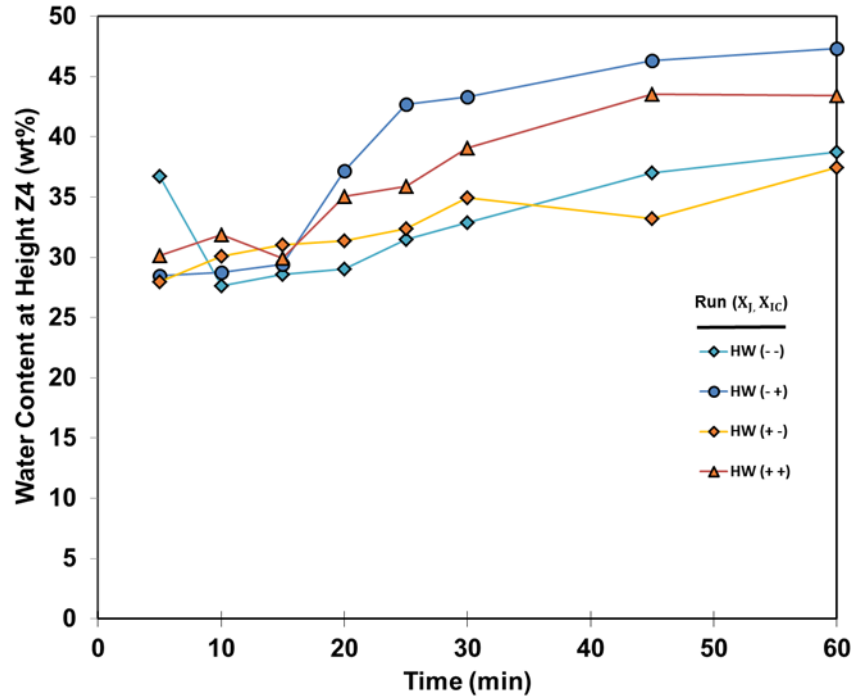


Figure 4-19: Comparison of four mixing conditions including low J and low IC, low J and high IC, high J and low IC and high J and high IC in terms of averaged water content (wt%) at height Z4 vs. time (min). Experiments were run with high-water froth (HW) at the sufficient BC = 200 ppm. Data reproduced with permission (Saraka, 2017).



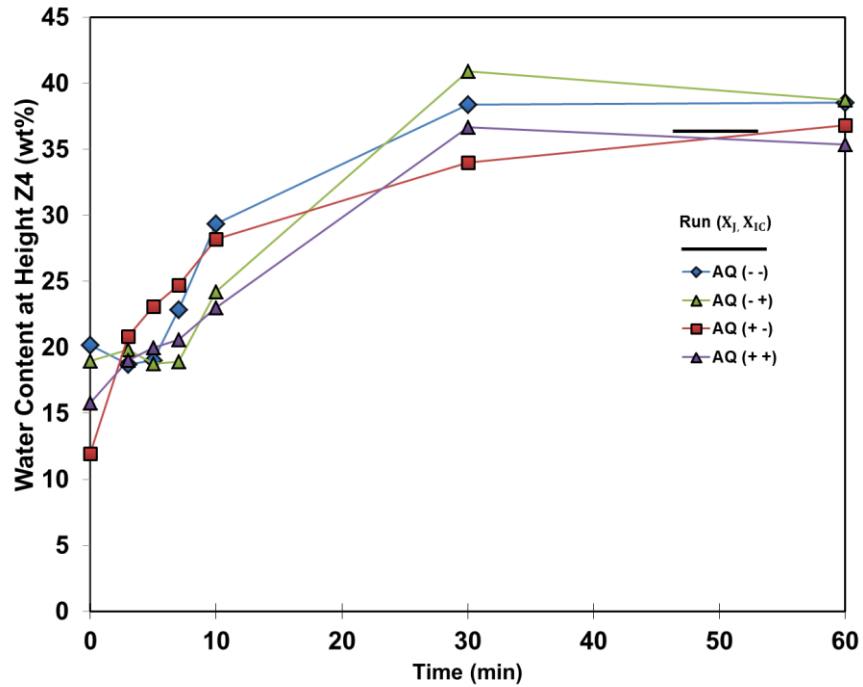


Figure 4-20: Comparison of four mixing conditions including low J and low IC, low J and high IC, high J and low IC and high J and high IC in terms of averaged water content (wt%) at height Z4 vs. time (min). Experiments were run with average-quality froth (AQ) at the sufficient BC = 150 ppm. Data reproduced with permission (Arora, 2016).

Figure 4-19 shows a significant increase in water amount at height Z4 at the end of settling in high-water froth. Figure 4-20 also shows a substantial increase in water amount at height Z4 in average-quality froth. Water amount is quite balanced in high-water and average-quality froth.

### 4.3.6 Effect of Bulk Concentration vs. Mixing Energy at Height Z1

The effects of BC and J, rather than proposing a predictive model, can be uncovered by calculating their coefficients throughout settling respectively as what has been done in previous study (Arora, 2016; Saraka, 2017). As shown in Equation 10, the water content (wt%) of a specific height and settling time depends on mixing energy, bulk concentration, and the interacting effect of these two factors. Since the experiments at centrepoint are not replicated, the analysis of coefficients does not include the centrepoint.

$$C(t, h) = \beta_0 + \beta_J X_J + \beta_{BC} X_{BC} + \beta_{BC*J} X_{BC} X_J \quad (10)$$

Since the induction time of high-solids froth can be up to 25 minutes, the analysis of effects focuses on the time after 25 minutes towards the end of settling, but the overall trend is still considered as well. Similarly, the analysis of effects for high-water froth focuses on the time after 40 minutes because of a longer induction time.

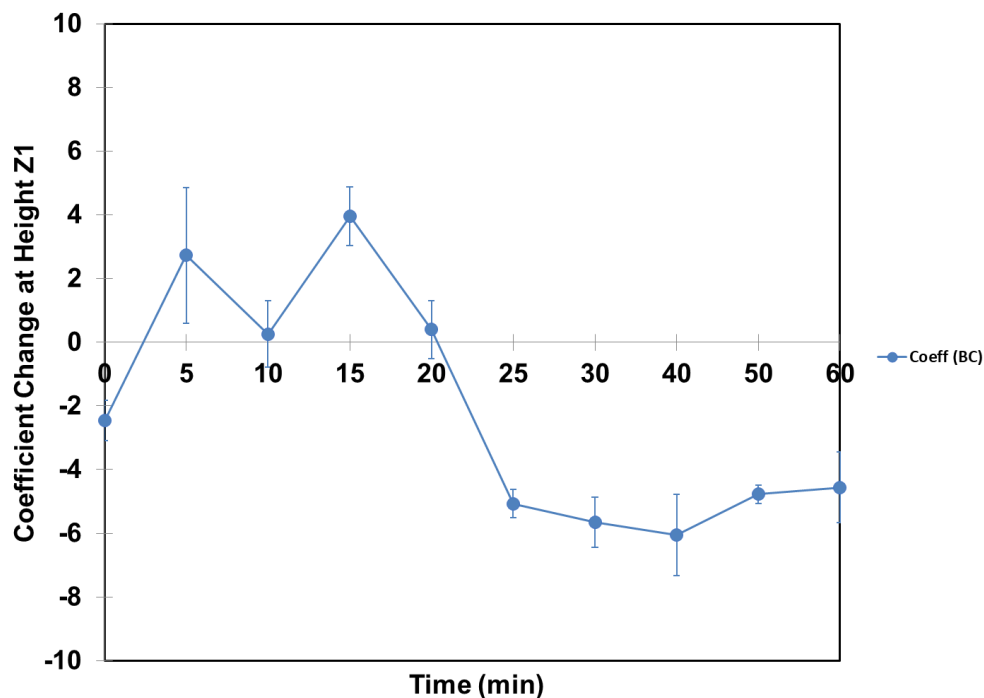


Figure 4-21: Effect of BC over settling time of height Z1 at IC = 12 wt% for high-solids froth.

Figure 4-21 shows that the effect of BC on high-solids froth changes from positive to negative at 20 minutes, which is around the same time as the induction time of 25 minutes in high-solids froth, and becomes very negative towards the end of settling, which means high BC leads to low final water content before reaching the overdosing limit.

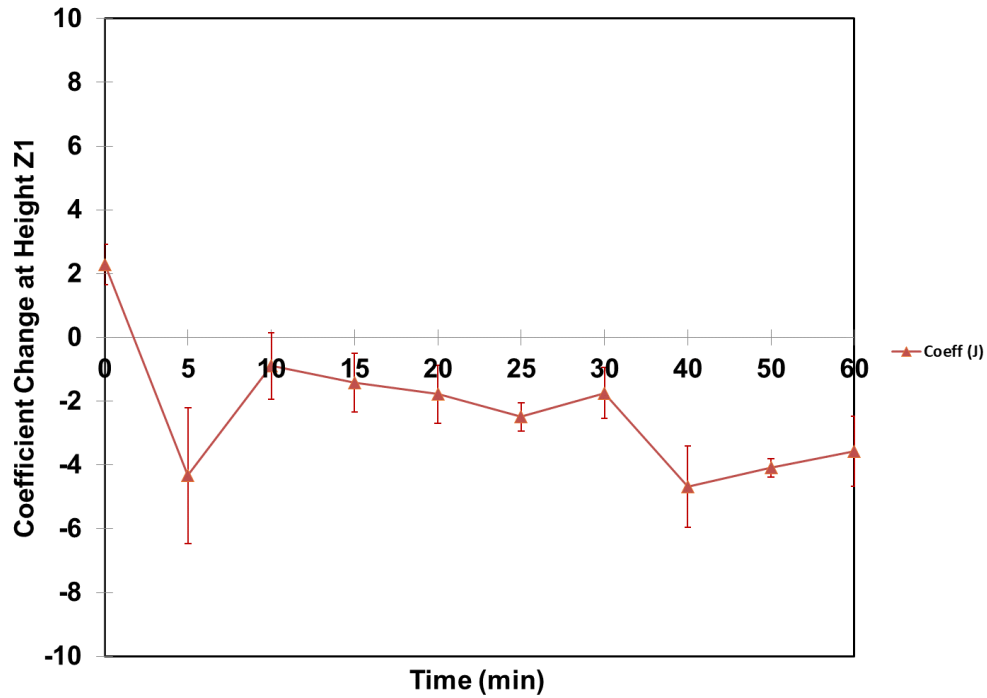


Figure 4-22: Effect of J over settling time at height Z1 at IC = 12 wt% for high-solids froth.

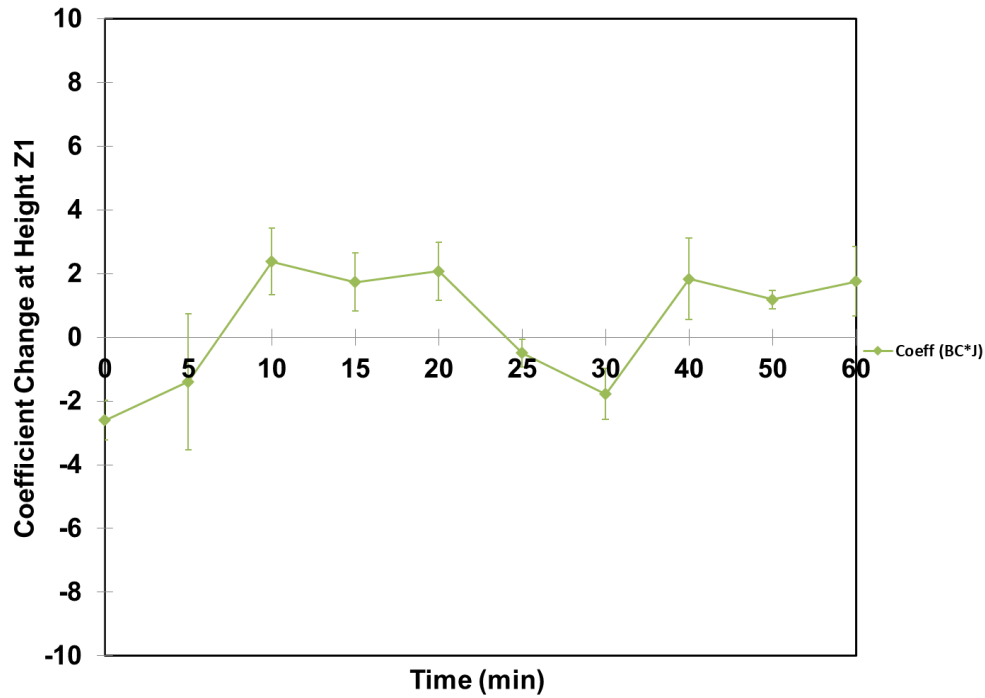


Figure 4-23: Effect of BC\*J over settling time of height Z1 at IC = 12wt% for high-solids froth.

Figure 4-22 shows that the effect of J stays negative during settling but is not as negative as the effect of BC, particularly towards the end. High J also leads to low final water content, but BC has a more significant effect than J. By contrast, Figure 4-23 shows that the interacting effect of BC\*J stays a bit positive throughout settling despite a dip between 25 and 30 minutes. The effect of BC\*J can be negligible compared to BC and J.

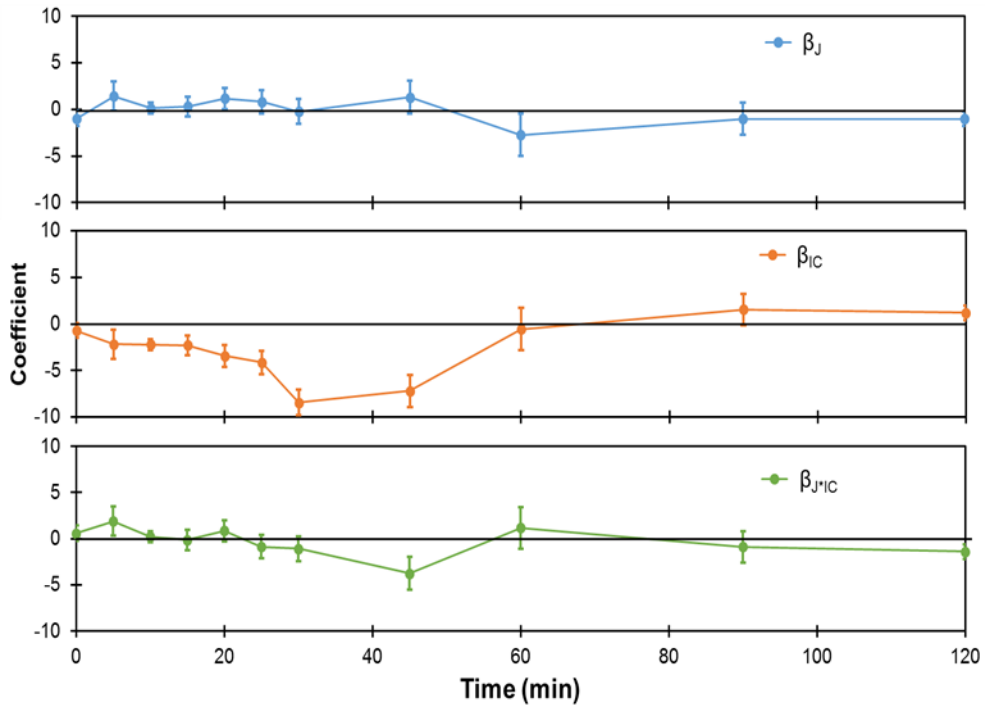


Figure 4-24: Effect of variables over settling time of height Z1 at BC = 200 ppm for high-water froth (Saraka, 2017).

Figure 4-24 shows that the effect of J is insignificant over settling; the effect of IC becomes very negative until 60 minutes of settling and stays a bit positive until the end; the interacting effect of J and IC is insignificant over settling. Since an induction time of up to 40 minutes is observed in high-water froth, which is around the same time when the IC effect starts to change from negative to positive, IC level is more related to the formation of induction time in high-water froth.

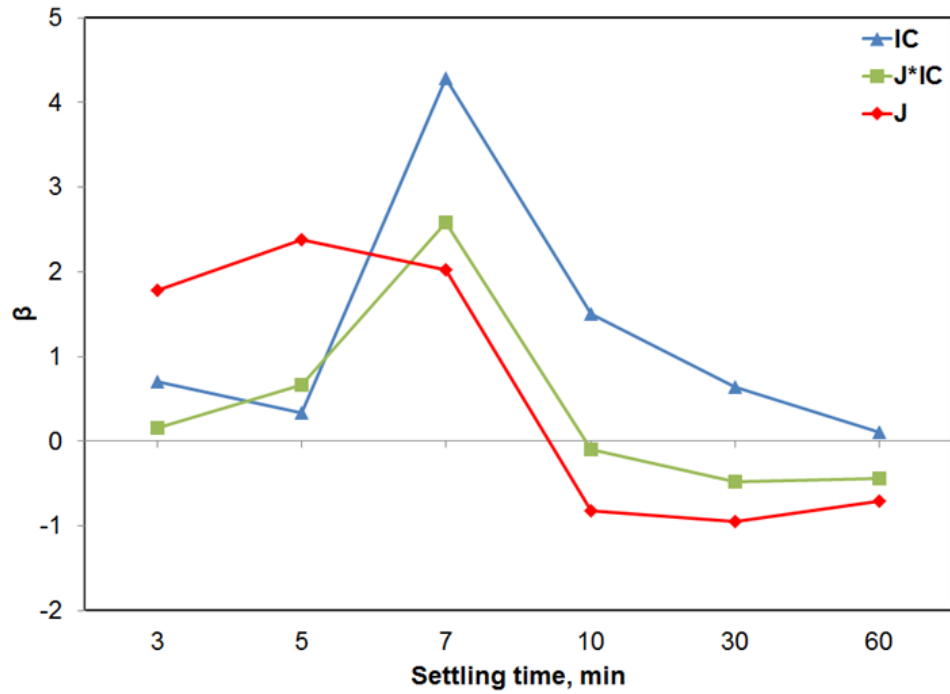


Figure 4-25: Effect of variables over settling time of height Z1 at BC = 150 ppm for average-quality froth (Arora, 2016).

Figure 4-25 shows that the effects of IC, J\*IC and J all change the sign from positive to negative at around 7 minutes of settling for average-quality froth. Since most of the water and solids finish settling within the first 10 minutes, which approximately aligns with the maximum value of all three effects, IC, J\*IC and J all plays an important role on final water content.

### 4.3.7 Effect of Bulk Concentration vs. Mixing Energy at Height Z2

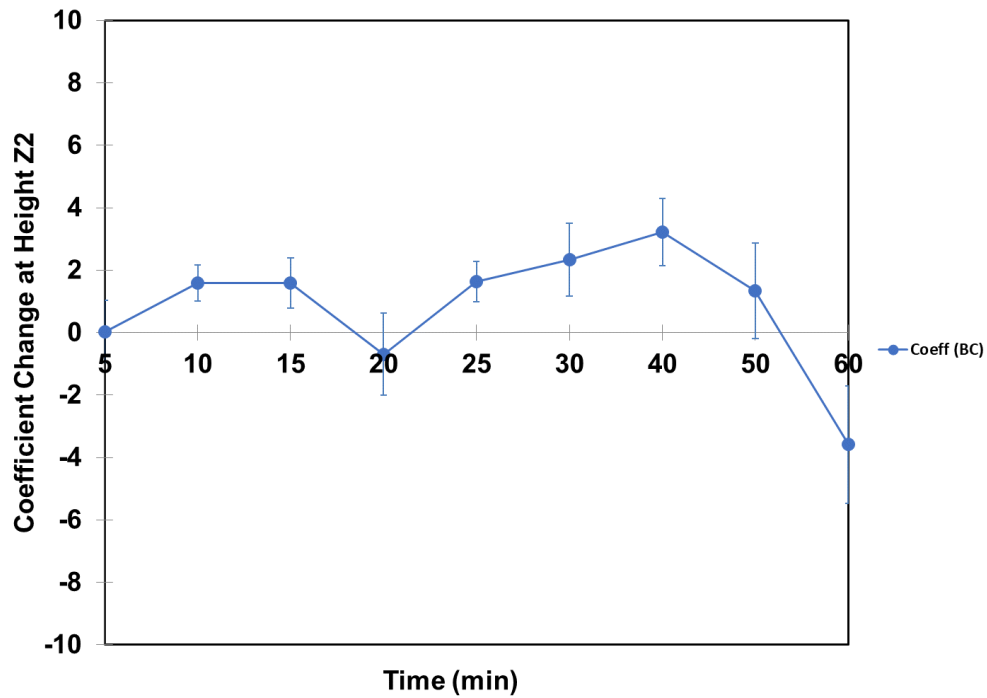


Figure 4-26: Effect of BC over settling time of height Z2 at IC = 12wt% for high-solids froth.

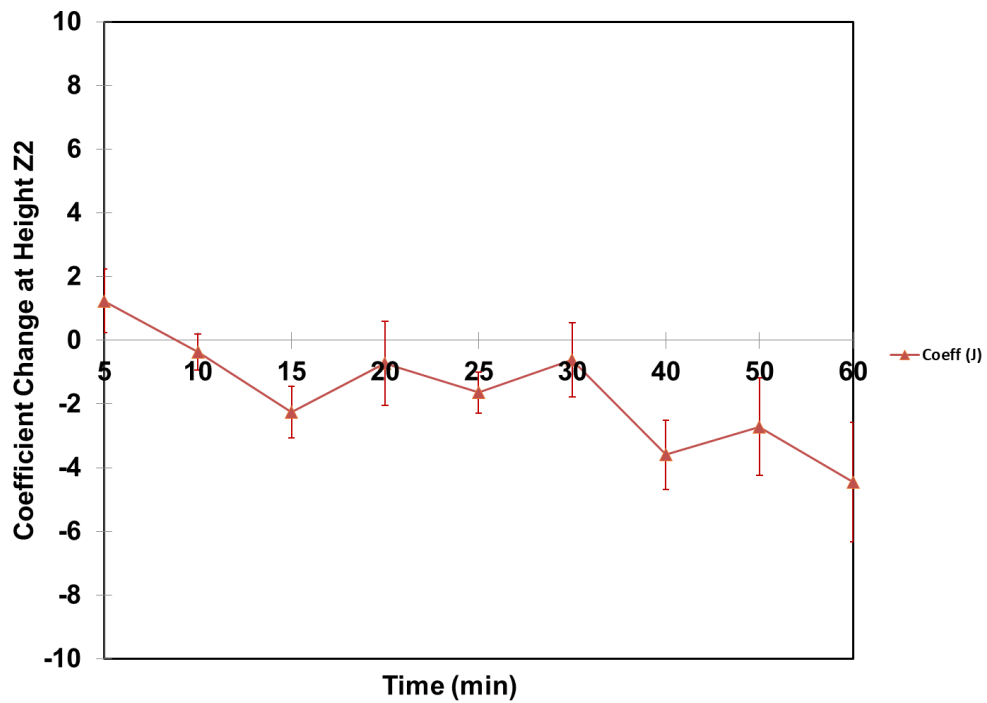


Figure 4-27: Effect of J over settling time of height Z2 at IC = 12wt% for high-solids froth.

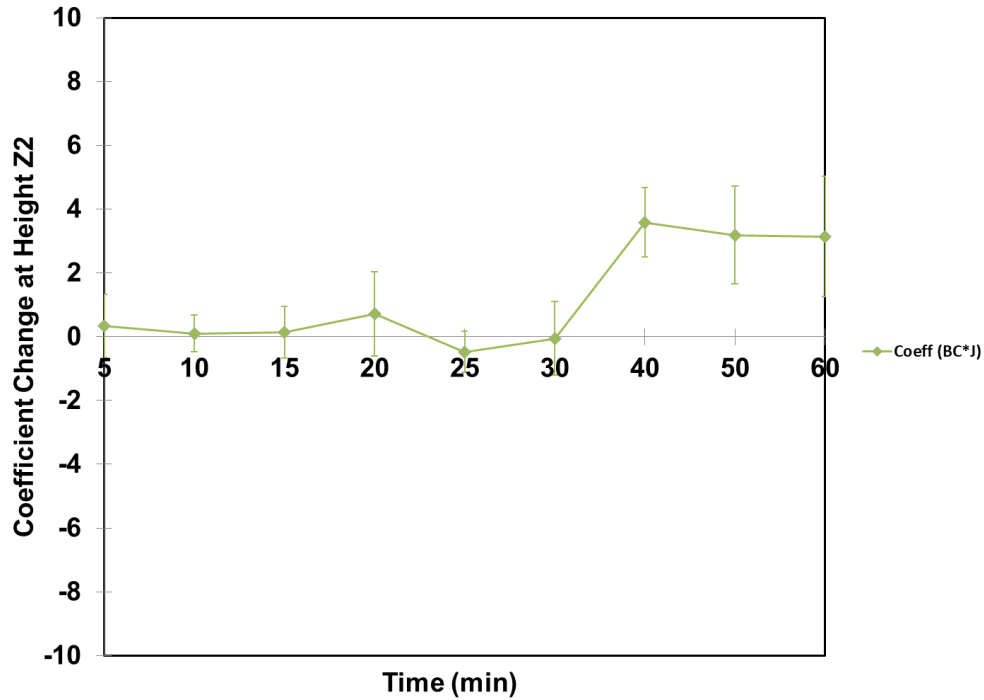


Figure 4-28: Effect of BC\*J over settling time of height Z2 at IC = 12wt% for high-solids froth.

Figure 4-26 shows that the effect of BC stays positive throughout the process by considering an outlier at 20 minutes, but it changes the sign from positive to negative at 40 minutes of settling, which is around the same time as the induction time at height Z2 in high-solids froth. By contrast, in Figure 4-27, the effect of J stays negative in general during settling. Figure 4-28 shows that the interacting effect of BC\*J becomes significantly positive after 30 minutes until the end. Overall, it shows that the settling at height Z2 is strongly affected by BC, J and BC\*J.



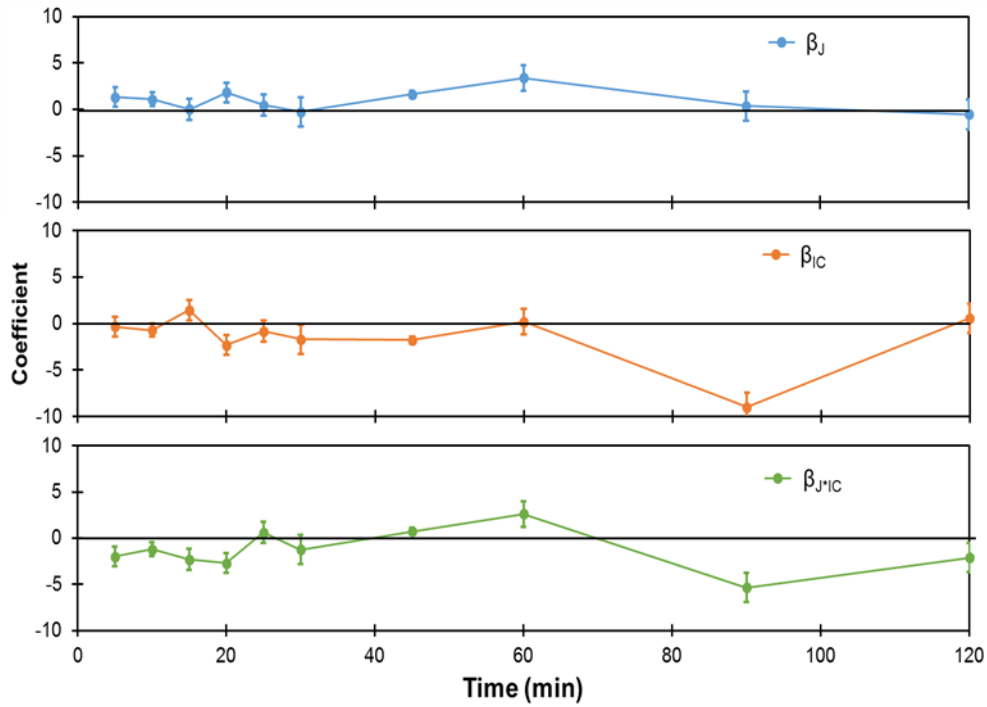


Figure 4-29: Effect of variables over settling time of height Z2 at BC = 150 ppm for average-quality froth (Saraka, 2017).

Figure 4-29 shows that the effects of IC, J\*IC all change the sign twice: from positive to negative at 60 minutes; from negative to positive at 90 minutes. Since the induction time at height Z2 for high-water froth is around 90 minutes, the effect of IC and J\*IC are more significant than J from 90 minutes until the end.

### 4.3.8 Effect of Bulk Concentration vs. Mixing Energy at Height Z3

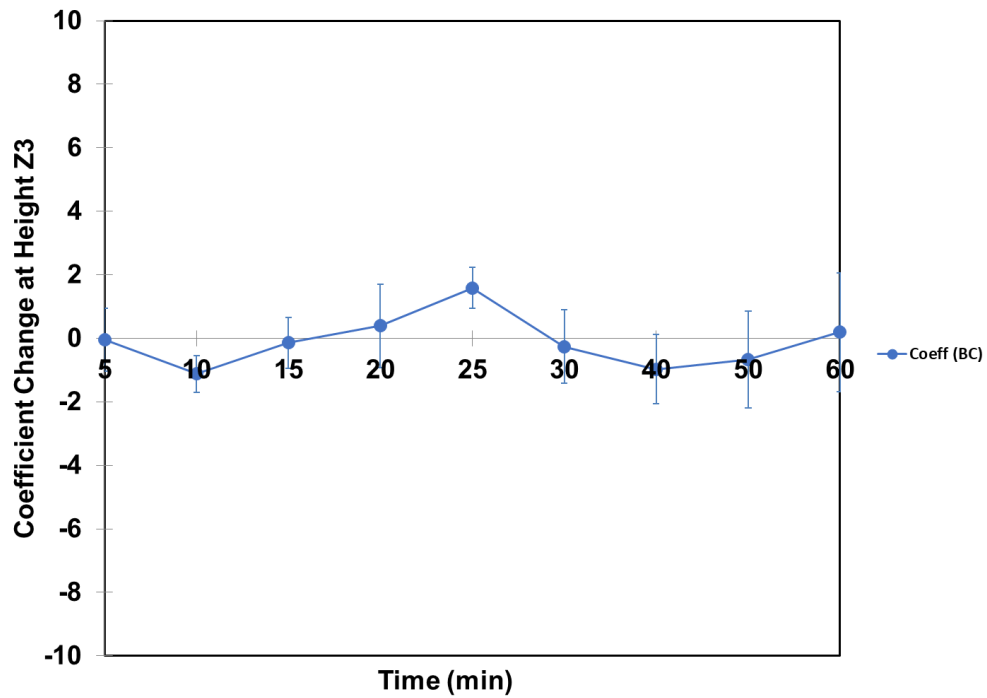


Figure 4-30: Effect of BC over settling time of height Z3 at IC = 12wt% for high-solids froth.

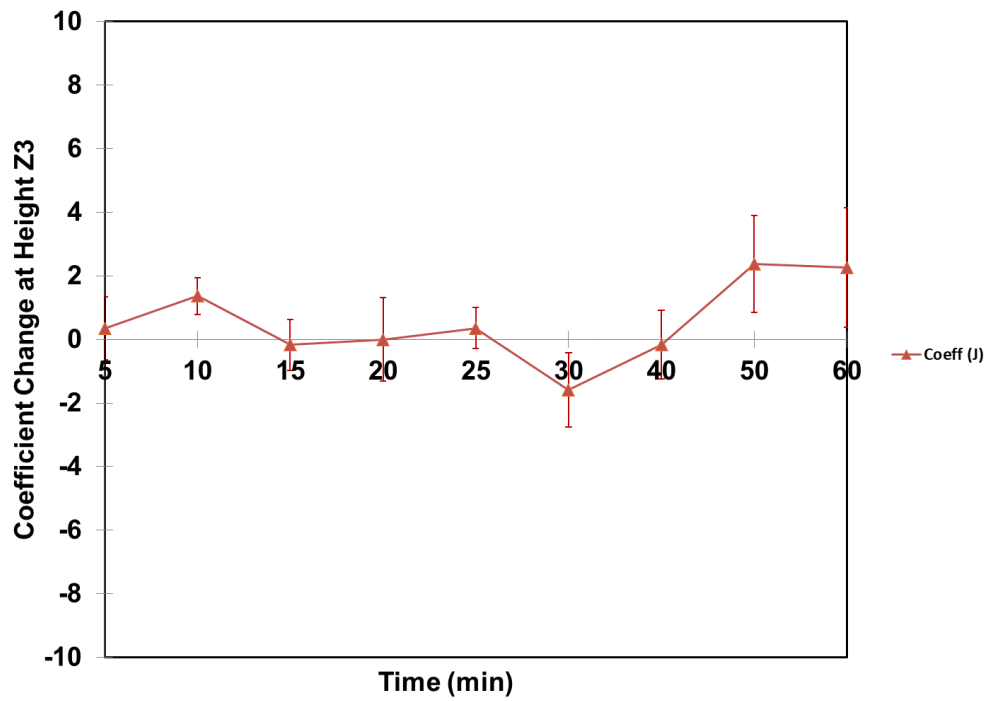


Figure 4-31: Effect of J over settling time of height Z3 at IC = 12wt% for high-solids froth.

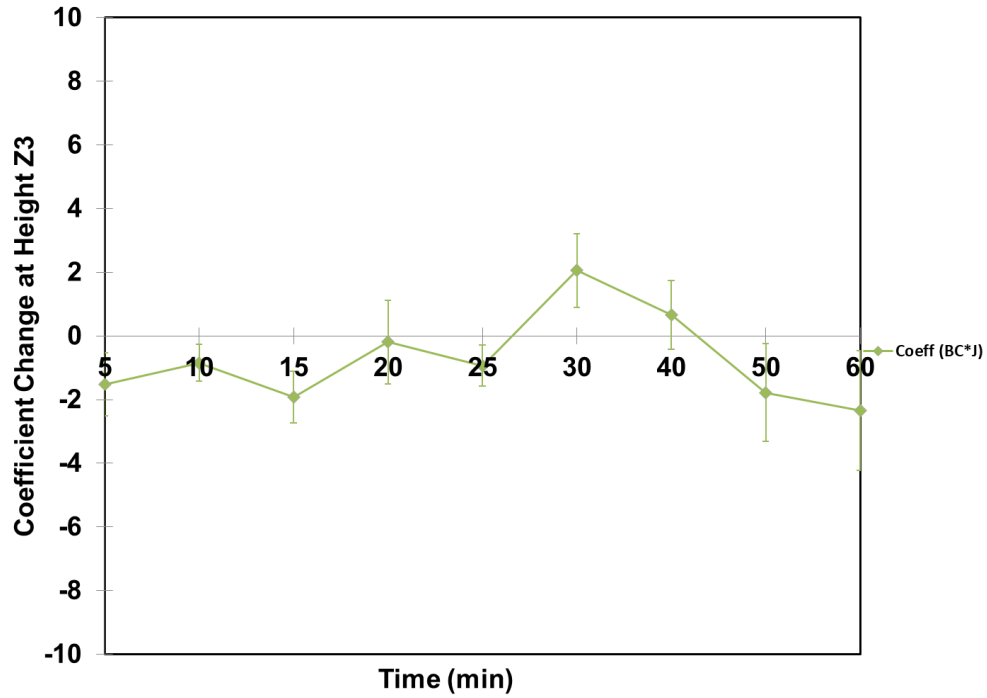


Figure 4-32: Effect of BC\*J over settling time of height Z3 at IC = 12wt% for high-solids froth.

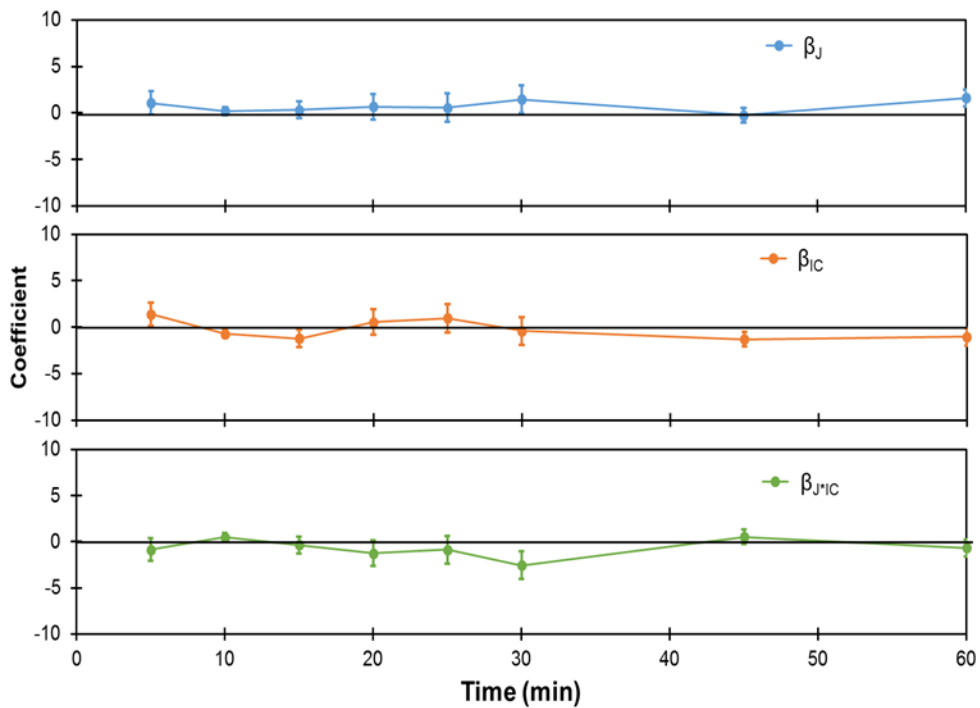


Figure 4-33: Effect of variables over settling time of height Z3 at BC = 150 ppm for average-quality froth (Saraka, 2017).

From Figure 4-30 to Figure 4-32, the effects of BC, J and BC\*J are not significant at height Z3 for high-solids froth during settling. Figure 4-33 shows that the effects of J, IC, and J\*IC are not significant at height Z3 for high-water froth during settling either. The settling at height Z3 for both high-solids and high-water froth are independent of BC, J and BC\*J.

#### 4.3.9 Effect of Bulk Concentration vs. Mixing Energy at Height Z4

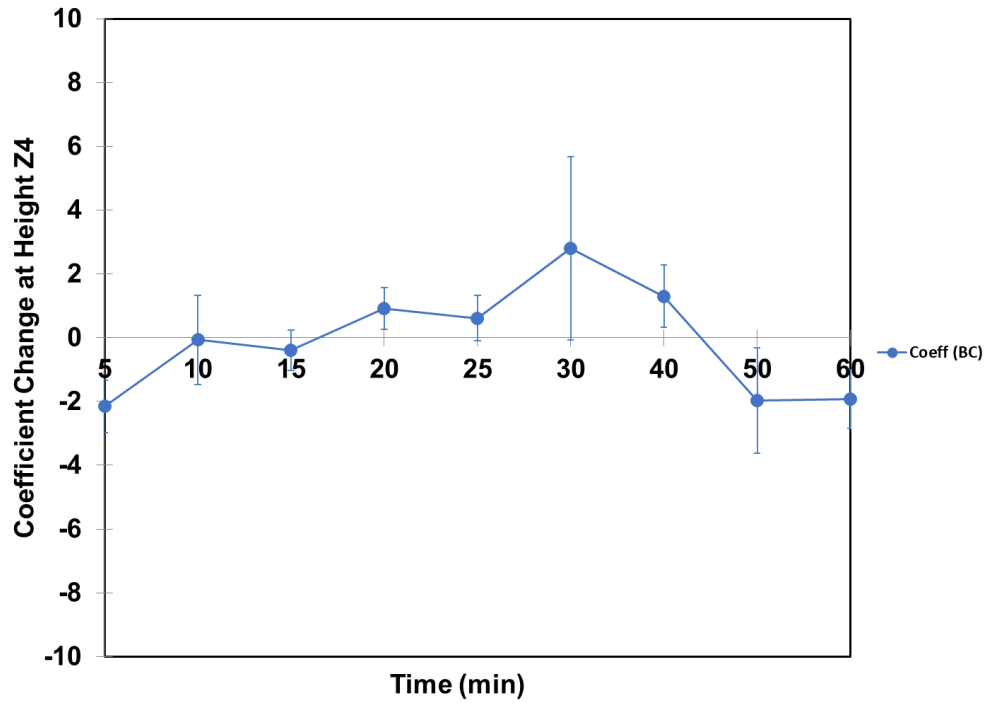


Figure 4-34: Effect of BC over settling time of height Z4 at IC = 12wt% for high-solids froth.

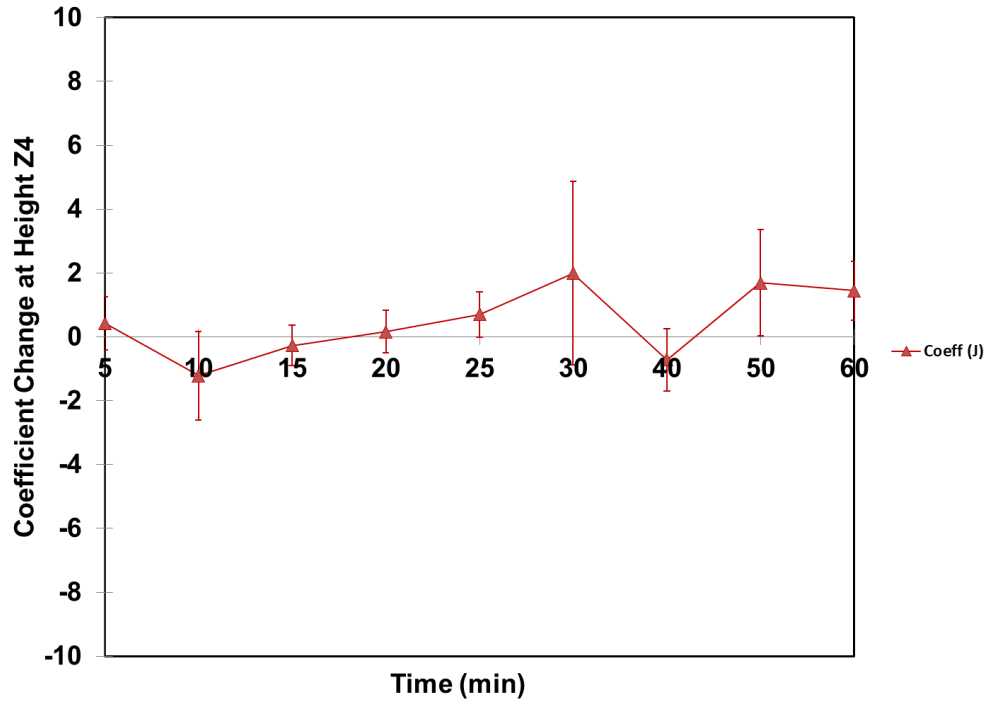


Figure 4-35: Effect of J over settling time of height Z4 at IC = 12wt% for high-solids froth.

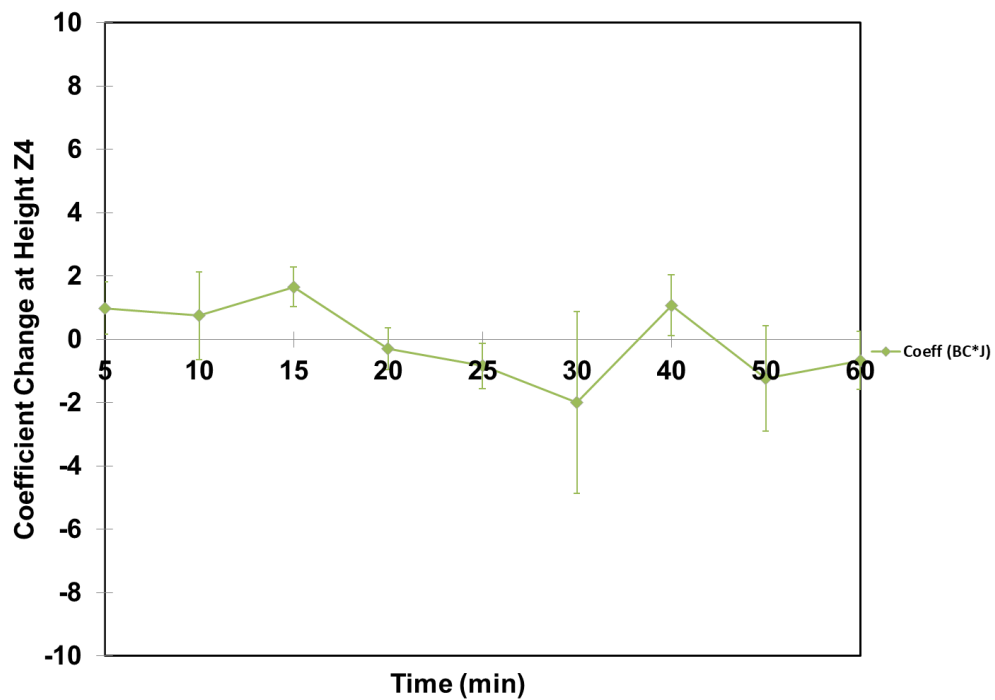


Figure 4-36: Effect of BC\*J over settling time of height Z4 at IC = 12wt% for high-solids froth.

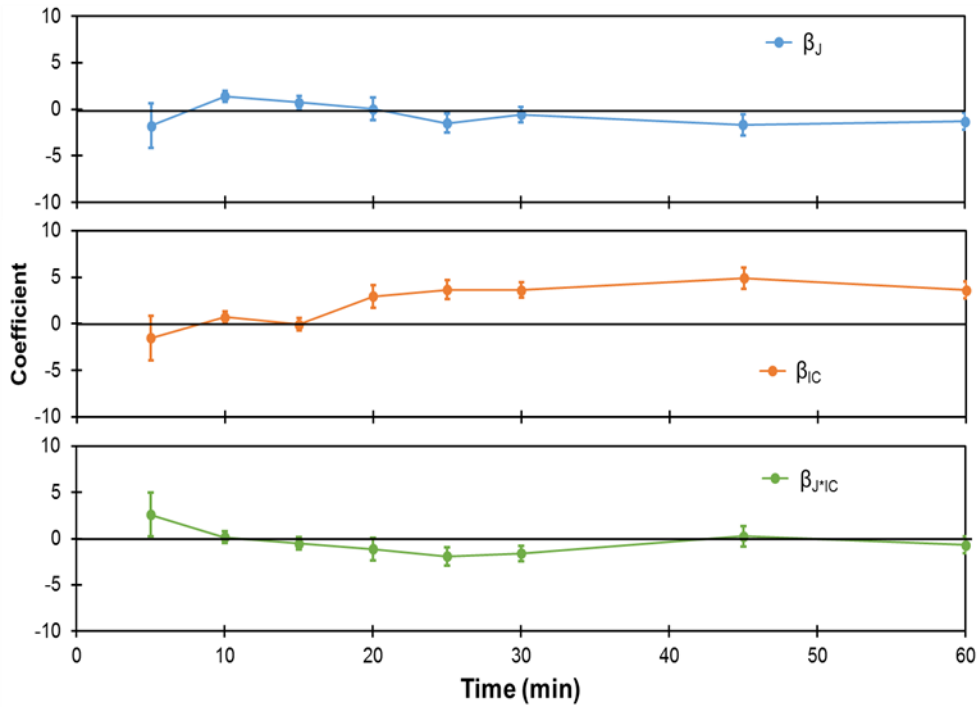


Figure 4-37: Effect of variables over settling time of height Z4 at BC = 150 ppm for average-quality froth (Saraka, 2017).

From Figure 4-34 to Figure 4-36, the effect of BC is bit negative, the effect of J is a bit positive at the end of settling; the interacting effect is insignificant during process. In Figure 4-37, the effects of J and J\*IC are negligible, but the effect of IC stays very positive until the end.

Overall, the effect of each factor and the interacting factor on final water content in each froth's settling is quite different. This difference further supports that each froth has a different settling behavior and should be treated differently.

#### 4.4 Dean Stark OWS

At the end of each experiment, a 100mL sample was collected at relative heights of 0.1, 0.5, and 0.9 based on the liquid height at the beginning of settling as what has been done in the previous study (Arora, 2016; Saraka, 2017). These samples were then sent to the industrial partner for OWS analysis to determine the fraction of oil, water, and solids (OWS) respectively. The full OWS data can be found in Appendix B.4.

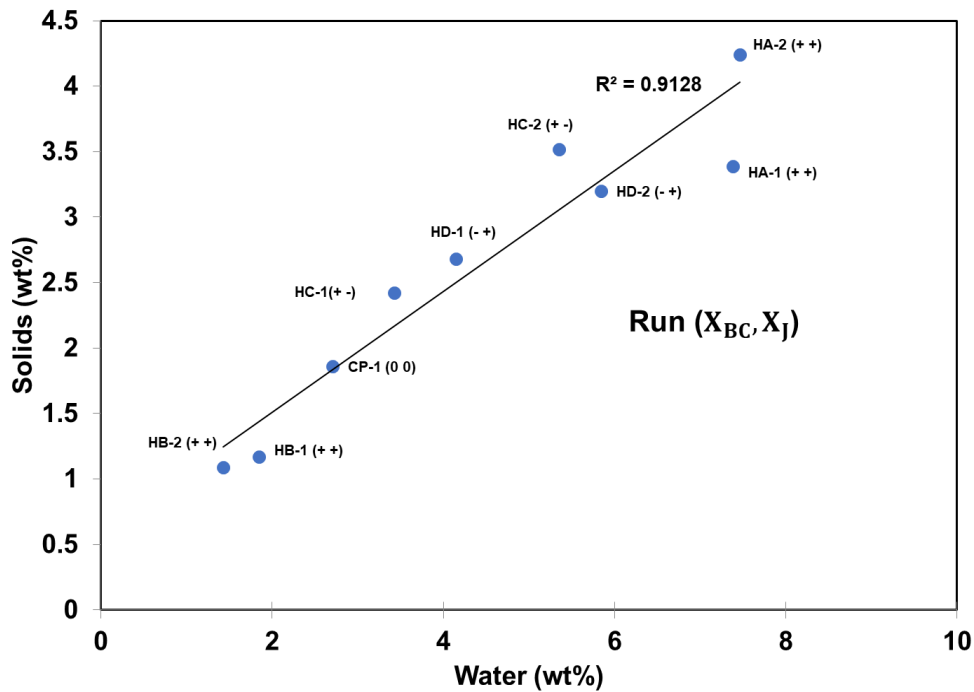


Figure 4-38: Water and solids content for several operating conditions with high-solids froth. Samples collected at the top height of the CIST ( $h/H=0.1$ ).

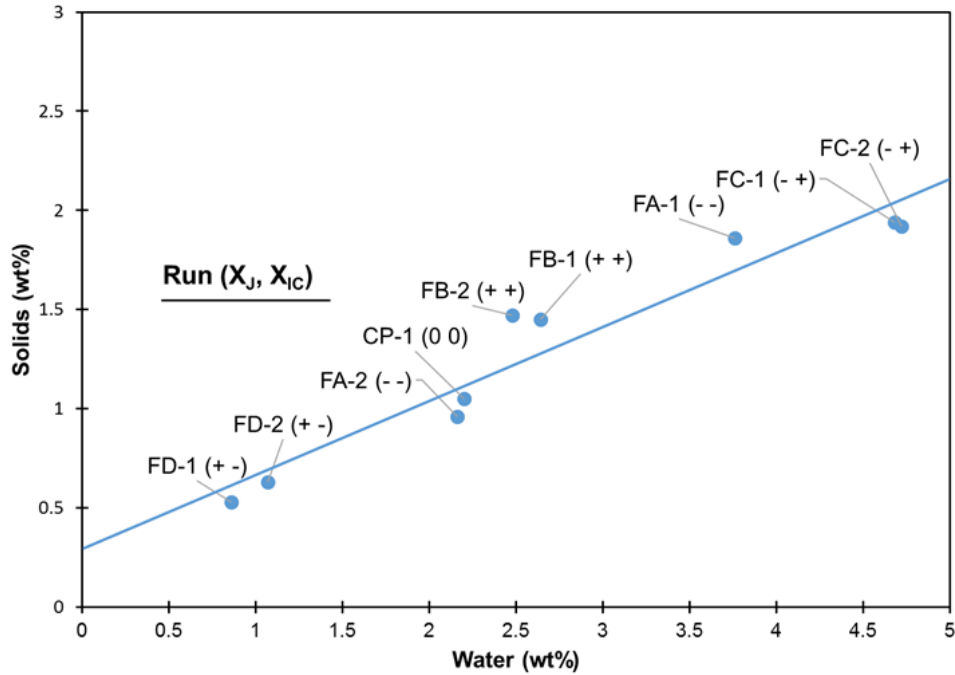


Figure 4-39: Water and solids content for several operating conditions with high-water froth.

Samples collected at the top height of the CIST ( $h/H=0.1$ ) (Saraka, 2017).

Figure 4-38 and Figure 4-39 show that the correlation between water (wt%) and solids (wt%) at the top height ( $h/H=0.1$ ) in high-solids and high-water froth can be captured by a linear equation respectively, which shows that the settling of water accompanies occurs at the same time as the settling of solids.

Table 4-11: The multivariate analysis for the water content at  $h/H = 0.1$ .

Term	Sum of Squares	d.f.	Mean Square	t	p-Value
J	13.39	1	13.19	-4.92	0.001713
BC	20.38	1	20.38	-3.99	0.005256
J*BC	0.05	1	0.05	-0.25	0.810
Error	3.36	4	0.84		
Total	37.19	7			

Table 4-12: The multivariate analysis for the solid content at  $h/H = 0.1$

Term	Sum of Squares	d.f.	Mean Square	t	p-Value
J	3.69	1	3.69	-3.57	0.009097



BC	3.52	1	3.52	-3.65	0.008178
J*BC	0.47	1	0.47	-1.30	0.234769
Error	1.10	4	0.28		
Total	8.78	7			

Table 4-11 and Table 4-12 show that the null hypothesis: J, BC and J\*BC do not have effects on the content of water and solids at  $h/H = 0.1$ , and differences are only due to experimental errors is rejected is tested statistically at p-value of 5%. This hypothesis is rejected for J and BC since their p-values are smaller than 5%. By contrast, the p-value of J\*BC is greater than 5%, and the null hypothesis cannot be rejected. Therefore, at the top height ( $h/H=0.1$ ), the water and solids content are affected by J and BC, but not the interacting effect of J\*BC.

# **Chapter 5: The FBRM Data: Chord Length Distributions of High-solids Froth Settling Experiments**

The FBRM instrument measures the chord length of particles passing the screen of the probe in settling experiments. The FBRM probe was placed into the vessel until it reached the designated location, which was discussed in Chapter 2.10, before naphtha blending started, and the chord length distribution was collected every 10s during each experiment.

## **5.1 Data Analysis Method**

Table 5-1 shows the chord length data selected from the raw data spreadsheet for each experiment. The FBRM raw data from each experiment was first divided to three stages: naphtha blending, demulsifier dispersion and settling process. The settling was further divided to five stages including 10 minutes, 20 minutes, 25 minutes, 30 minutes and 60 minutes after settling began respectively.

Table 5-1: Chord length data selection for each high-solids froth settling experiment

Notation	Explanation
NB Starts	Naptha blending starts
NB Ends	Naptha blending ends
DD Starts	Demulsifier dispersion starts
The data of NB Ends is the same as DD Starts	
DD Ends	Demulsifier dispersion ends
0 minutes	Settling starts
The data of DD Ends is the same as 0 minutes	
10 minutes	10 minutes after settling starts
20 minutes	20 minutes after settling starts
25 minutes	25 minutes after settling starts
30 minutes	30 minutes after settling starts
60 minutes	60 minutes after settling starts

Table 5-2 shows the data usability of each experiment based on its fouling index. The fouling index is a percentage, which indicates the degree of to which the FBRM probe is covered by stagnant fluids (Mettler Toledo, 2011b). The experiment with a lower fouling index is closer to real-time mixing conditions (Mettler Toledo, 2011b). Sapphire treatment was performed on the probe every two experiments in order to mediate the fouling effect as in previous study (Saraka, 2017). However, since the bitumen froth is a highly complex and dirty system to work with, the probe can still easily get stuck in bitumen and solids that can hardly be removed during experiments. Hence, some of experiments still have high fouling index even after sapphire treatment. In the end, the analysis of chord length data for high-solids froth focused on the data of the second replicate, which includes four experiments without the centerpoint, because of a lower fouling index in general.

Table 5-2: The operating condition, fouling index and data usability of the FBRM data for each high-solids froth experiment

Experiment	$X_{BC}$	$X_J$	Fouling index	Usability
HA-1	-1	-1	below 20%	Yes
HB-1	+1	+1	above 40%	No
HC-1	+1	-1	below 20%	Yes
HD-1	-1	+1	above 50%	No
CP-1	0	0	below 20% up to 1 hour of the experiment	Yes
HA-2	-1	-1	below 5%	Yes
HB-2	+1	+1	below 20%	Yes
HC-2	+1	-1	below 10%	Yes
HD-2	-1	+1	below 20% up to 1 hour of the experiment	Yes

## 5.2 Low Bulk Concentration and Low Mixing Energy

There are three figures depicting the chord length distribution for each selected experiment including naphtha blending, demulsifier dispersion and settling with different times respectively. Both unweighted and square weighted data are shown in this section. Square weighted data focuses more on large particles and therefore has a larger average chord length compared to number weighted data which focuses more on small particles.

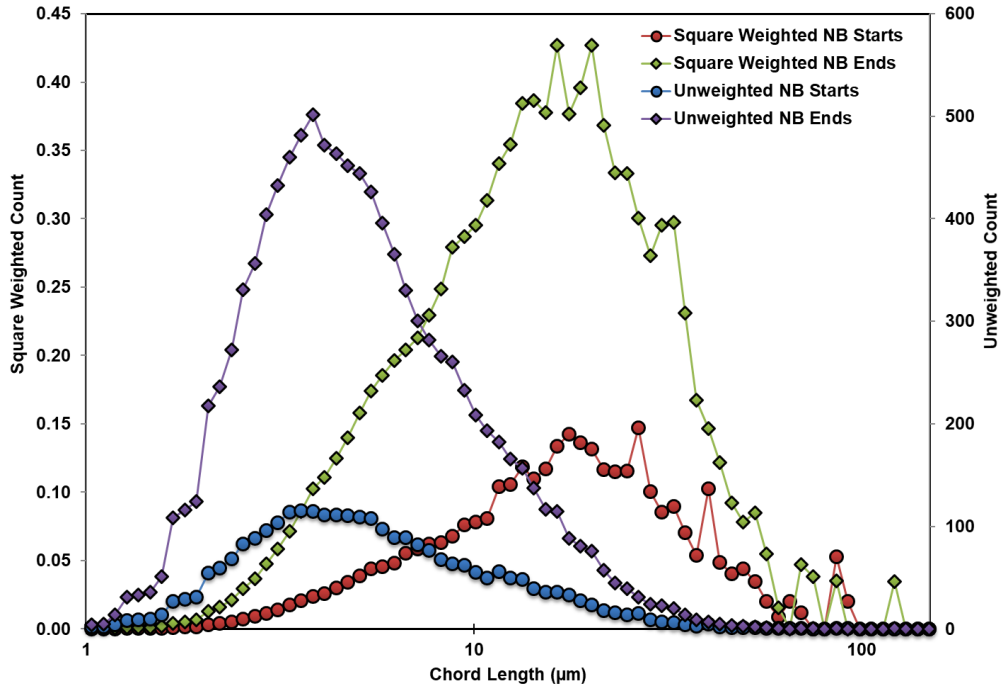


Figure 5-1: Square weighted and unweighted chord length distribution at the beginning and the end of naphtha blending for low BC and low J operating conditions for high-solids froth settling experiment.

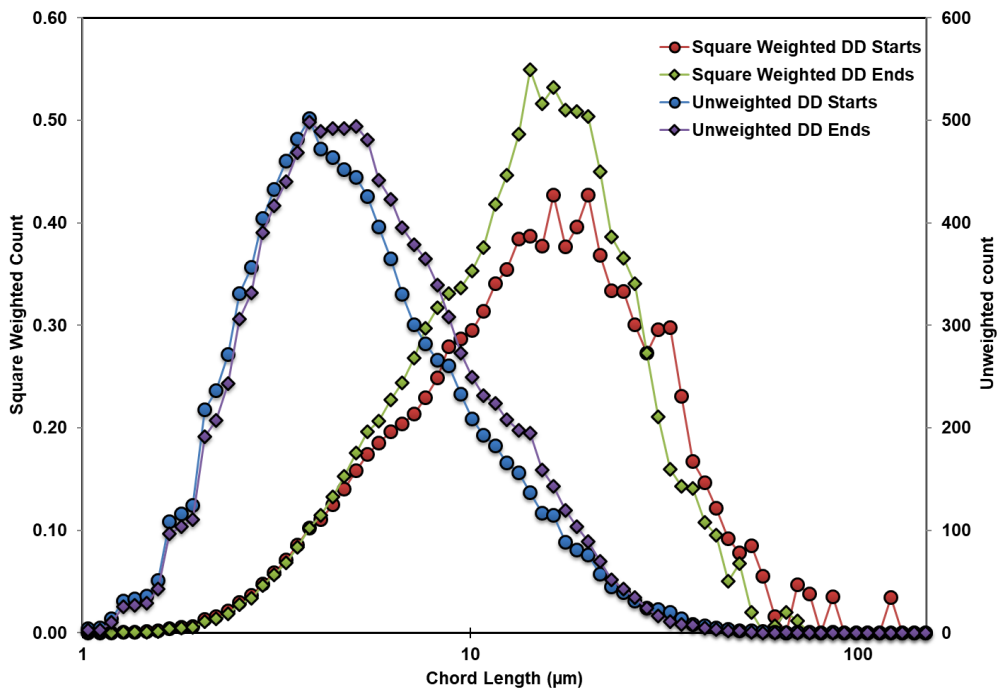


Figure 5-2: Square weighted and unweighted chord length distribution at the beginning and the end of demulsifier dispersion for low BC and low J operating conditions for high-solids froth settling experiment.

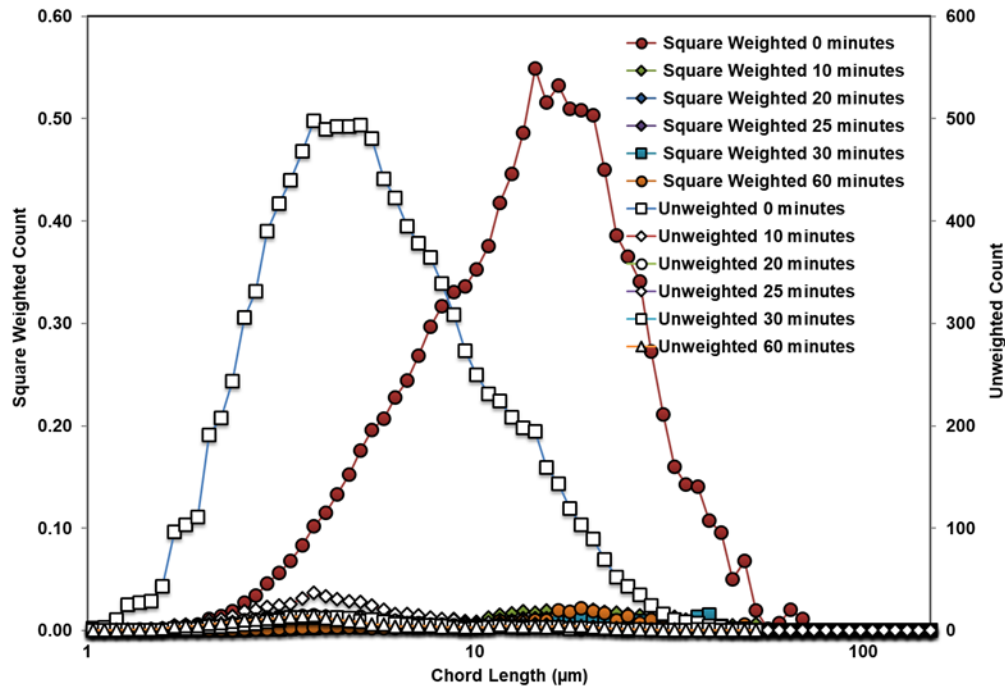


Figure 5-3: Square weighted and unweighted chord length distribution over settling for low BC and low J operating conditions for high-solids froth settling experiment.

Figure 5-1 shows a significant increase in counts during naphtha blending. Figure 5-2 shows a bit of increase in counts during demulsifier dispersion. Figure 5-3 shows an obvious decrease in count after 10 minutes of settling, but few changes in counts after 10 minutes until the end.

### 5.3 High Bulk Concentration and High Mixing Energy

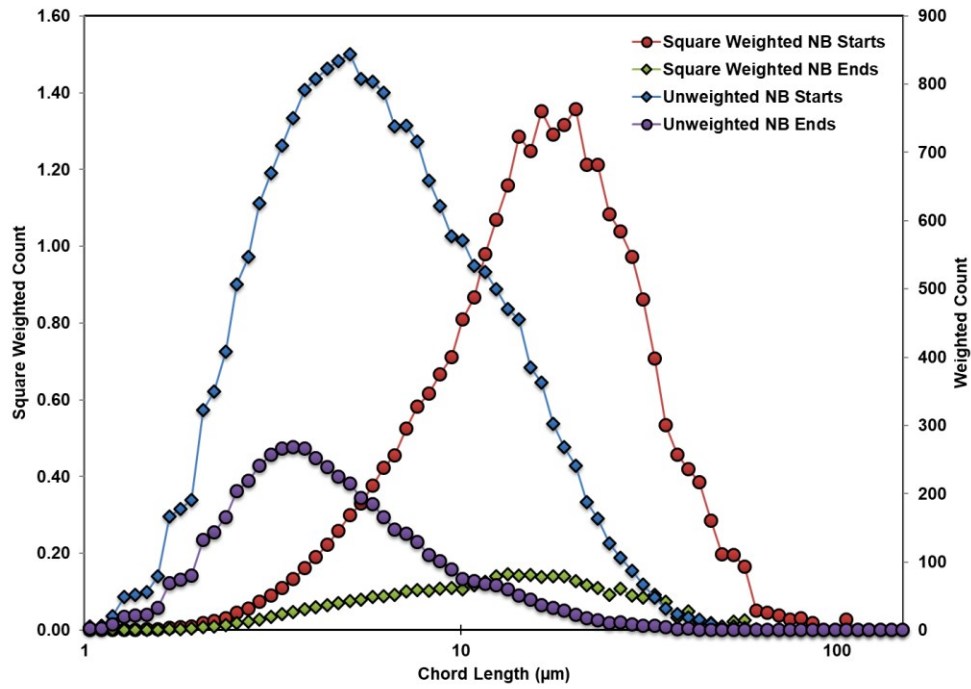


Figure 5-4: Square weighted and unweighted chord length distribution at the beginning and the end naphtha blending for high BC and high J operating conditions for high-solids froth settling experiment.

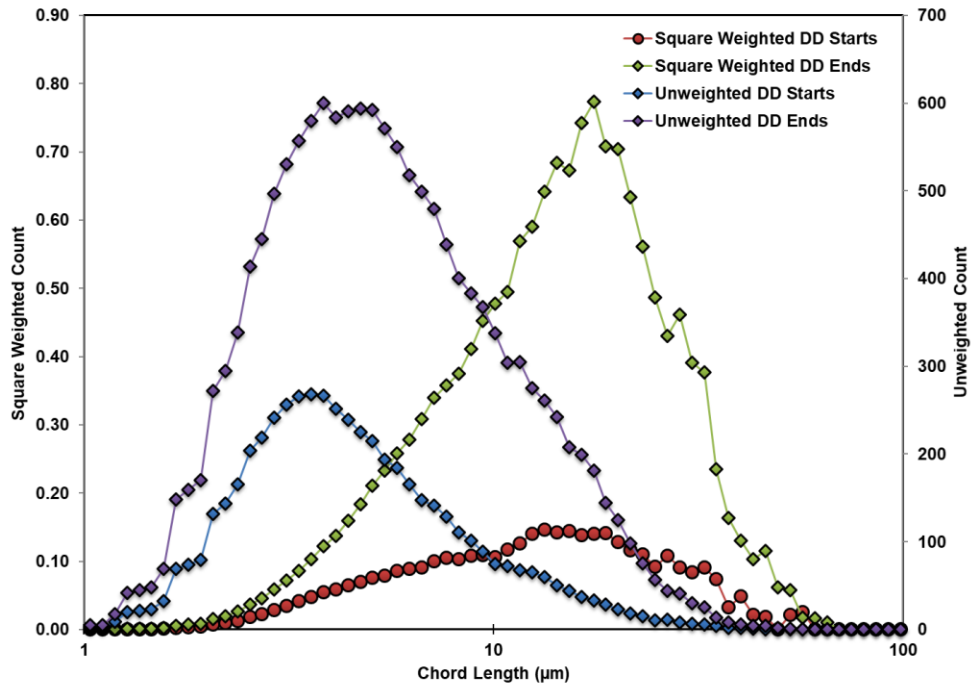


Figure 5-5: Square weighted and unweighted chord length distribution at the beginning and the end of demulsifier dispersion for high BC and high J operating conditions for high-solids froth settling experiment.

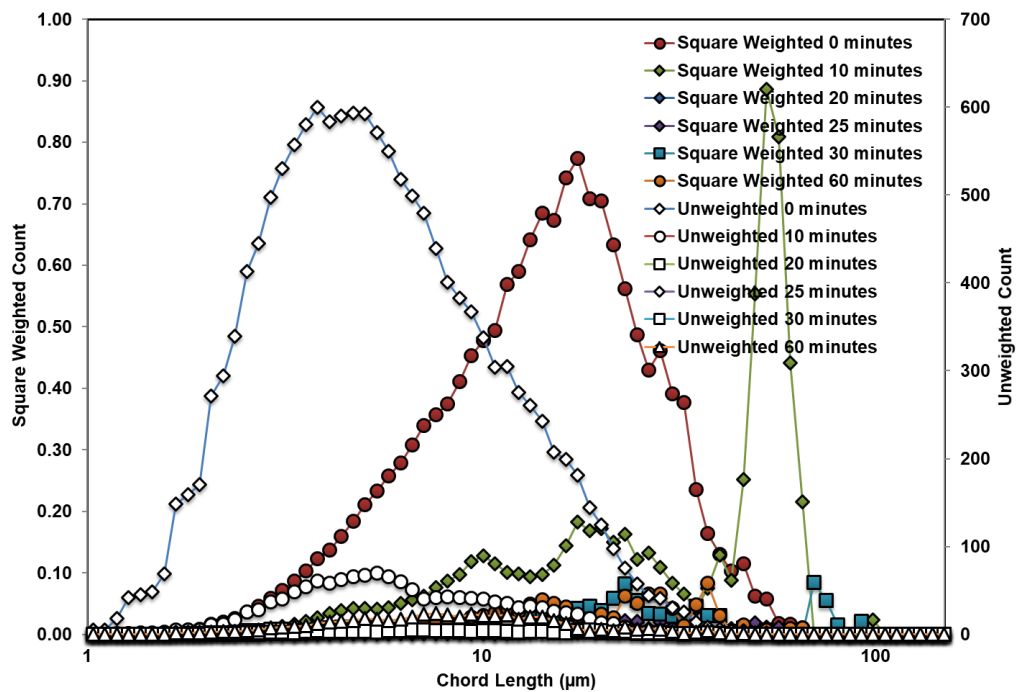




Figure 5-6: Square weighted and unweighted chord length distribution over settling for high BC and high J operating conditions for high-solids froth settling experiment.

Figure 5-4 shows a significant decrease in count during naphtha blending. Figure 5-5 shows a significant increase in count during demulsifier dispersion. Figure 5-6 shows a significant decrease in count after 10 minutes of settling, and an obvious increase in larger drops between 60 $\mu$ m and 80 $\mu$ m. In addition, few changes in counts are observed after 10 minutes until the end.

#### 5.4 High Bulk Concentration and Low Mixing Energy

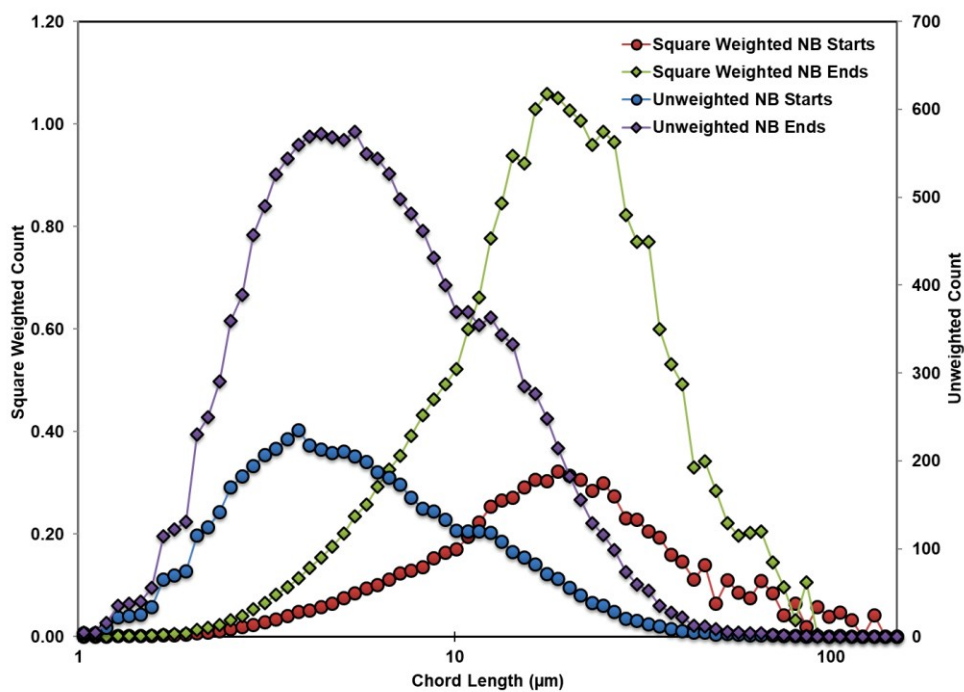


Figure 5-7: Square weighted and unweighted chord length distribution at the beginning and the end of naphtha blending for high BC and low J operating conditions for high-solids froth settling experiment.

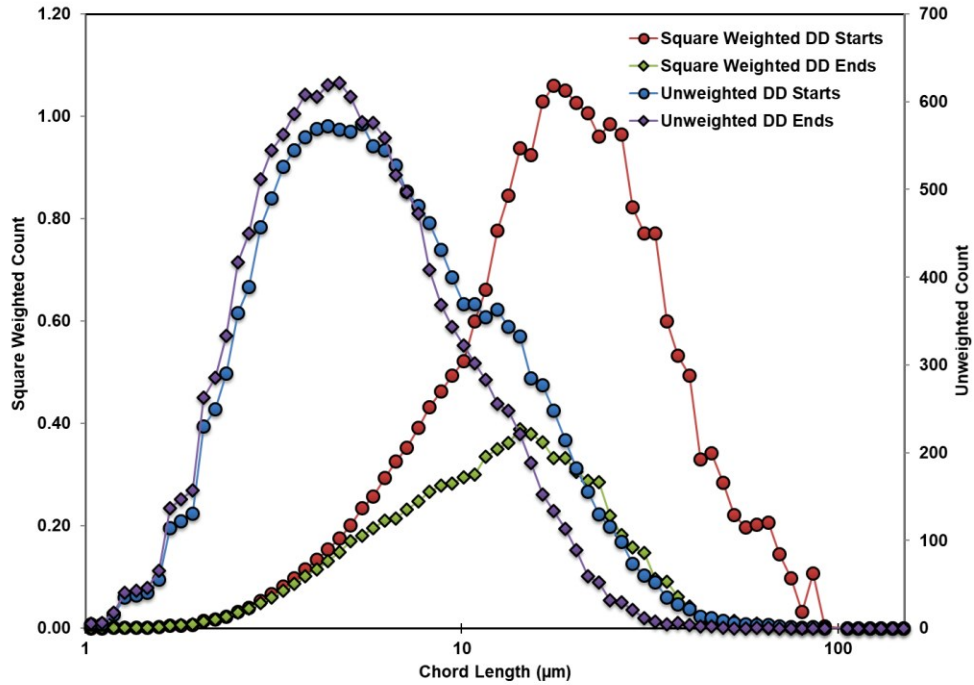


Figure 5-8: Square weighted and unweighted chord length distribution at the beginning and the end of demulsifier dispersion for high BC and low J operating conditions for high-solids froth settling experiment.

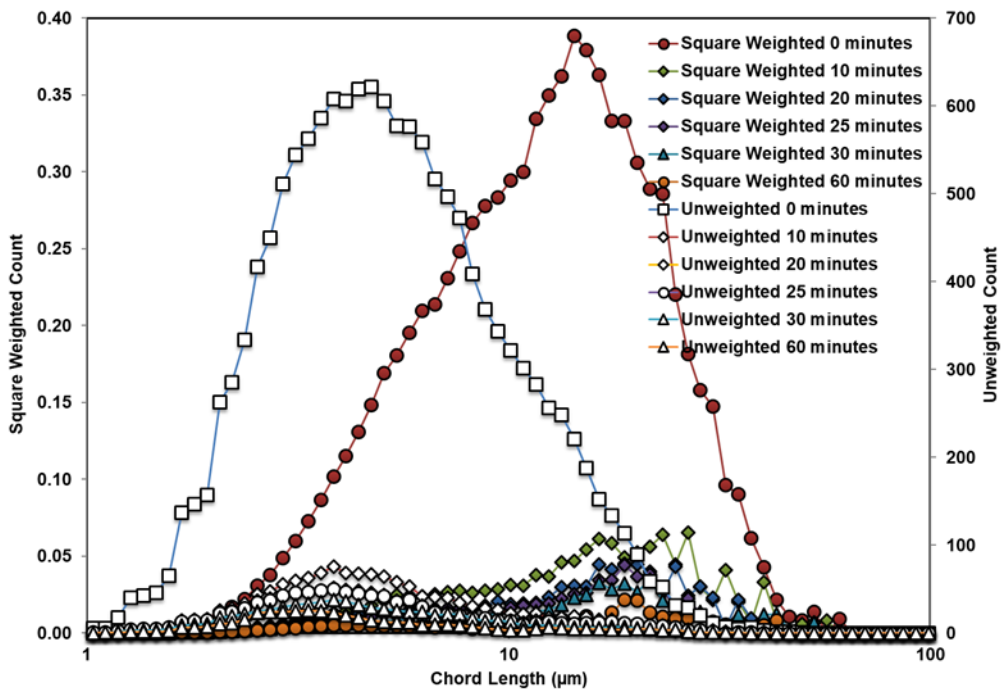


Figure 5-9: Square weighted and unweighted chord length distribution over settling for high BC and low J operating conditions for high-solids froth settling experiment.

Figure 5-7 shows a significant increase in counts during naphtha blending. Figure 5-8 shows a significant decrease in square weighted counts during demulsifier dispersion when considering large particles. Figure 5-9 shows an obvious decrease in count after 10 minutes of settling, but few changes in counts after 10 minutes until the end.

### 5.5 Low Bulk Concentration and High Mixing Energy

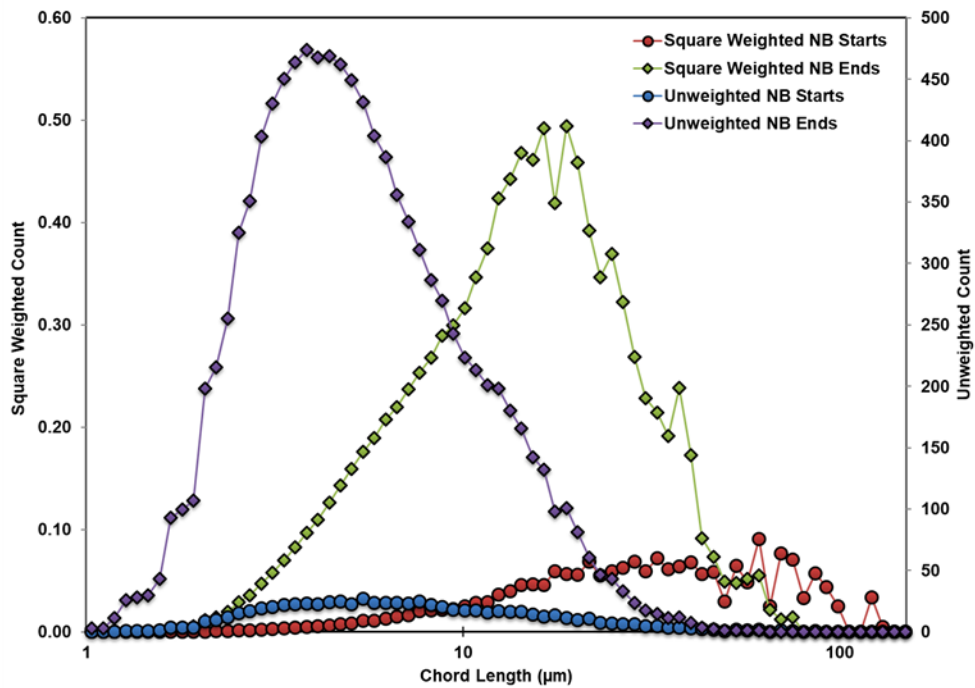


Figure 5-10: Square weighted and unweighted chord length distribution at the beginning and the end of naphtha blending for low BC and high J operating conditions for high-solids froth settling experiment.

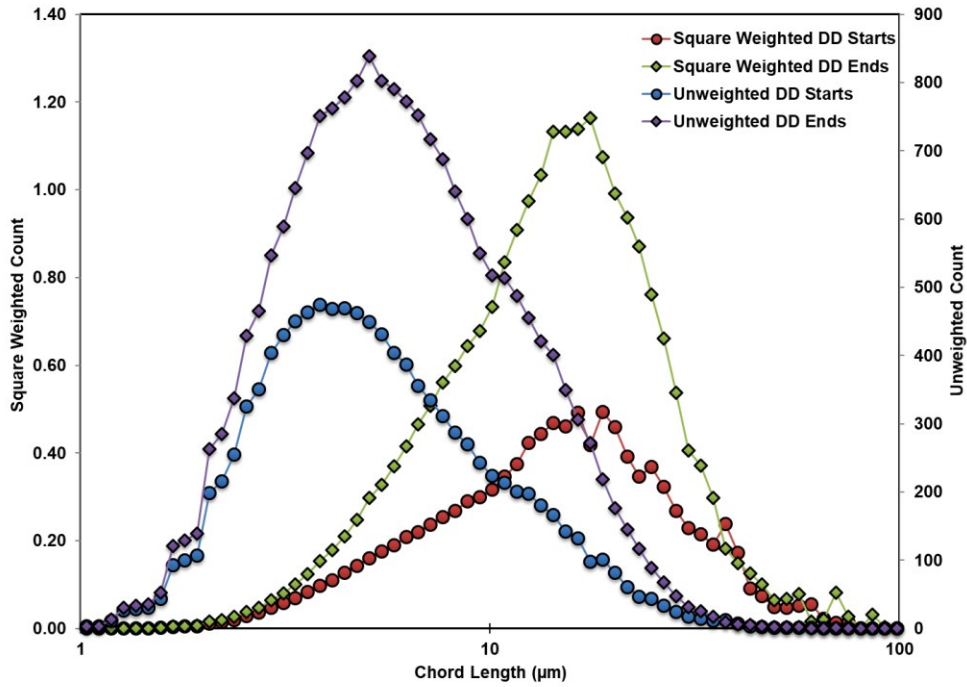


Figure 5-11: Square weighted and unweighted chord length distribution at the beginning and the end of demulsifier dispersion for low BC and high J operating conditions for high-solids froth settling experiment.

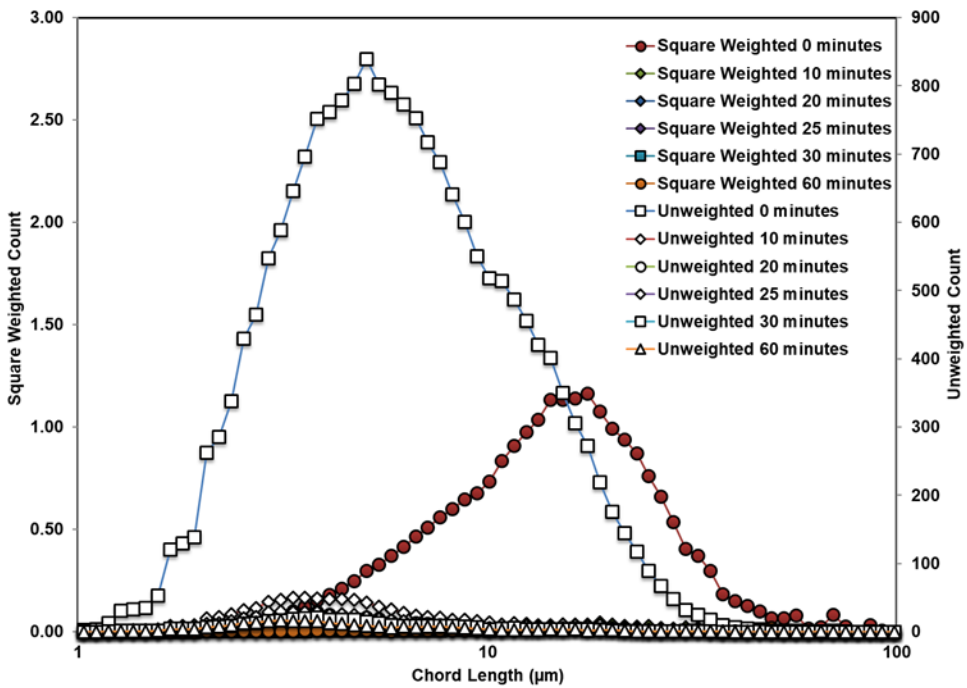


Figure 5-12: Square weighted and unweighted chord length distribution over settling for low BC and high J operating conditions for high-solids froth settling experiment

Figure 5-10 shows a significant increase in count during naphtha blending. Figure 5-11 also shows a significant increase in count during demulsifier dispersion. Figure 5-12 shows a significant decrease in counts after 10 minutes, but few changes until the end.

### 5.6 Square Weighted Data: Comparison at Different Stages

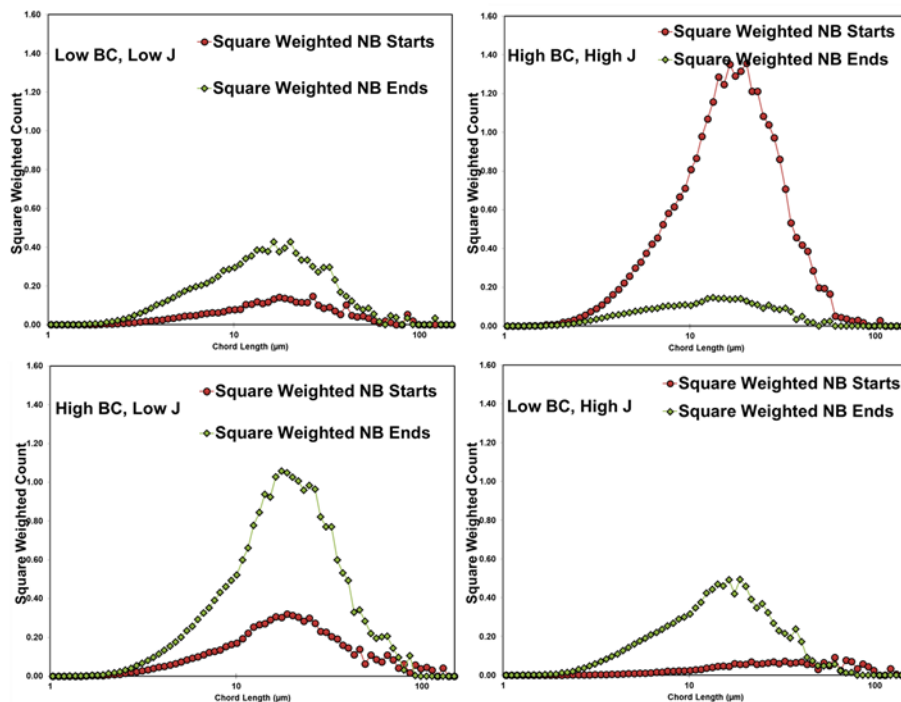


Figure 5-13: Square weighted chord length distributions at the beginning and the end of naphtha blending for four different operating conditions of high-solids froth settling experiment.

From Figure 5-13, except for the high BC and high J operating conditions, all other three operating conditions show an increase in count for drops during naphtha blending. In theory, naphtha blending is where no demulsifier is injected and mixing energy is kept constant, so chord length distribution of different operating conditions are expected to be the same. This is

an unexpected result. The changes of counts may reflect actual changes in the fluid, or they may be either due to the stacking or removing of fluid drops on the probe since fouling index fluctuates once impellers are turned off.

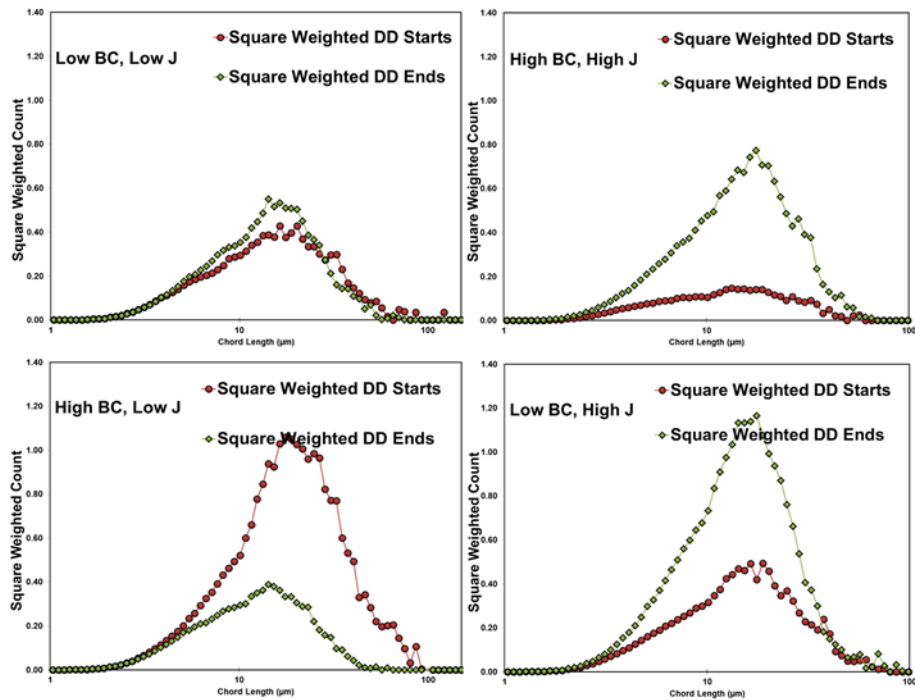


Figure 5-14: Square weighted chord length distributions at the beginning and the end of demulsifier dispersion for four different operating conditions of high-solids froth settling experiment.

From Figure 5-14, except for the high BC and low J operating conditions, the other three operating conditions show an increase in counts of drops but little shifts of chord length during demulsifier dispersion. In theory, because demulsifier dispersion is where a certain amount of demulsifier is injected to help the coalescence and flocculation of water drops and solids, larger drops or flocs are expected to be generated. Hence, the increase in counts can be due to the formation of large loosely-connected water flocs passing the probe, where more separated drops but no single large water drops are detected.

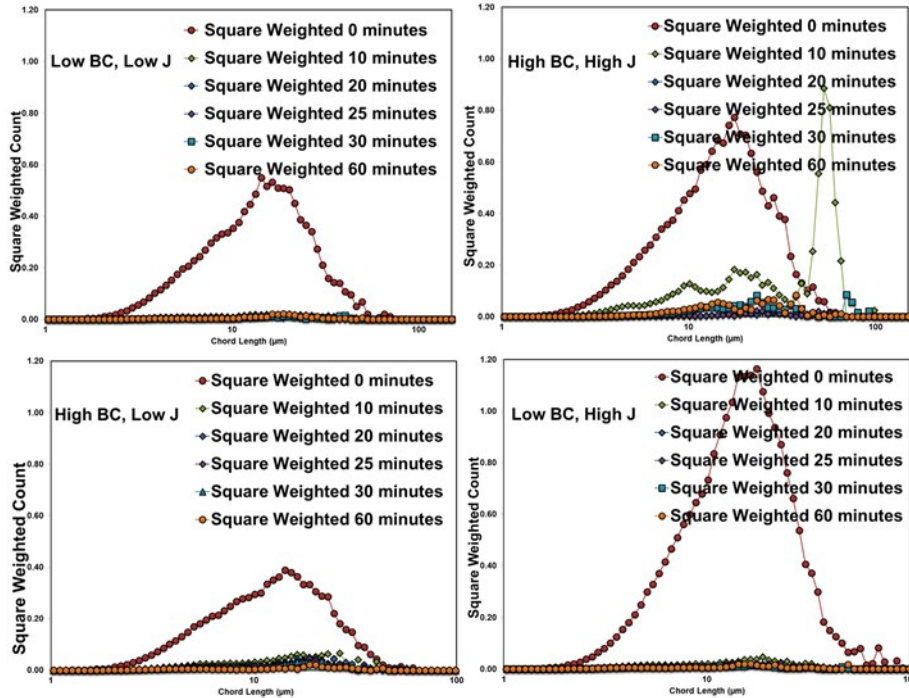


Figure 5-15: Square weighted chord length distributions over settling for four different operating conditions of high-solids froth settling experiment.

Figure 5-15 shows a decrease in counts of particles for all four operating conditions after the first 10 minutes, but few changes of counts are observed after 10 minutes until the end. In addition, the best operating conditions of high BC and high J shows an increase in chord length after the first 10 minutes of settling.

To summarize the above selected FBRM data of high-solid froth settling experiments, some important observations are as follows:

- In general, there is an increase in count during naphtha blending, which can be due to the accumulation of stagnant fluid on the probe surface or due to dispersion of water drops, which is expected.
- In general, an increase in count is observed but without shifts in chord length during demulsifier dispersion. The increase in counts during demulsifier dispersion can be due to the formation of large loosely-connected flocs. The loosely-connected flocs consist of many separate water drops, which are detected by the probe as individual water drop.

Since no coalescence happens, no larger water drops are detected. Hence, no shift in chord length can be observed.

- Most of the count changes happen in the first 10 minutes of settling. The best operating conditions: high BC and high J show an obvious increase in drop size, which can be due to the formation of larger drops during settling.

When considering the KF data, the FBRM data is expected to have few changes during the first 25 minutes since an induction time is observed. It can be explained that the probe surface has an accumulation of stagnant fluid. Since the FRBM application to froth dewatering is a relatively new method, microscope images were also collected and analyzed in order to further understand the settling behavior of water and solids in different froths.



# **Chapter 6: Analysis of Microscope Images of Bitumen Froth with Different Qualities Using a Mixed Approach: Qualitative and Quantitative Methods**

Microscope images of settling experiments for bitumen froth with different qualities were analyzed using a mixed qualitative and quantitative method (Xu and Saraka, 2017). This method was first developed based on the 10x microscope images of average-quality and high-water froths and was then adapted for high-solids froth. By using this mixed method, microscope images of these three froths can be compared using the same baseline to gain some insights into separation mechanisms in all three froths.

## **6.1 Capturing Microscope Images for High-Water Froth Settling**

The microscope images of average-quality froth were taken based on the following instructions (Arora, 2016): (1) images are taken according to the sampling schedule developed for average-quality froth (2) images are evenly spaced out on each microscope slide, sweeping from left to right and top to the bottom (3) roughly 15 microscope images are taken at 10x to obtain an overview on the slide, and around 50 images are taken at 40x to obtain more detail on different spots. This image capture protocol was first developed for average-quality froth and was applied in high-water froth with little change. No microscope images were taken at the lowest height, Z4, for high-water froth, since these images are mostly jammed with free water and are not useful for analysis. In the end, there were approximately 15 microscope images taken at 10x and around 50 images taken at 40x for high-water froth from height Z1 to height Z3.

## 6.2 Mixed Approach to Analyze 10x Microscope Images

Compared to average-quality froth, a great amount of free water is observed on both the 10x and 40x images of high-water froth. The MATLAB algorithm developed by Nitin Arora to quantitatively capture spherical water drops on the 40x images of average-quality froth can only be applied on some of the 40x images for high-water froth, since most of the 40x images are occupied by free water, which makes the edges of spherical water drops too blurred to be recognized by the algorithm. In general, free water instead of spherical water drops are dominant on the images of high-water froth, such as small free water, large free water, small free water flocs and large free water flocs.

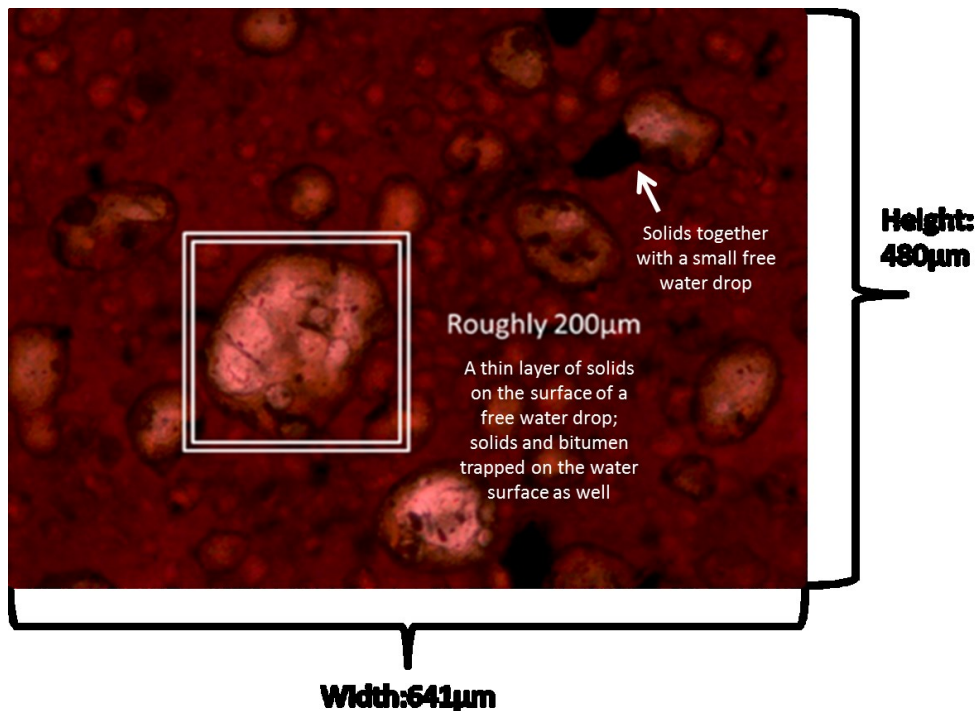


Figure 6-1: Estimation of the size of a single small free water drop observed on the 10x microscope image for the high-water froth. Experiment was run at good mixing conditions (high J and low IC) at BC = 200 ppm.

Figure 6-1 shows that the diameter of a small free water drop observed in high-water froth is approximately 200 µm. (Rao and Liu, 2013) has defined that any water drops bigger than 60 µm

are considered as free water. In this case, the free water drop observed in high-water froth is much bigger than the criteria defined in this research.

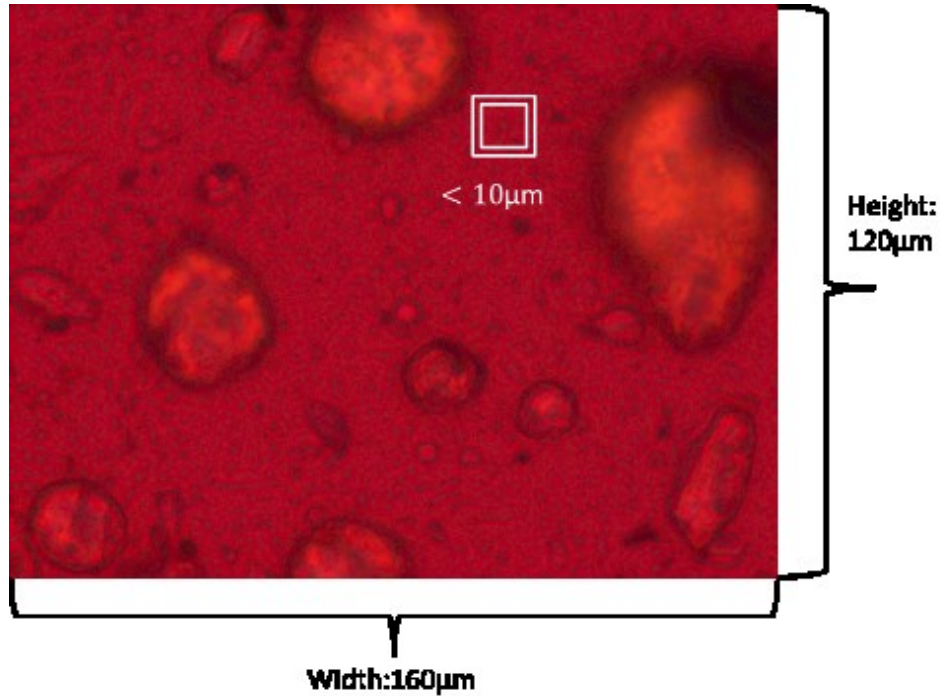


Figure 6-2: Estimation of the size of a single spherical water drop observed on the 40x microscope image for the high-water froth. Experiment was run at good mixing conditions (high J and low IC) at BC = 200 ppm.

Figure 6-2 shows that the diameter of a small spherical water drop observed in high-water froth is approximately  $<10\mu\text{m}$ . Although 40x images of different slides do not show a clear difference since they are usually jammed with free water, there are enough differences in water structures on 10x images between high-water and average-quality froth. Hence, 10x images are analyzed both qualitatively and quantitatively to understand the settling dynamics of each froth.

There are two steps to apply this mixed method. First, the qualitative approach is to review all of the 10x microscope images and pick a group of the most representative images. Second, the quantitative approach is to count the 10x microscope images which show similar water

structures and water coverage on the slide. The % of occurrence is calculated through the equation as follows:

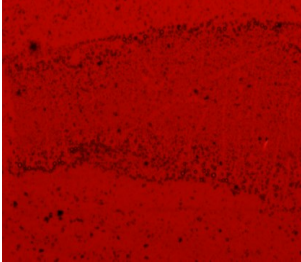
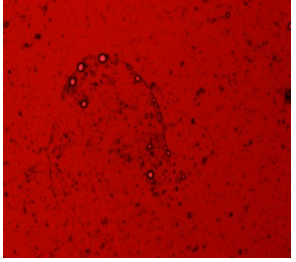
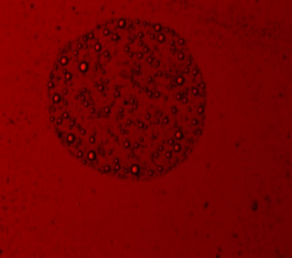
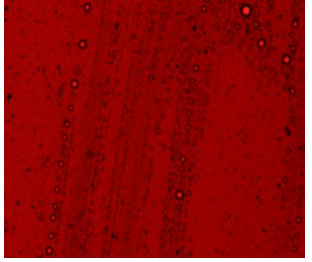
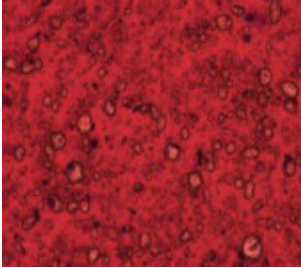
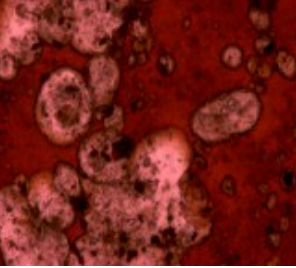
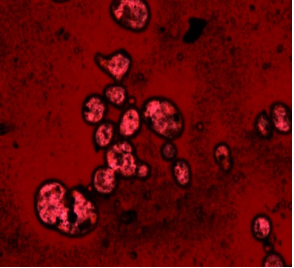
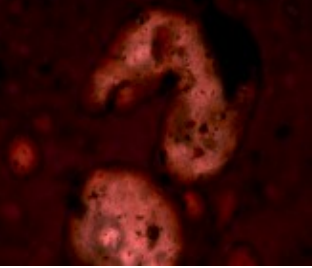
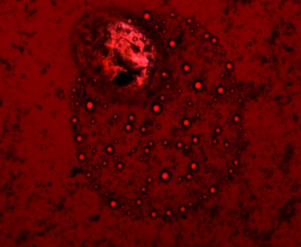
$$\% = \frac{\text{the number of 10x microscope images which are similar to the representative image}}{\text{the total number of 10x microscope images taken}}$$

Although the process of picking the most representative image can be subjective, the % of occurrence gives confidence in this image to some extent that it can represent the settling behavior of the froth at a certain settling height and certain settling time. By using this mixed method, the microscope images of high-water froth and average-quality froth can be compared both qualitatively and quantitatively by using a single representative 10x microscope image.

### 6.3 Microscope Analysis of High-Water and Average-Quality Froth

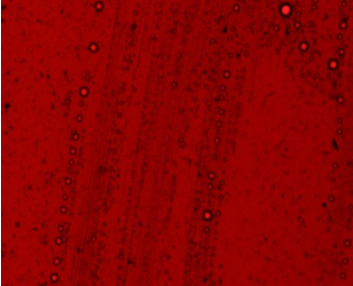
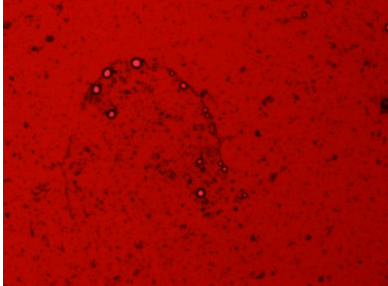
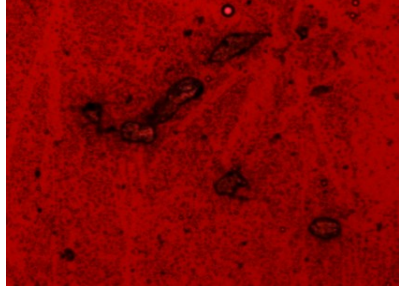
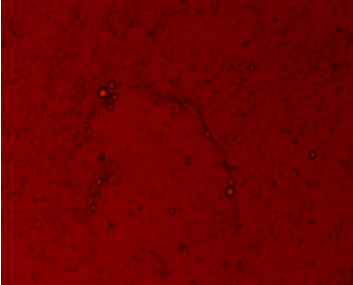
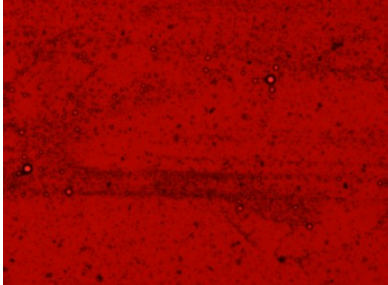

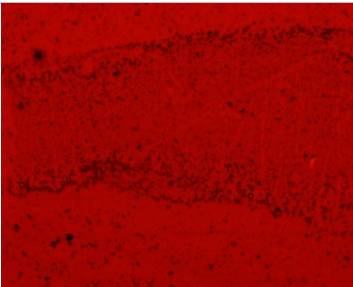
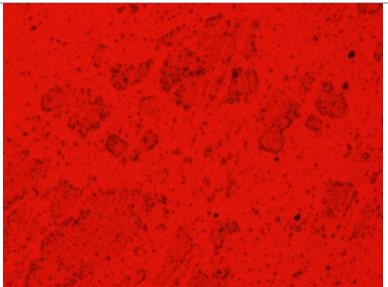
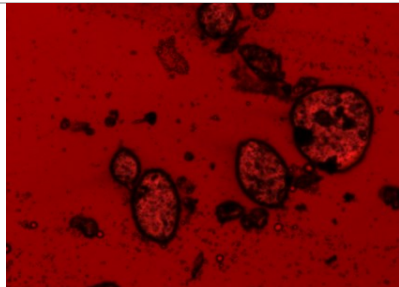
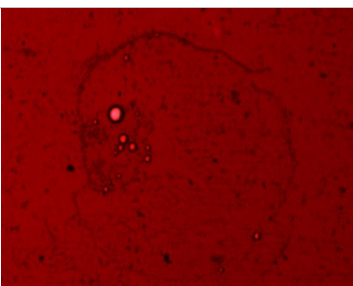
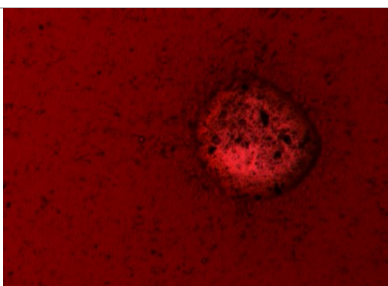
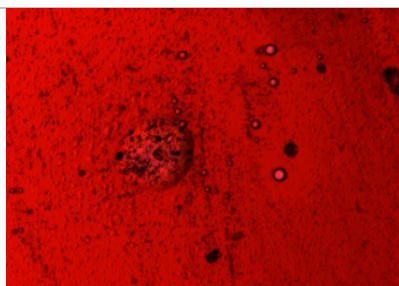
Table 6-1 shows the representative water structures observed in these two different froths. Overall, many small spherical water drops are observed in average-quality froth. Free water is also observed but is not dominant. By contrast, a great amount of free water and free water flocs are observed in high-water froth.

Table 6-1: Possible water structures observed on the 10x microscope images of average-quality and high-water froth during settling.

Structures made of spherical water drops with sharp edges in average froth				
Structures made of free water with irregular surface in high-water froth				
Combined Structure in average froth				

As shown from Table 6-2 to Table 6-5, many spherical water drops are observed in average-quality froth under different mixing conditions. In addition, a thin layer of solids at the surface of water is observed. In general, most of the large free water disappears on the images after 10 minutes at height Z1.

Table 6-2: Representative 10x microscope images of average-quality froth experiments with operating conditions: low mixing energy (-) and low injection rate (-).

Experimental Code	Sampling Height Z1	Sampling Height Z2	Sampling Height Z3
3 minutes			
Occurrence (%)	92%	92%	81%
5 minutes			
Occurrence (%)	91%	85%	75%
7 minutes			
Occurrence (%)	89%	95%	76%
10 minutes			
Occurrence (%)	71%	74%	68%


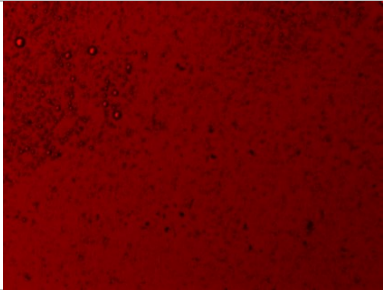
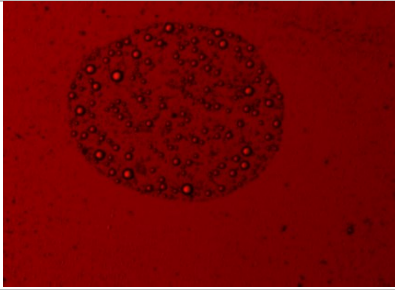
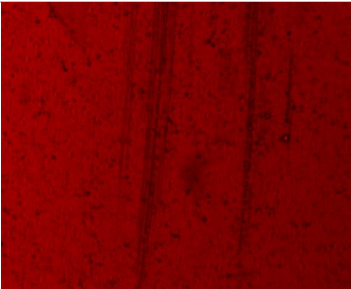
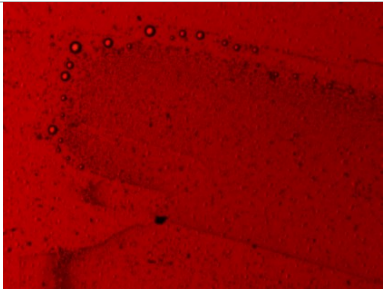
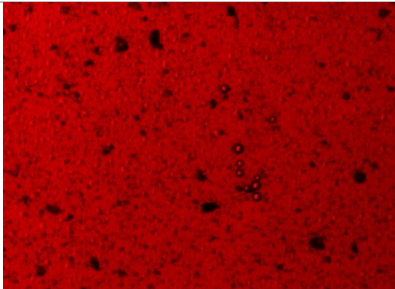
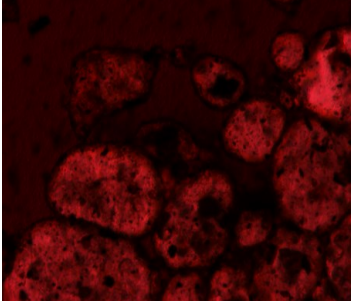

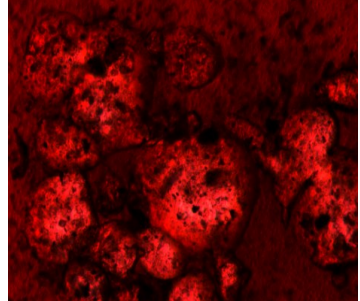
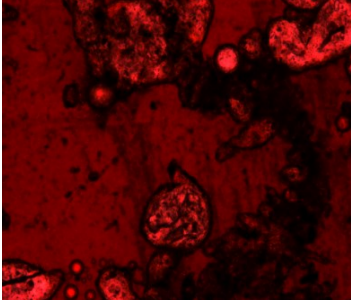
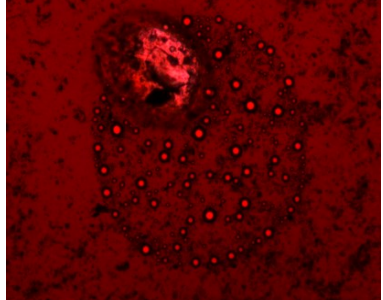
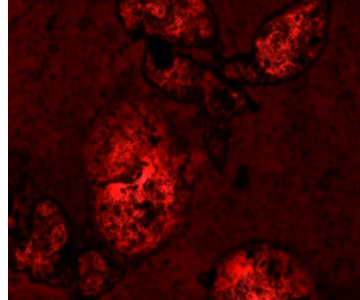
30 minutes			
Occurrence (%)	80%	82%	78%
60 minutes			
Occurrence (%)	76%	93%	69%

Table 6-3: Representative 10x microscope images of average-quality froth experiments with operating conditions: high mixing energy (+) and low injection rate (-).

Experimental Code	Sampling Height Z1	Sampling Height Z2	Sampling Height Z3
3 minutes			
Occurrence (%)	80%	85%	76%
5 minutes			
Occurrence (%)	79%	56%	69%

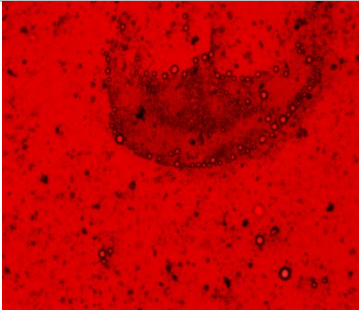
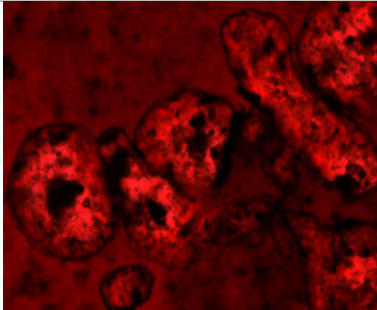
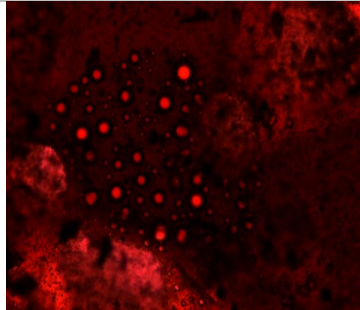
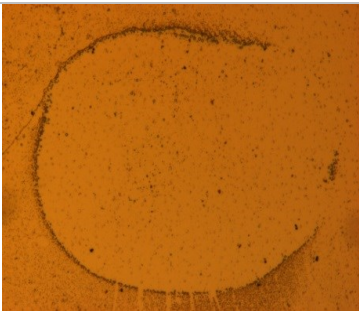
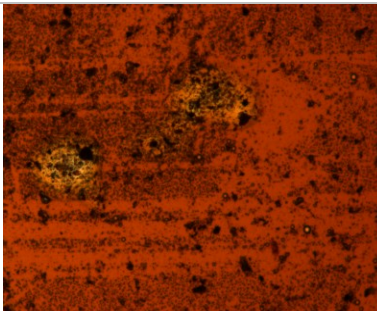
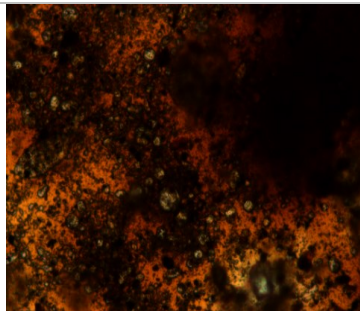
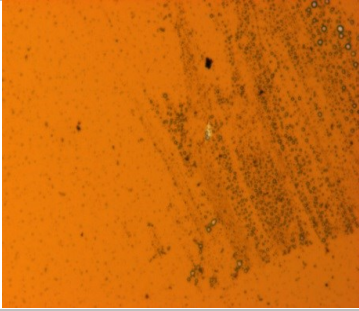
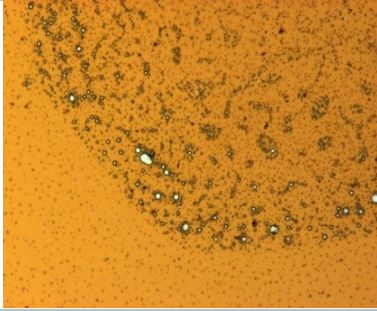
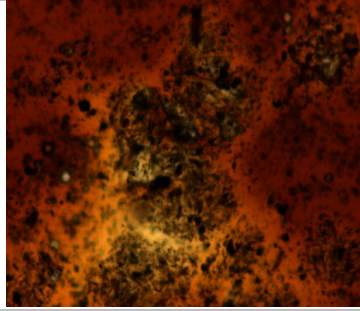
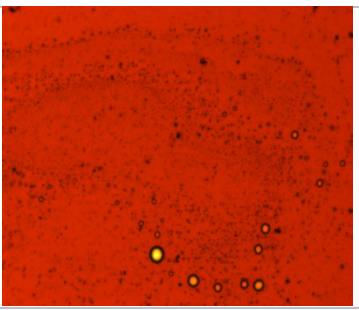
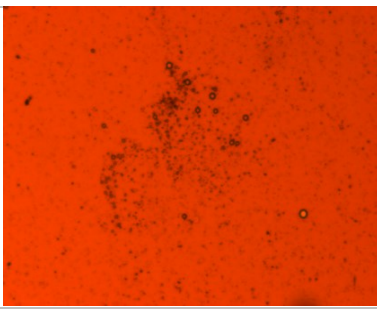
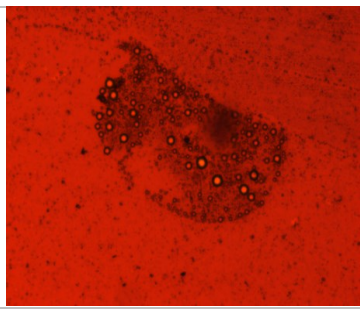
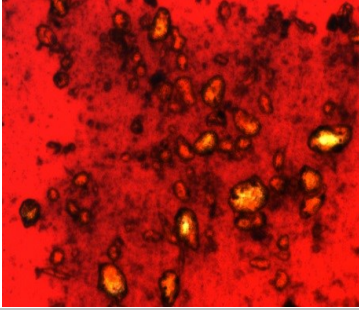
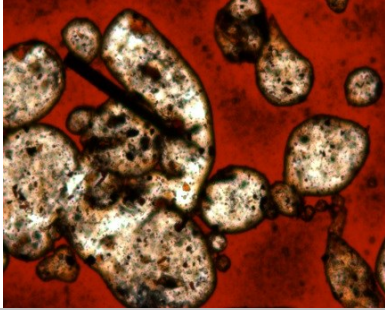
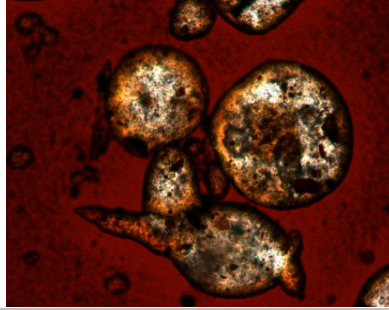
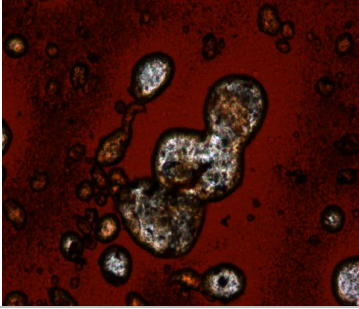
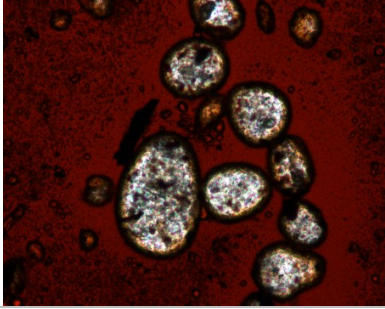
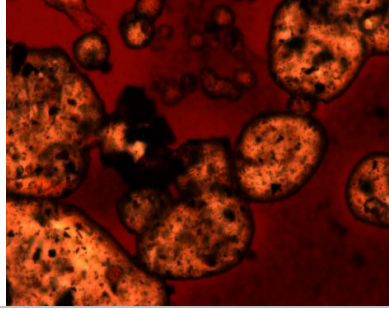
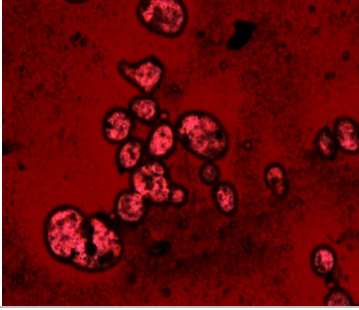
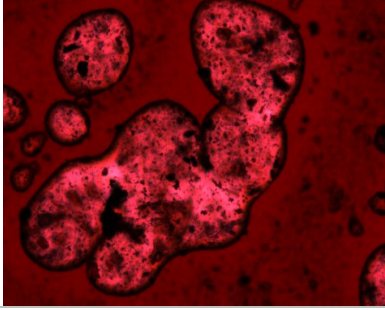
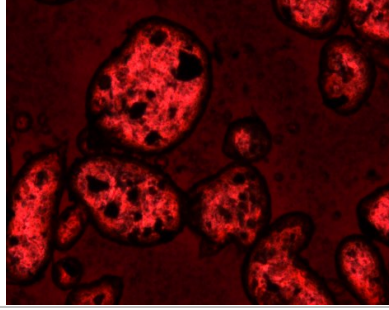
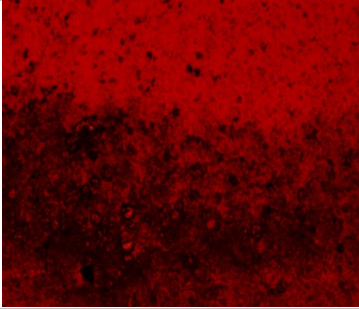
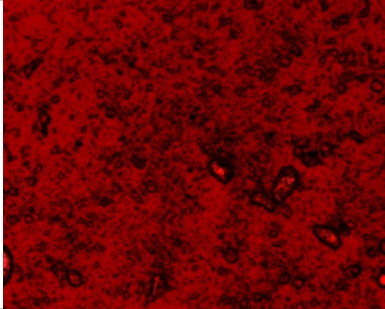
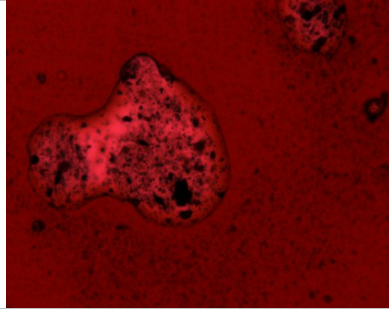
7 minutes			
Occurrence (%)	81%	86%	91%
10 minutes			
Occurrence (%)	71%	100%	90%
30 minutes			
Occurrence (%)	77%	67%	61%
60 minutes			
Occurrence (%)	63%	82%	70%



Table 6-4: Representative 10x microscope images of average-quality froth experiments with operating conditions: low mixing energy (-) and high injection rate (+).

Experimental Code	Sampling Height Z1	Sampling Height Z2	Sampling Height Z3
3 minutes			
Occurrence (%)	89%	67%	72%
5 minutes			
Occurrence (%)	84%	57%	93%
7 minutes			
Occurrence (%)	91%	88%	89%
10 minutes			
Occurrence (%)	77%	94%	72%

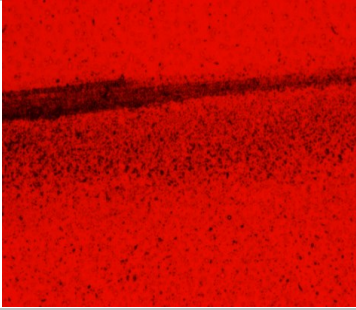
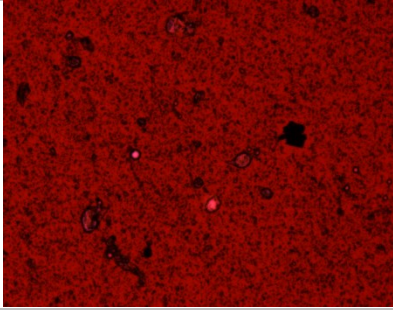
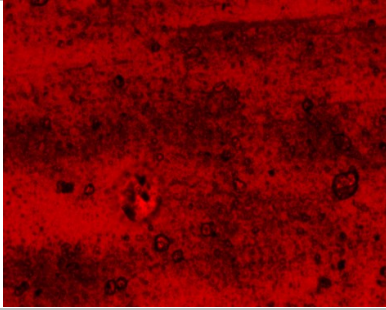
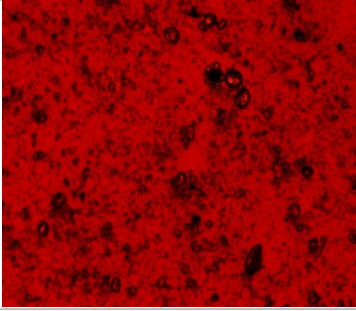
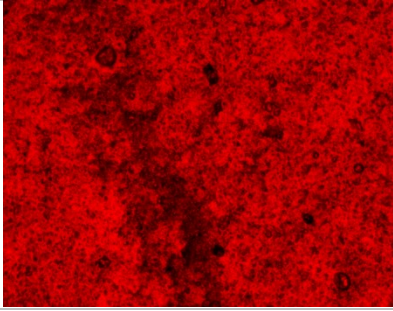
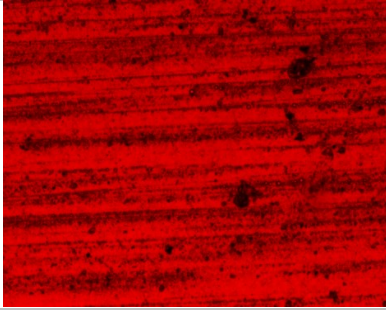
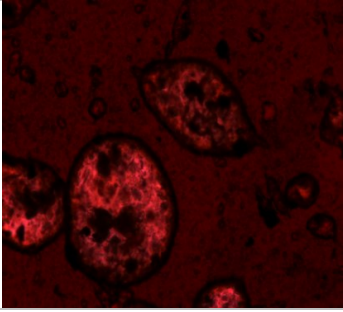
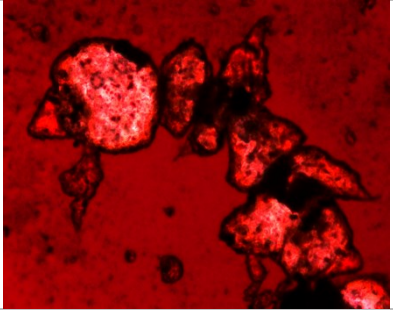
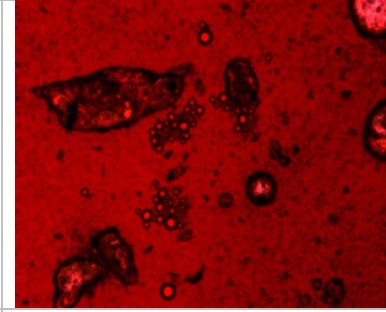
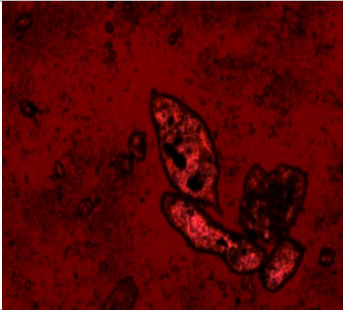
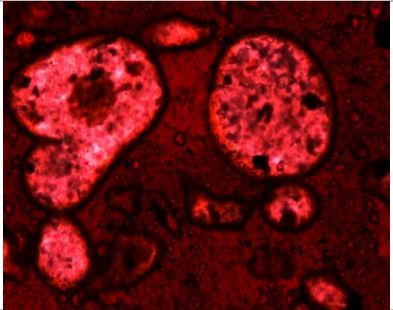
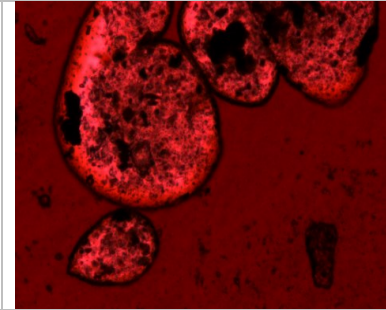
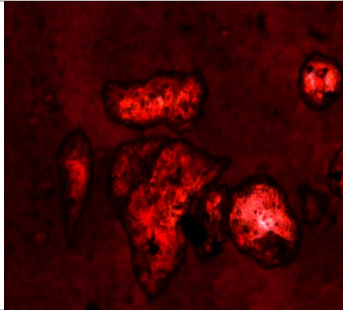
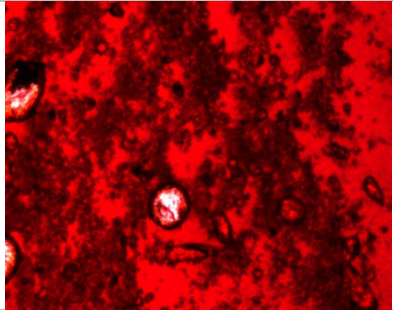
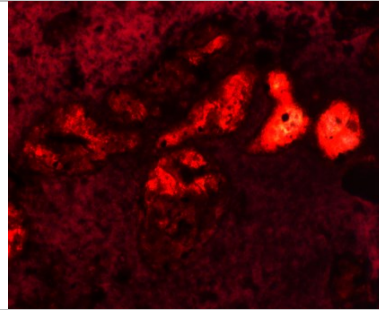
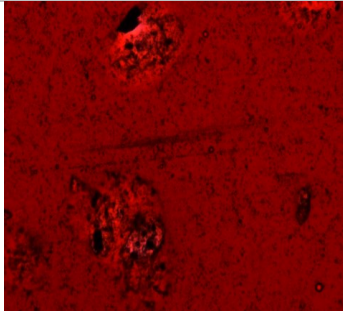
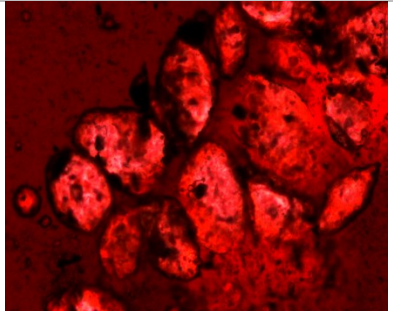
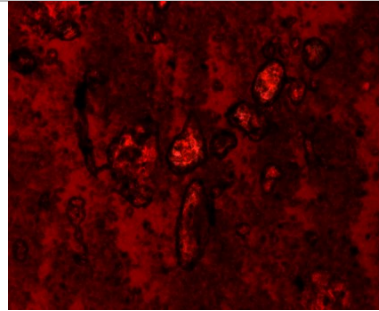
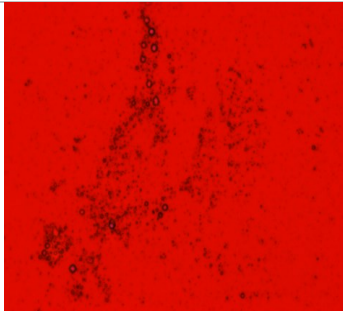
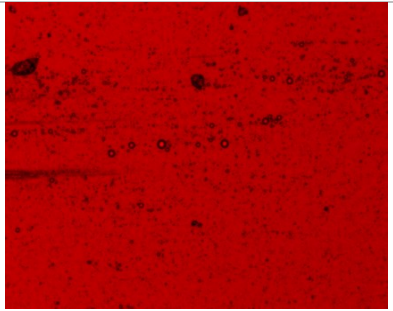
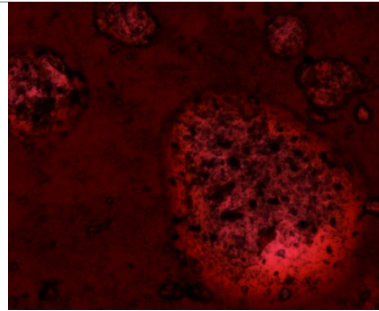
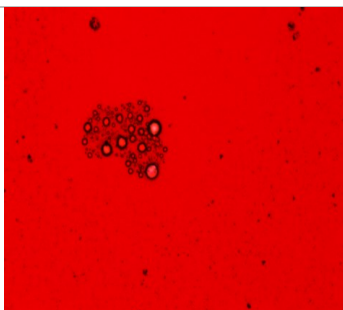
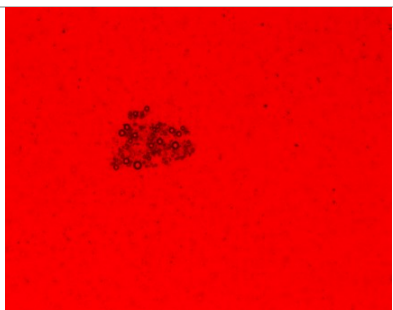
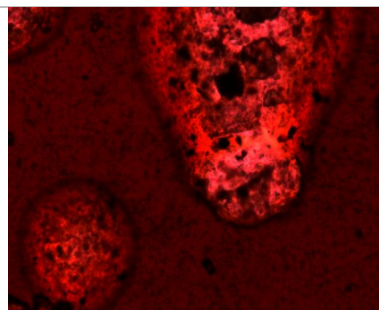
30 minutes			
Occurrence (%)	79%	91%	100%
60 minutes			
Occurrence (%)	100%	100%	100%

Table 6-5: Representative 10x microscope images of average-quality froth experiments with operating conditions: high mixing energy (+) and high injection rate (+).

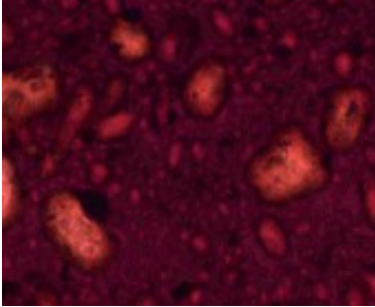
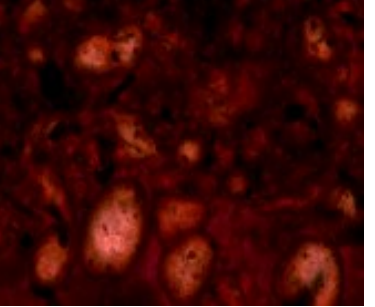
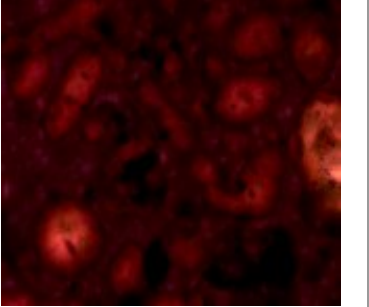
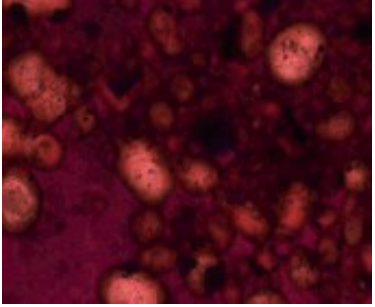
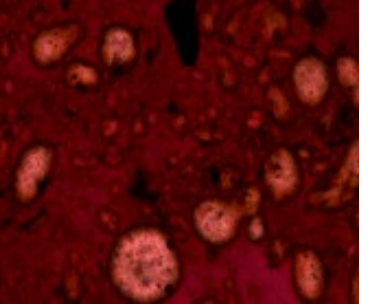
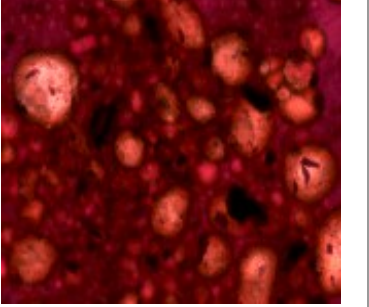
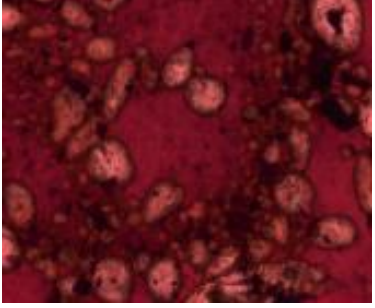
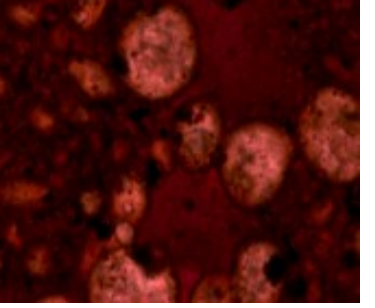
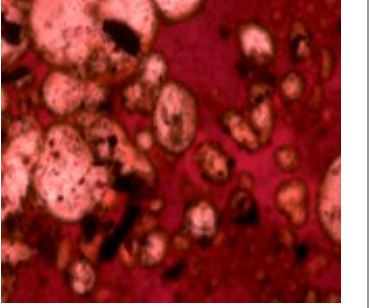
Experimental Code	Sampling Height Z1	Sampling Height Z2	Sampling Height Z3
3 minutes			
Occurrence (%)	82%	74%	94%
5 minutes			
Occurrence (%)	84%	74%	70%

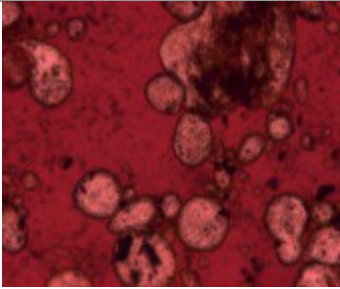
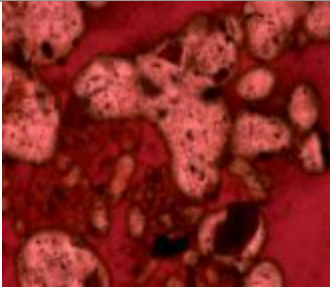
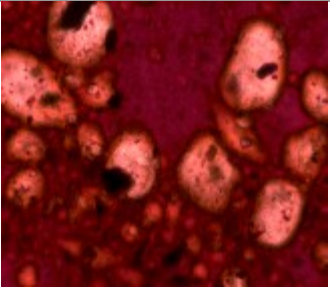
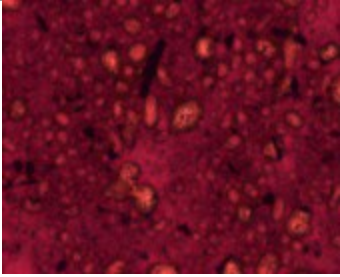
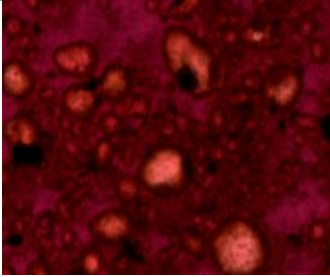
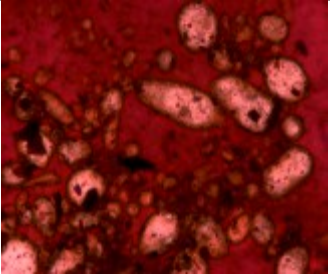
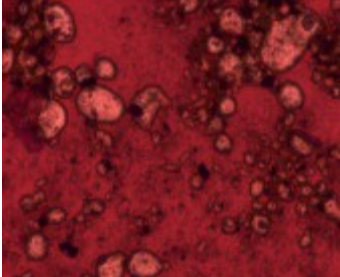
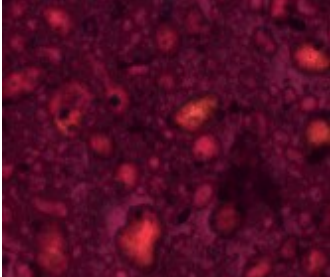
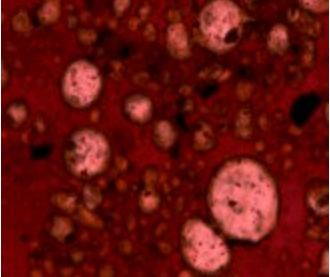
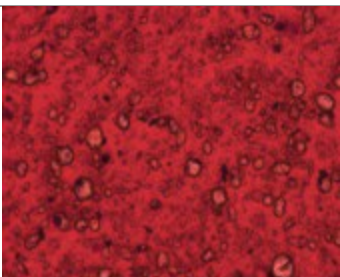
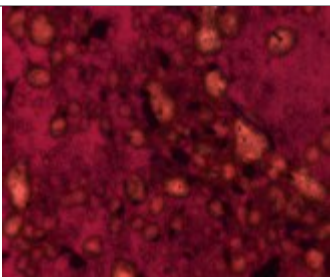
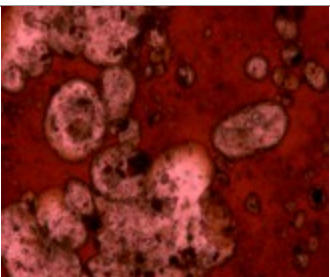
7 minutes			
Occurrence (%)	71%	82%	80%
10 minutes			
Occurrence (%)	82%	100%	74%
30 minutes			
Occurrence (%)	94%	88%	75%
60 minutes			
Occurrence (%)	58%	67%	70%

As shown from Table 6-6 to Table 6-9, free water rather than spherical water drops is dominant in high-water froth under different mixing conditions. In general, the microscope images of height Z1, Z2, and Z3 are mostly packed with water during induction time of approximately 30

minutes at height Z1. Height Z2 is also packed with free water for approximately 45 minutes, and height Z3 is packed with free water throughout settling.

Table 6-6: Representative 10x microscope images of high-water froth experiments with operating conditions: low mixing energy (-) and low injection rate (-).

Settling Time	Sampling Height Z1	Sampling Height Z2	Sampling Height Z3
5 minutes			
Occurrence (%)	75	100	94
10 minutes			
Occurrence (%)	94	100	100
15 minutes			
Occurrence (%)	81	56	100

20 minutes			
Occurrence (%)	94	63	94
25 minutes			
Occurrence (%)	100	90	94
30 minutes			
Occurrence (%)	100	94	100
45 minutes			
Occurrence (%)	88	100	88

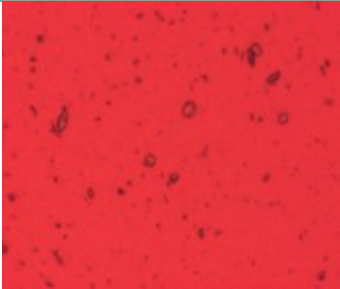
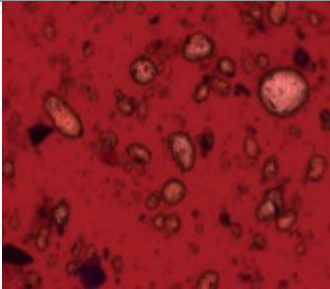
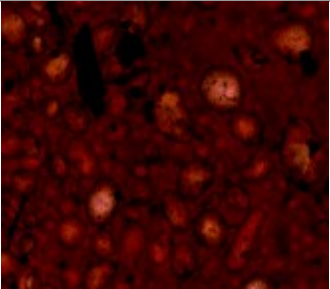
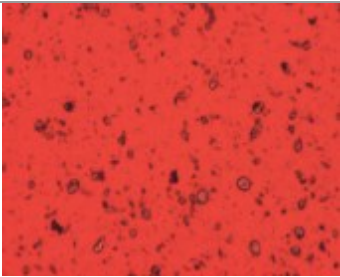
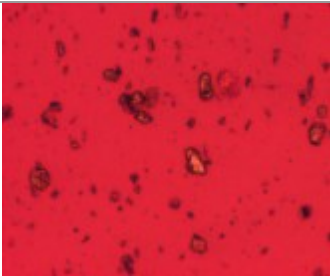
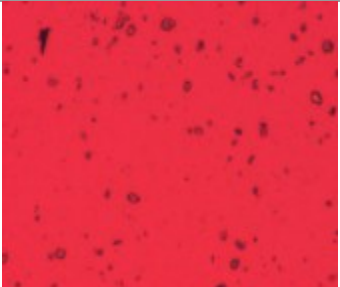

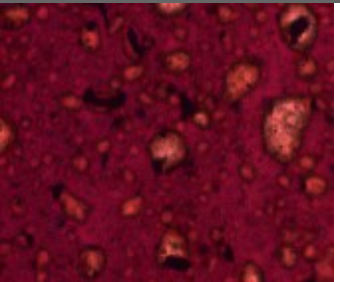
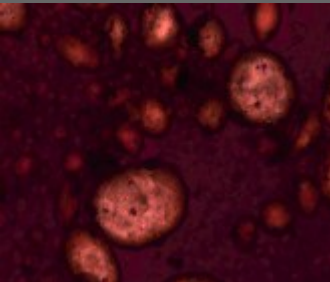
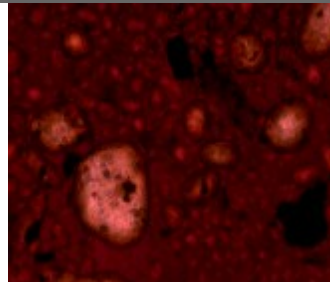
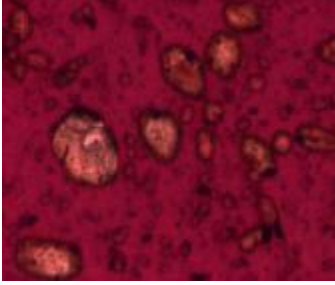
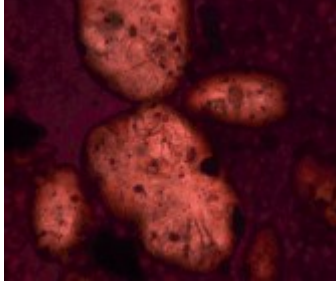
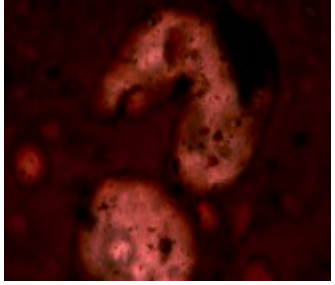
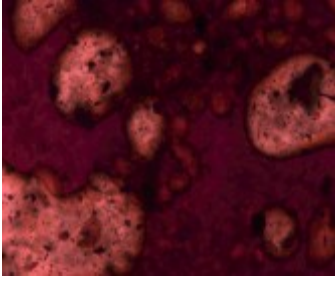
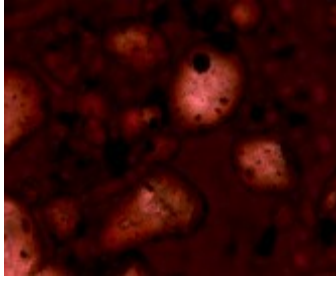
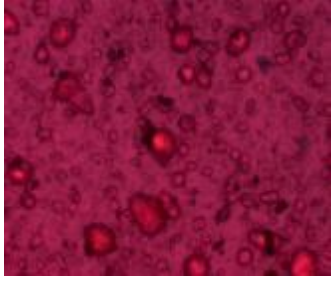
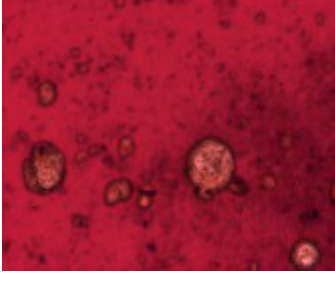
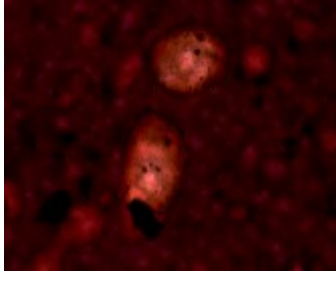
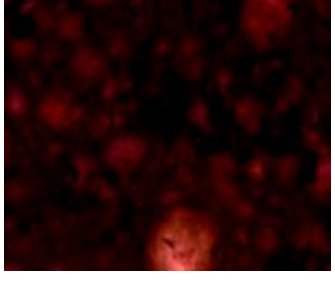
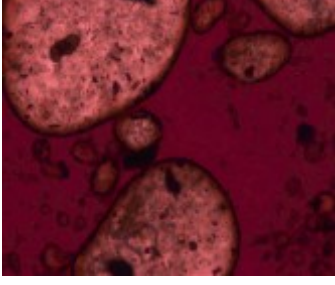
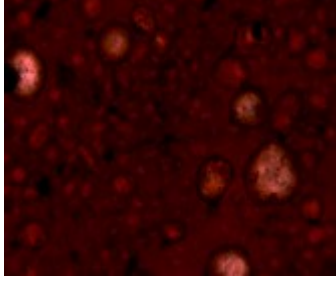
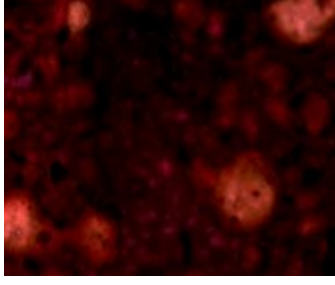
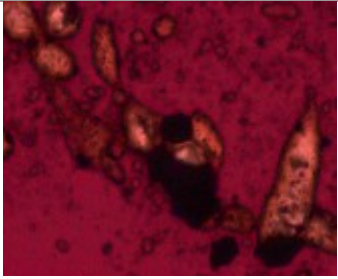
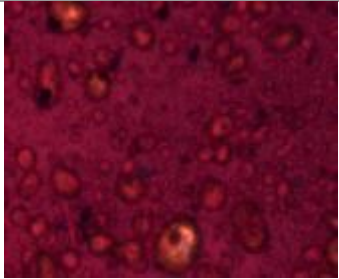
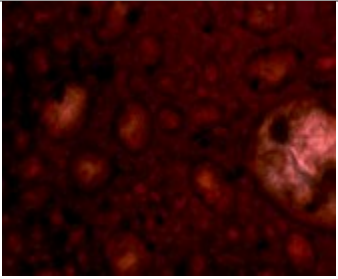
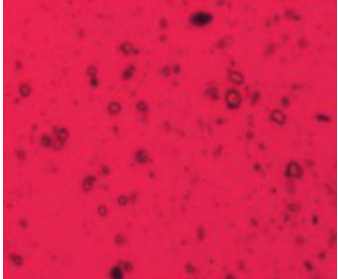
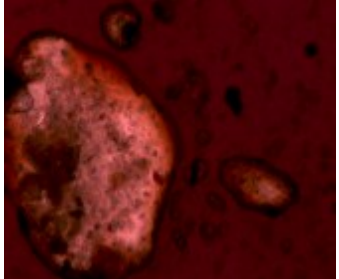


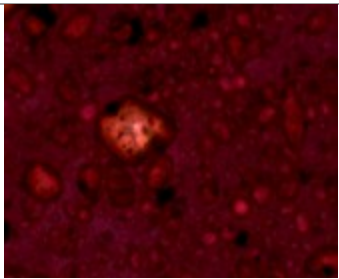
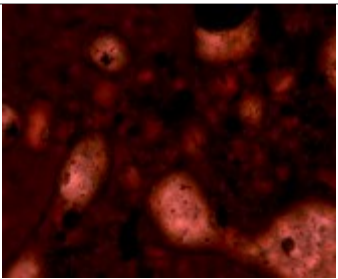

60 minutes			
Occurrence (%)	89	94	100
90 minutes			NA
Occurrence (%)	100	67	
120 minutes			NA
Occurrence (%)	93	100	

Table 6-7: Representative 10x microscope images of high-water froth experiments with less optimal mixing conditions: high mixing energy (+) and low injection rate (-).

Settling Time	Sampling Height Z1	Sampling Height Z2	Sampling Height Z3
5 minutes			

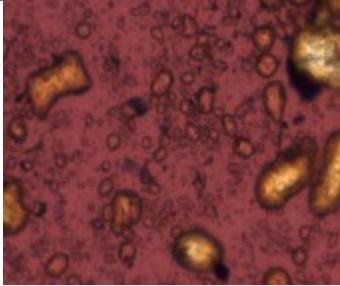
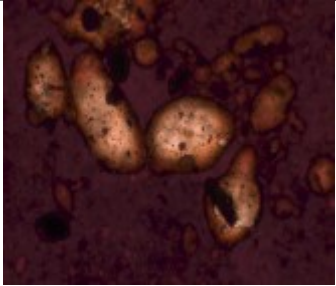
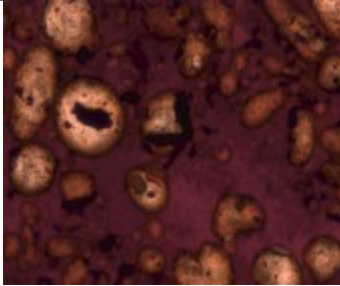
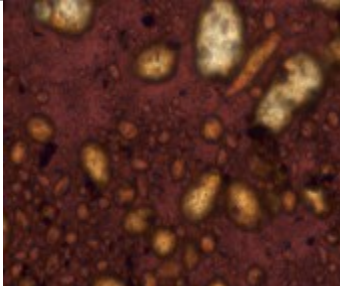
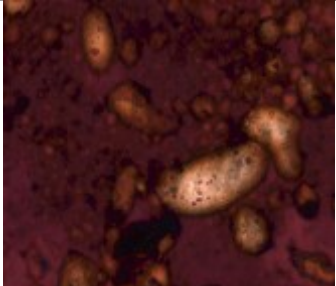
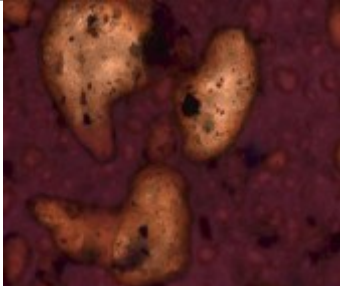
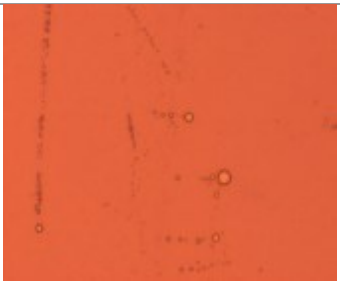
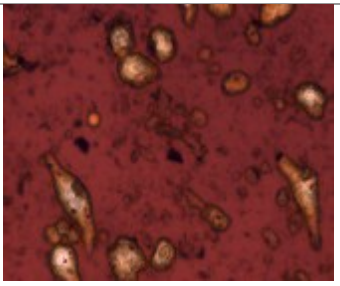
Occurrence (%)	86	53	83
10 minutes			
Occurrence (%)	53	87	100
15 minutes			
Occurrence (%)	100	100	50
20 minutes			
Occurrence (%)	50	93	100
25 minutes			
Occurrence (%)	75	73	100

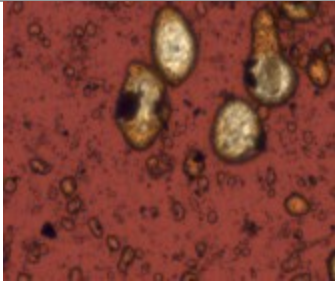
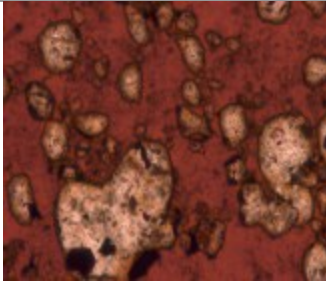
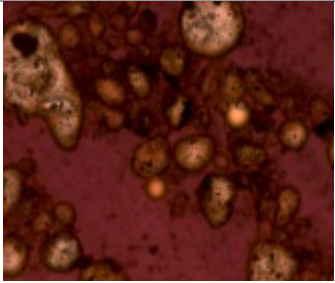
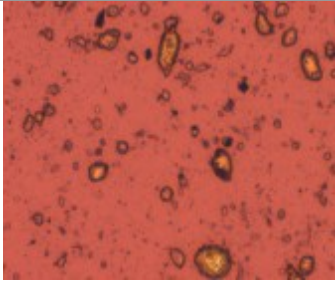
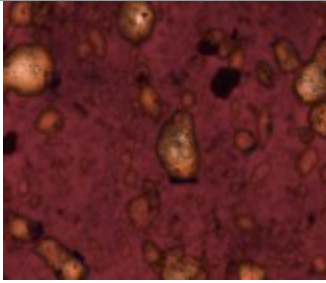
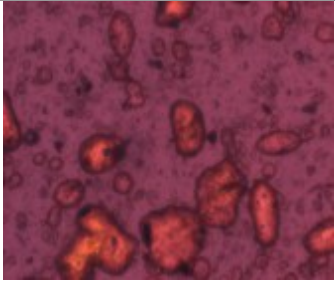
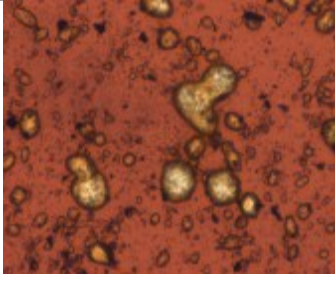
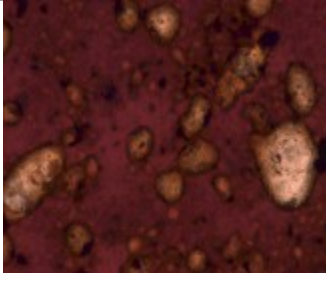
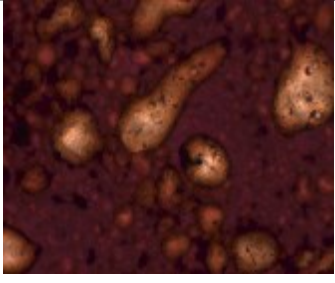
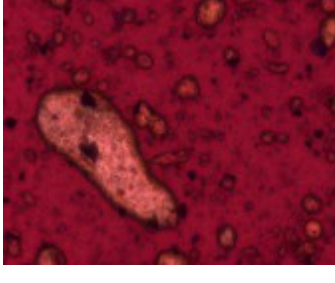
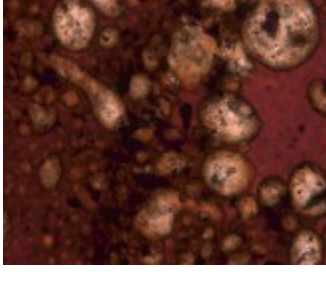
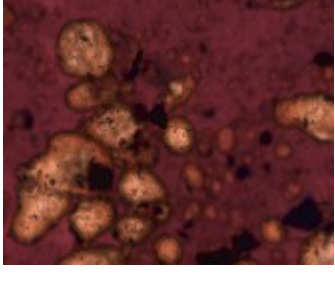
30 minutes			
Occurrence (%)	75	71	92
45 minutes			
Occurrence (%)	92	73	100
60 minutes			
Occurrence (%)	100	20	100
90 minutes		NA	NA
Occurrence (%)	100		



120 minutes		NA	NA
Occurrence (%)	100		

Table 6-8: Representative 10x microscope images of high-water froth experiments with less optimal mixing conditions: low mixing energy (-) and high injection rate (+).

Settling Time	Sampling Height Z1	Sampling Height Z2	Sampling Height Z3
5 minutes			
Occurrence (%)	83	100	100
10 minutes			
Occurrence (%)	100	100	87
15 minutes		NA	
Occurrence (%)	100		86

20 minutes			
Occurrence (%)	100	100	100
25 minutes			
Occurrence (%)	92	100	79
30 minutes			
Occurrence (%)	100	100	100
45 minutes			
Occurrence (%)	92	100	100

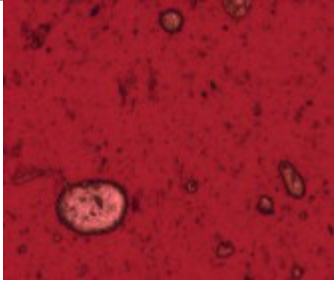
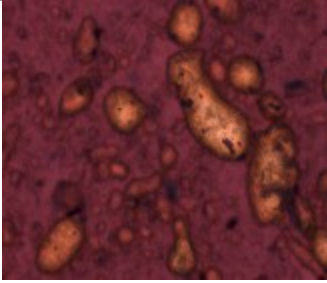
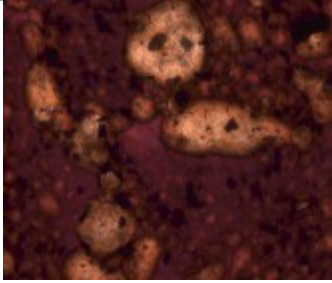
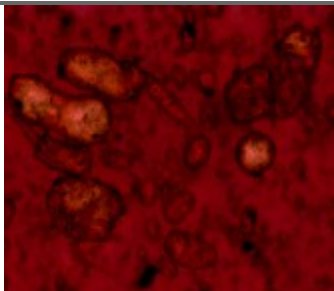
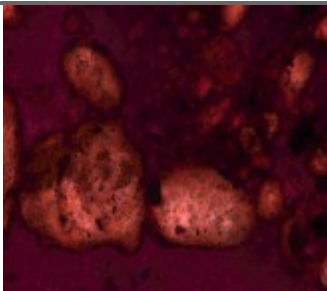
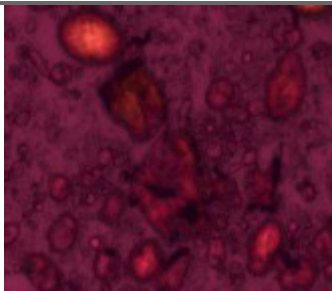
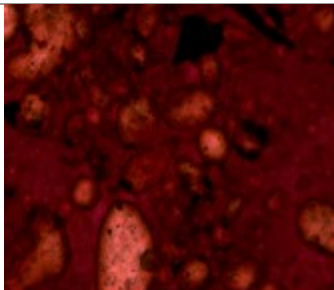
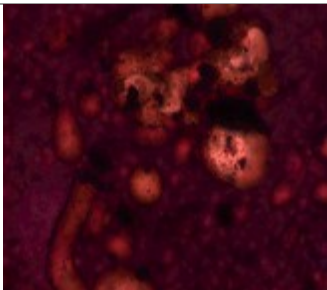
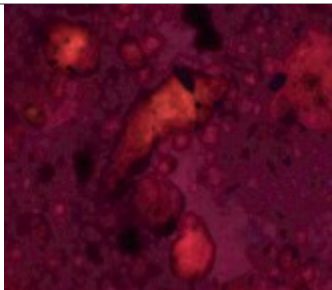
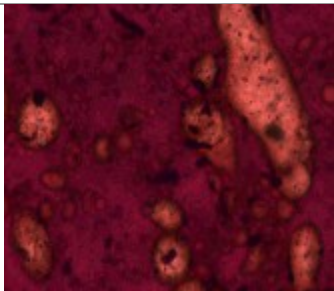
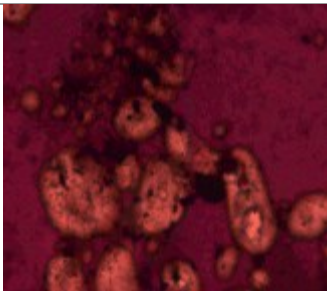
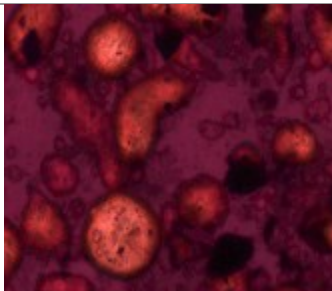
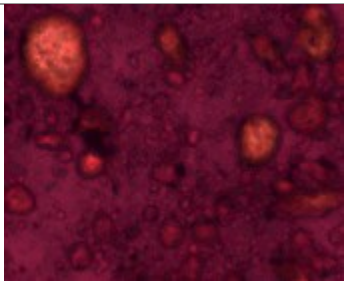
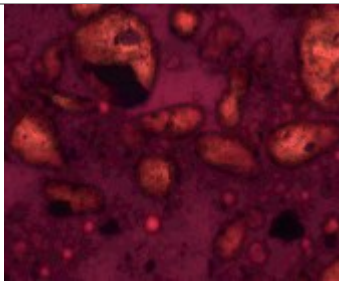
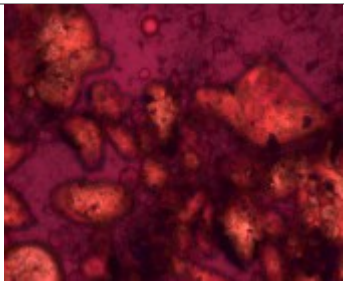
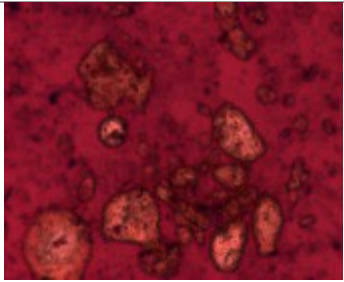
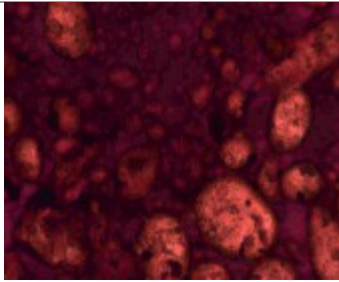
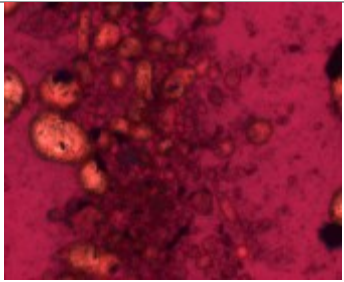
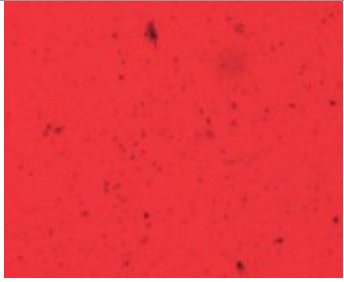
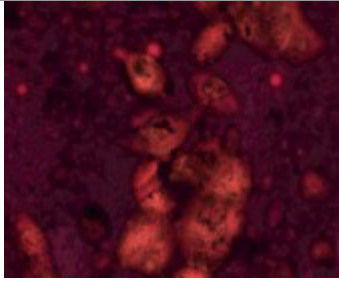
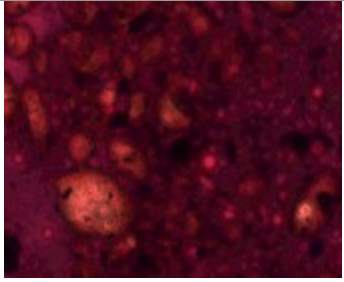

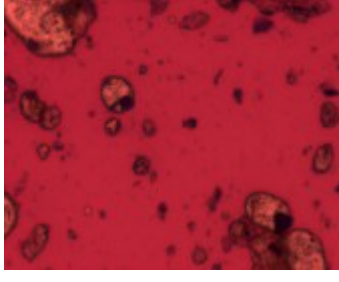
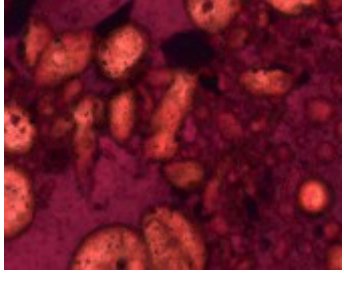
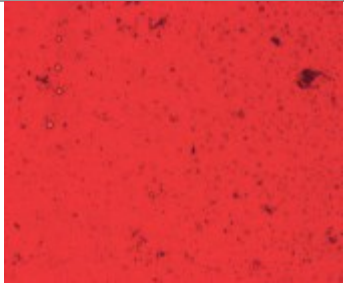
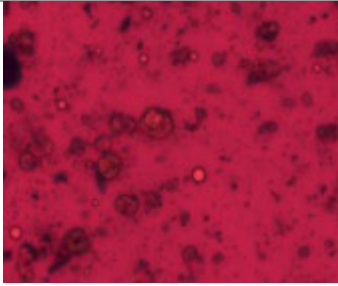
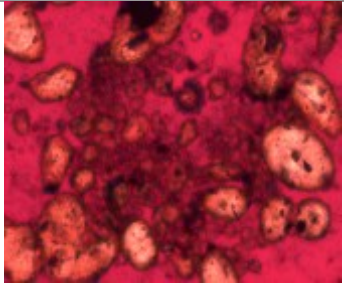
60 minutes			
Occurrence (%)	100	100	100

Table 6-9: Representative 10x microscope images of high-water froth experiments with the best mixing conditions: high mixing energy (+) and high injection rate (+).

Settling Time	Sampling Height Z1	Sampling Height Z2	Sampling Height Z3
5 minutes			
Occurrence (%)	100	100	100
10 minutes			
Occurrence (%)	100	100	100
15 minutes			

Occurrence (%)	100	87	100
20 minutes			
Occurrence (%)	100	100	100
25 minutes			
Occurrence (%)	82	93	100
30 minutes			
Occurrence (%)	100	100	100
45 minutes			
Occurrence (%)	100	88	100

60 minutes			
Occurrence (%)	100	100	95

When considering the settling behavior in high-water froth, flocculation-induced coalescence is proposed to be the dominant settling mechanism. In this case, free water is assumed to be evenly distributed after demulsifier dispersion. The vessel volume can be divided to four equal zones based on sampling heights from Z1 to Z4. Each zone from Zone 1 to 4 is packed with free water, which consists of large free water, small free water, and a small amount of spherical water drops. These water structures are closely connected at the beginning of settling. The flocs are large enough to occupy the whole space of each zone, and hence make the overall settling from top to bottom stagnant to some extent.

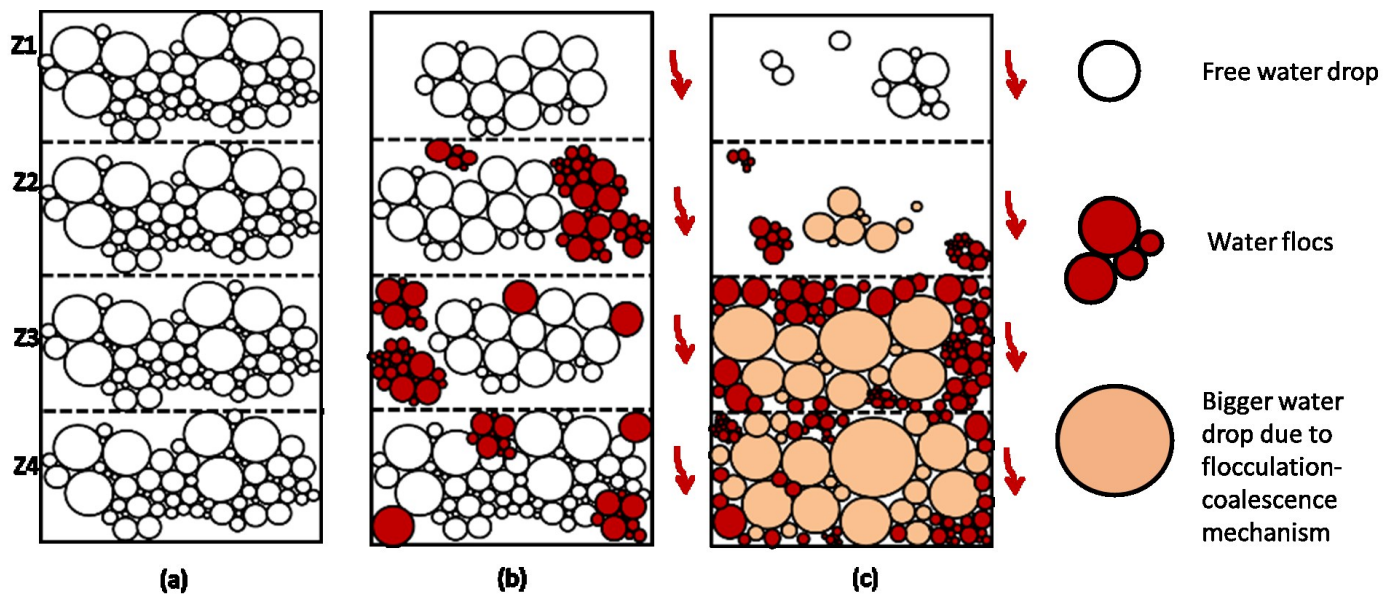


Figure 6-3: Graphic demonstration of the proposed settling mechanism of free water in high-water froth experiments (a) at the beginning of settling, naturally present free-water are evenly distributed in each height zone (b) during the induction time, flocculation-induced coalescence happen in the bottom height zones, free space is squeezed, and some naturally present free-water flow to the empty space (c) at the end of settling, the bottom height zones are packed and top height zone is quite empty.

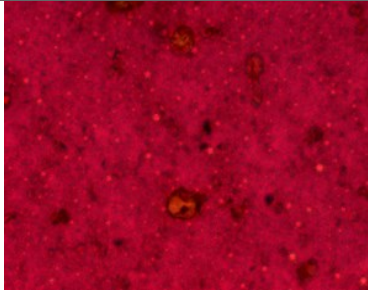
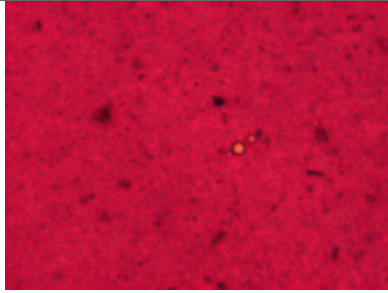
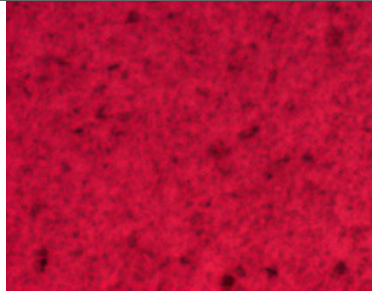
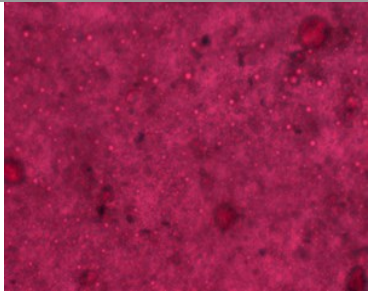

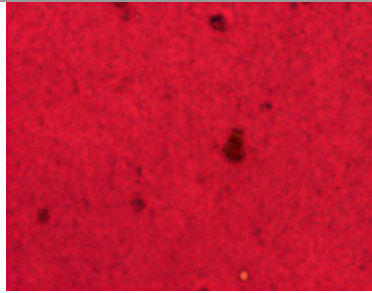
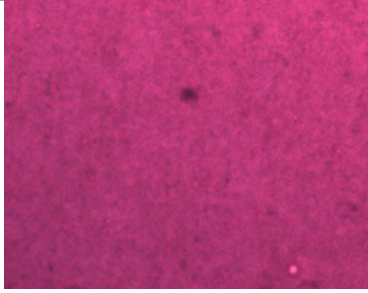
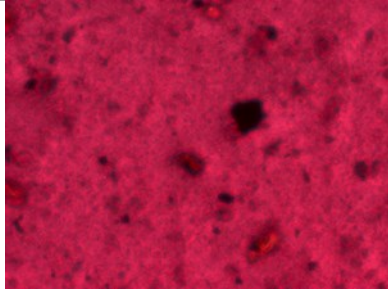
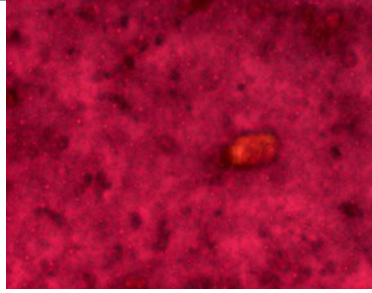
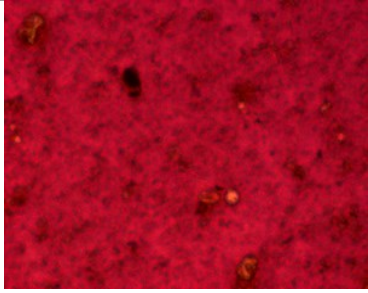

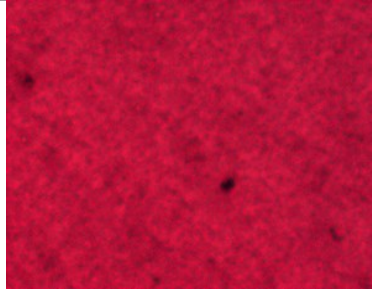
Figure 6-3 demonstrates the proposed flocculation-induced coalescence settling: (a) at the beginning, there is not enough space available in Zone 3 and 4 to accept water flocs from Zone 1 and Zone 2, but flocculation-inducing coalescence can happen in Zone 3 and 4; (b) the flocculation-inducing coalescence helps release free space in Zone 3 and 4, and small water flocs and small free water from Zone 1 and 2 can flow to this free space; when Zone 4 is fully packed with water and no more space can be squeezed, Zone 3 starts accepting most of water flocs; and (c) the acceptance of water flocs continues until both Zone 4 and 3 are fully packed.

#### 6.4 Method Improvement and Analysis on High-Solids Froth

Since 10x microscope images are more important for this type of froth, more 10x microscope images should be taken to give a more reliable occurrence (%). Only around 15 microscope images were taken at 10x for average-quality and high-water froths by following the image capture protocol. To improve the reliability of the analysis method, the number of 10x microscope images taken for high-solids froth is increased to be around 30 images.

From Table 6-10 to Table 6-13, both many spherical drops and small free water are observed in high-solids froth under different operating conditions. These water drops are usually associated with “hazy” substances, which are expected to be solids. In general, an induction time of approximately 30 minutes at height Z1 is observed in high-solids froth. Some microscope images show little objects under other operating conditions, which can be due to inadequate resolution of the microscope.

Table 6-10: Representative 10x microscope images of high-solids froth experiments with operating mixing conditions: low bulk concentration (-) and low mixing energy (-).

Settling Time	Sampling Height Z1	Sampling Height Z2	Sampling Height Z3
5 minutes			
Occurrence (%)	70	96	94
10 minutes			
Occurrence (%)	88	82	71
15 minutes			
Occurrence (%)	100	79	83
20 minutes			
Occurrence (%)	100	100	100

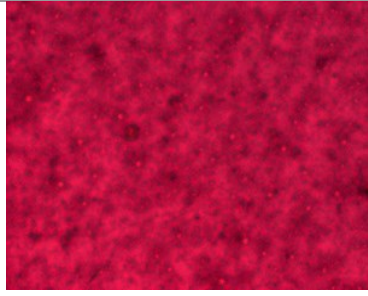
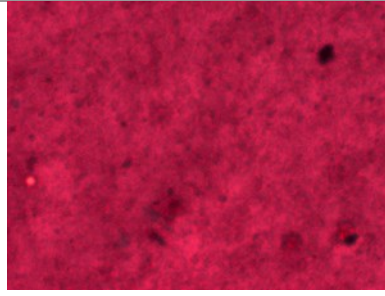
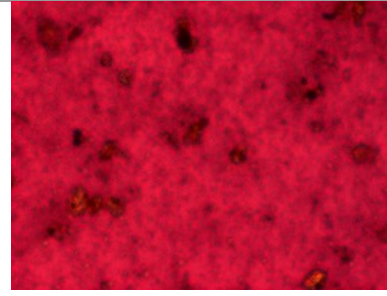
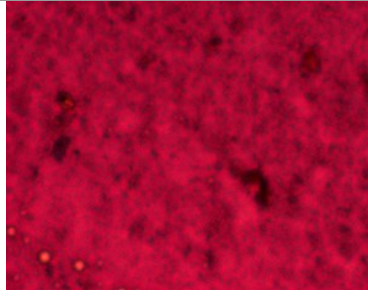
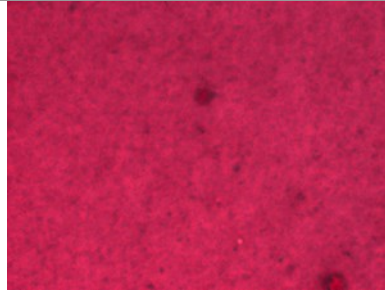
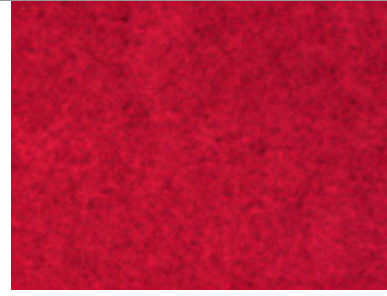
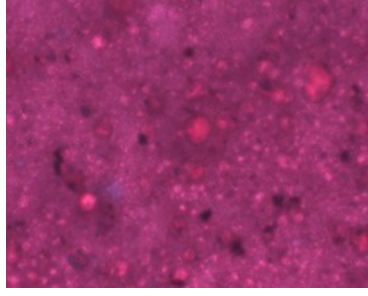
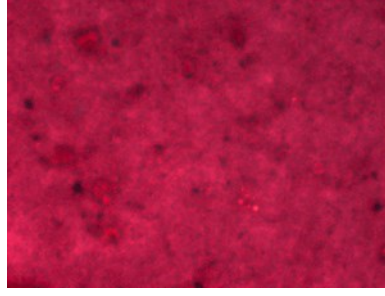
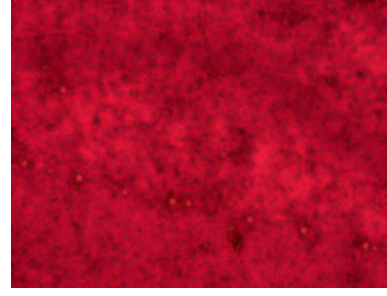
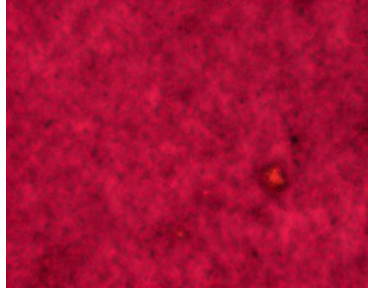
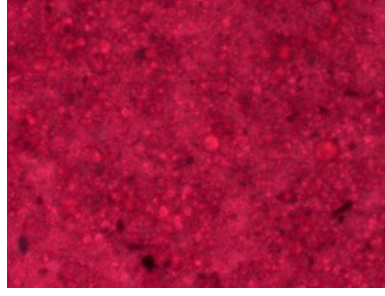
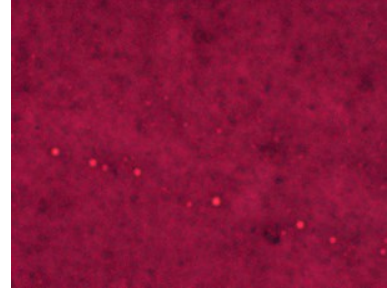
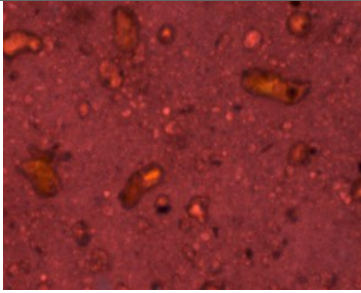
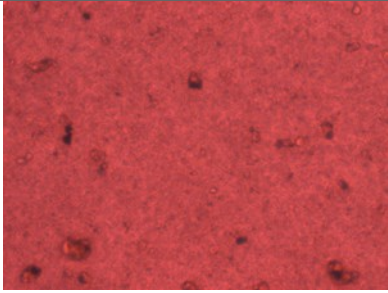
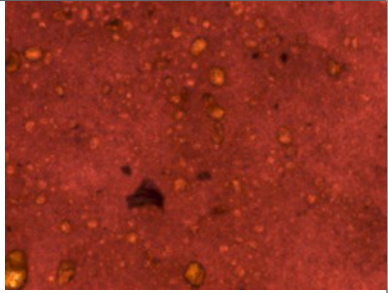
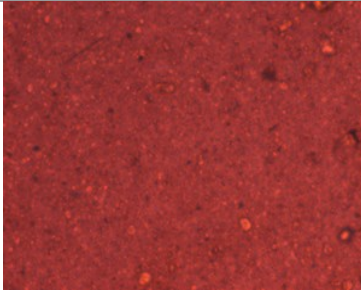
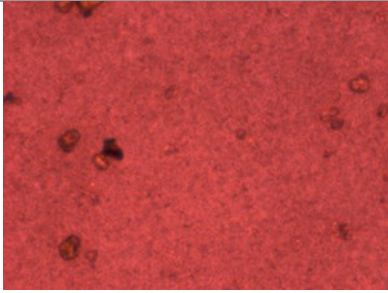
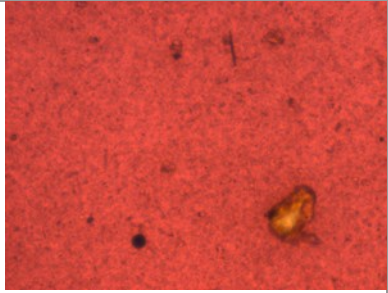
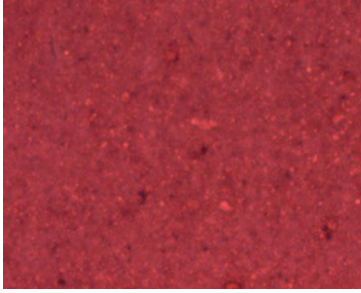
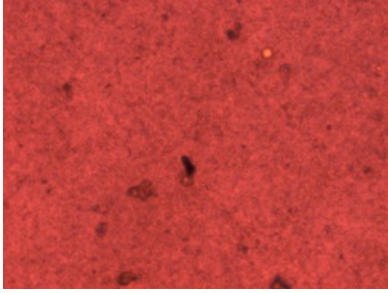

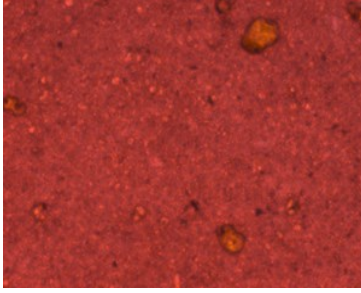
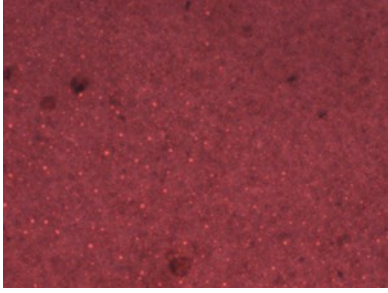
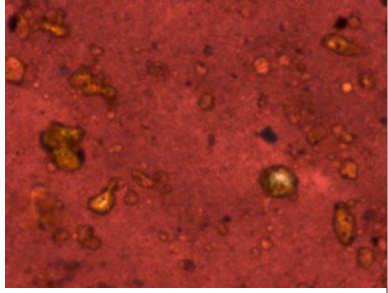
25 minutes			
Occurrence (%)	100	80	100
30 minutes			
Occurrence (%)	100	74	100
40 minutes			
Occurrence (%)	100	100	100
60 minutes			
Occurrence (%)	100	87	96



Table 6-11: Representative 10x microscope images of high-solids froth experiments with operating conditions: high bulk concentration (+) and low mixing energy (-).

Settling Time	Sampling Height Z1	Sampling Height Z2	Sampling Height Z3
5 minutes			
Occurrence (%)	91	76	100
10 minutes			
Occurrence (%)	91	100	84
15 minutes			
Occurrence (%)	100	100	100
20 minutes			
Occurrence (%)	100	100	100

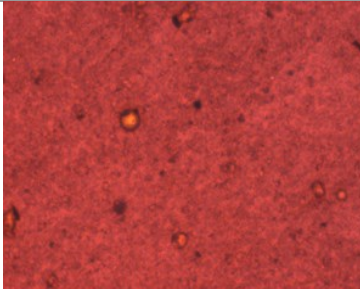
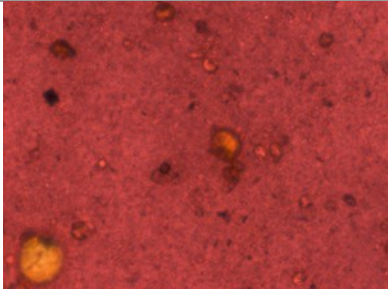
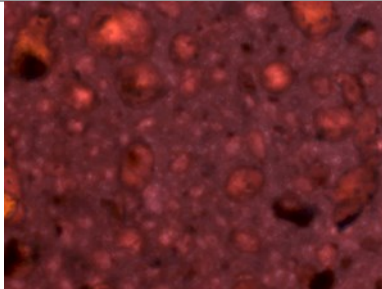
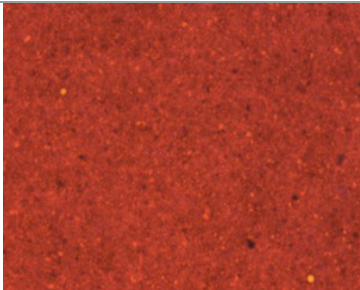
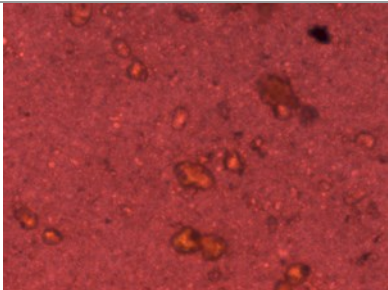
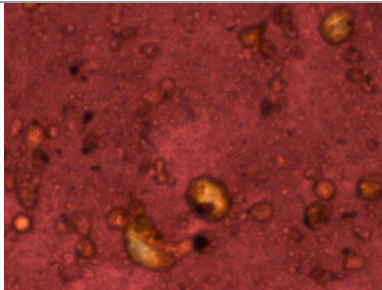
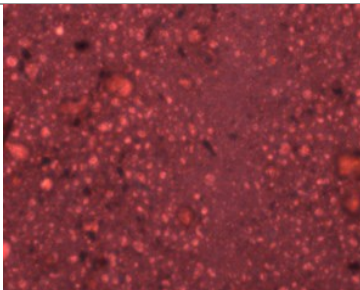
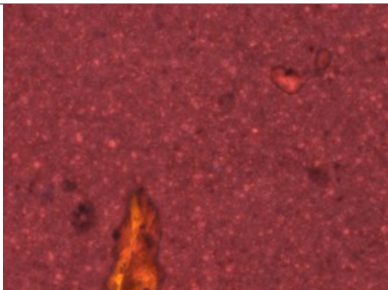
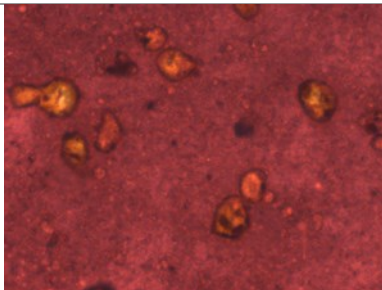
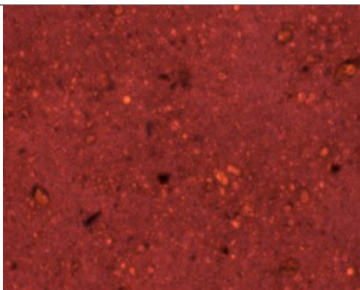
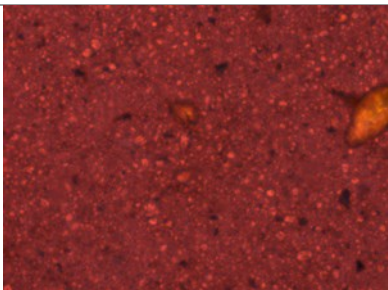
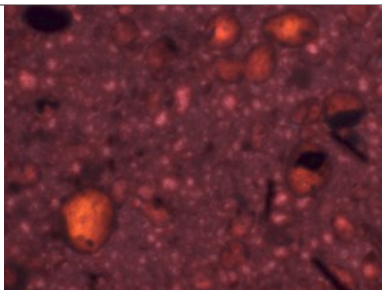

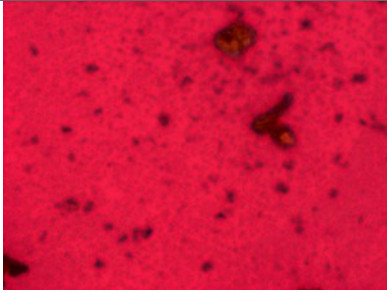

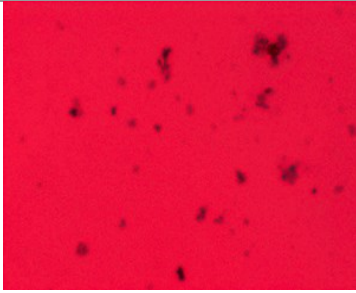
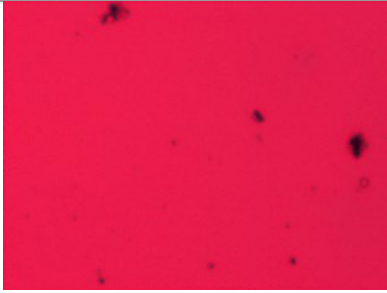
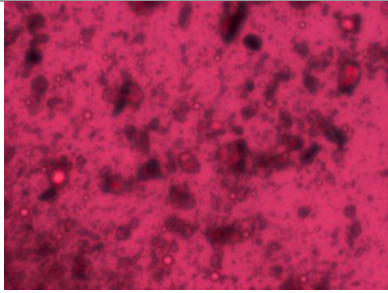
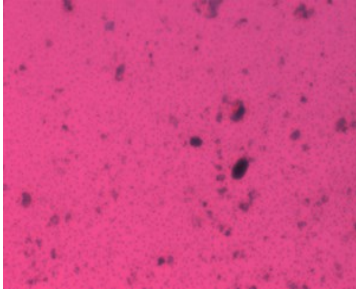
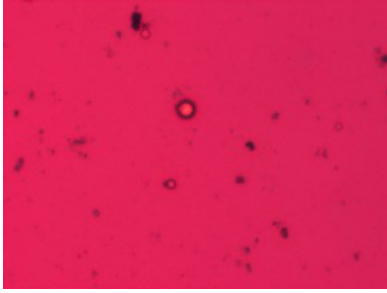
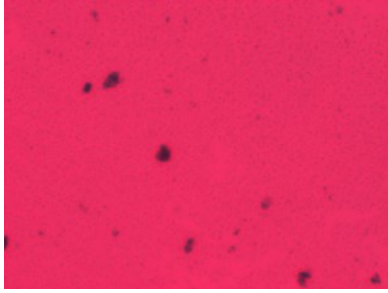
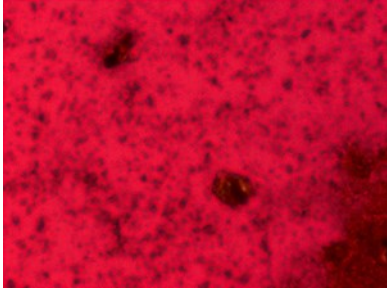
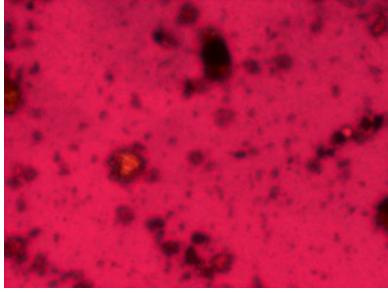
25 minutes			
Occurrence (%)	92	87	100
30 minutes			
Occurrence (%)	100	92	100
40 minutes			
Occurrence (%)	100	100	87
60 minutes			
Occurrence (%)	100	100	100

Table 6-12: Representative 10x microscope images of high-solids froth experiments with optimal mixing conditions: low bulk concentration (-) and high mixing energy (+).

Settling Time	Sampling Height Z1	Sampling Height Z2	Sampling Height Z3
5 minutes			
Occurrence (%)	100	82	100
10 minutes			
Occurrence (%)	100	100	76
15 minutes			
Occurrence (%)	47	100	56
20 minutes	NA		
Occurrence (%)		59	88

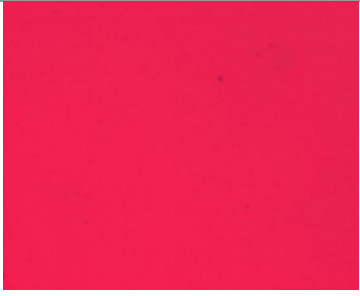
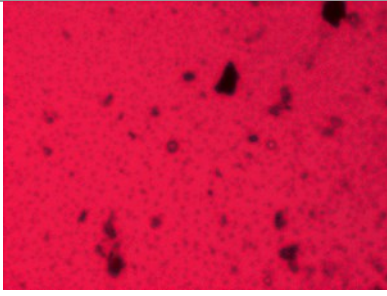
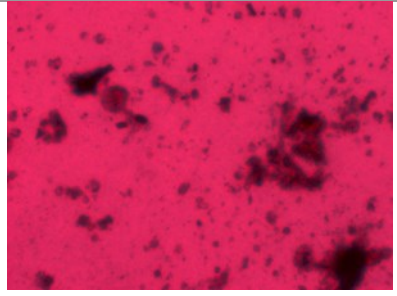

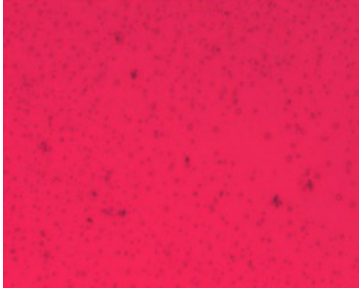
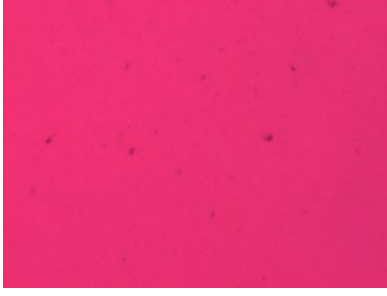
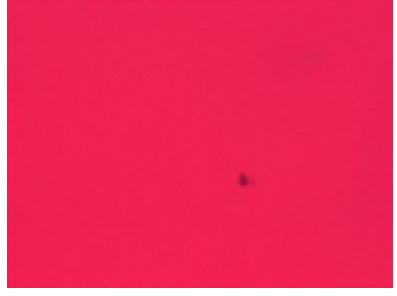

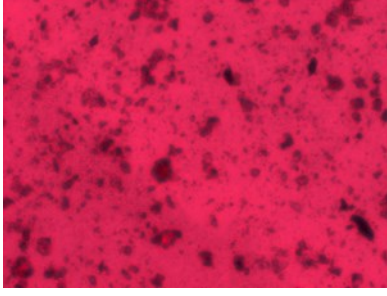
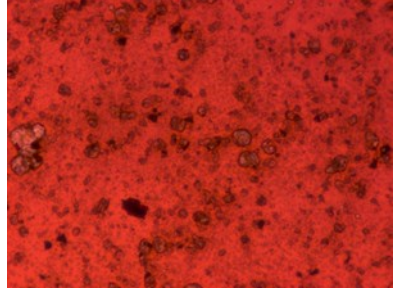
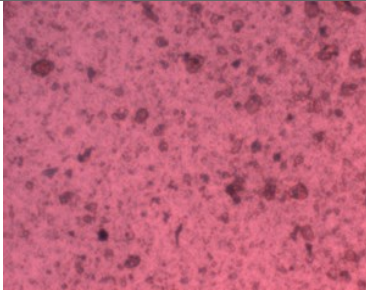
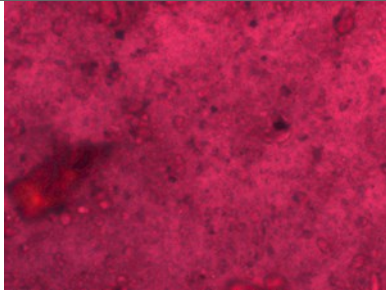
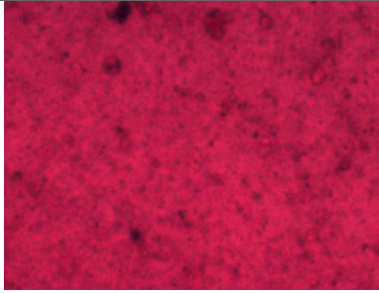
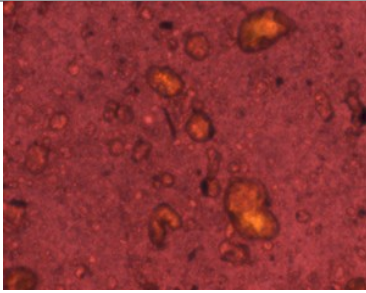
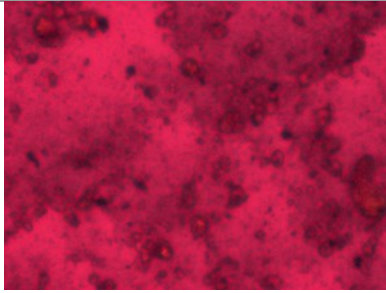
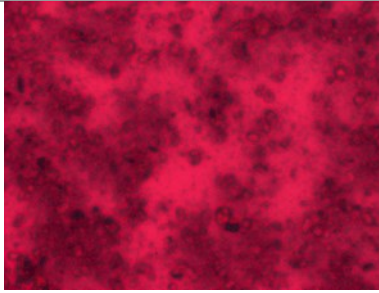
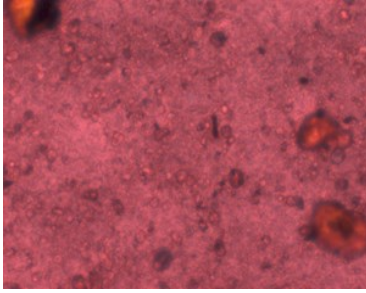
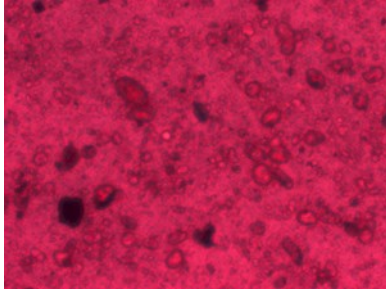
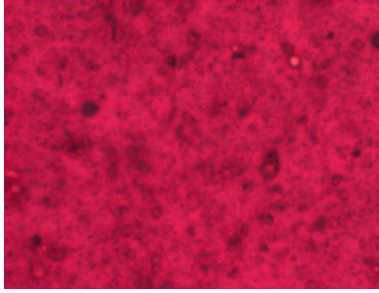
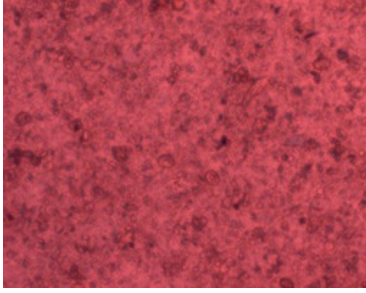
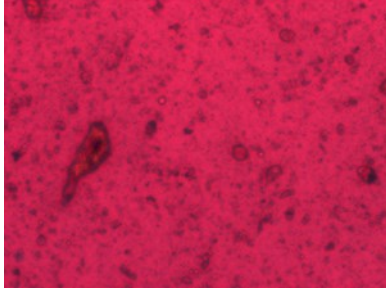
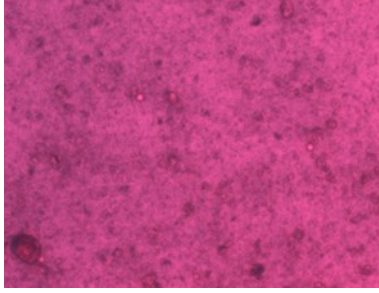
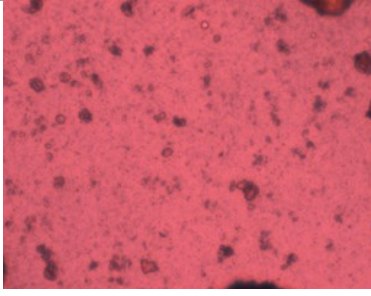
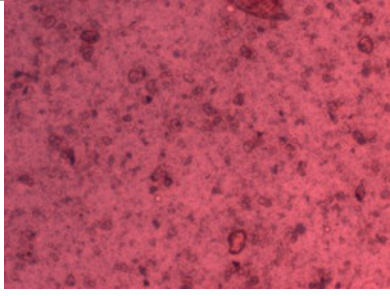
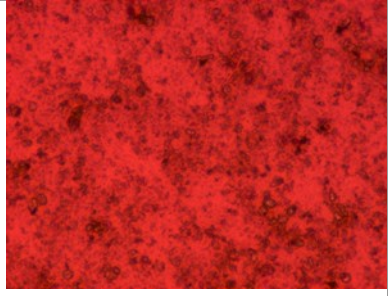
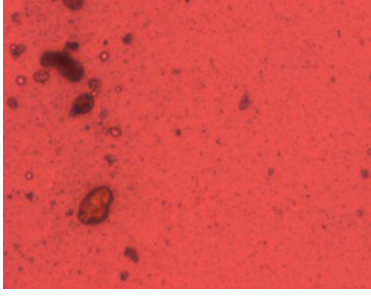
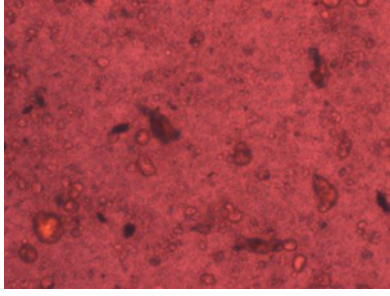
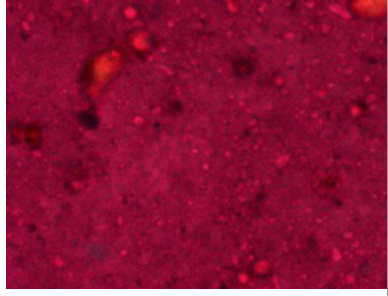
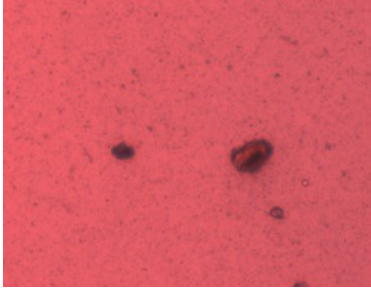
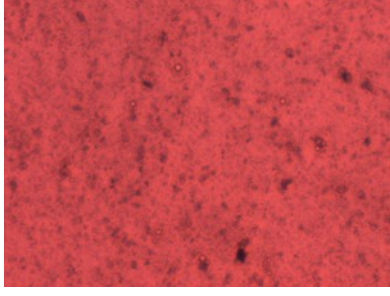
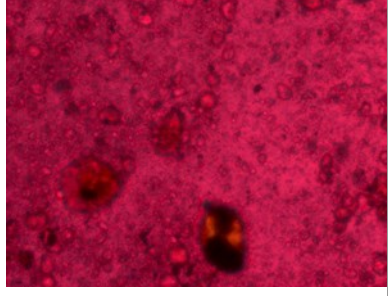
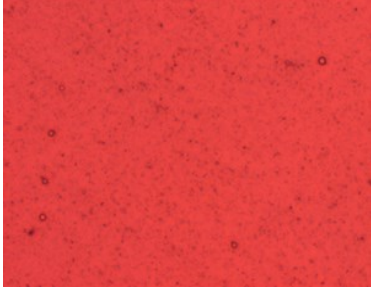
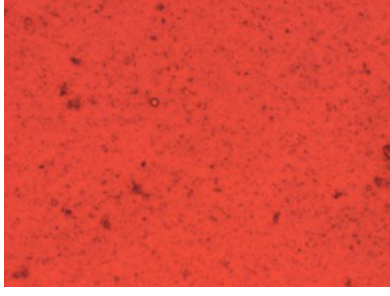
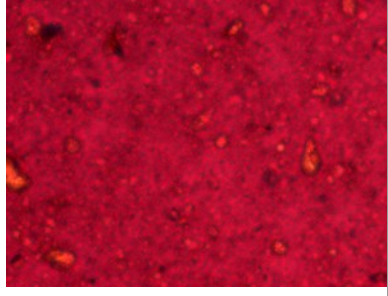
25 minutes			
Occurrence (%)	100	67	51
30 minutes		NA	NA
Occurrence (%)	100		
40 minutes			
Occurrence (%)	100	100	100
60 minutes			
Occurrence (%)	100	80	87

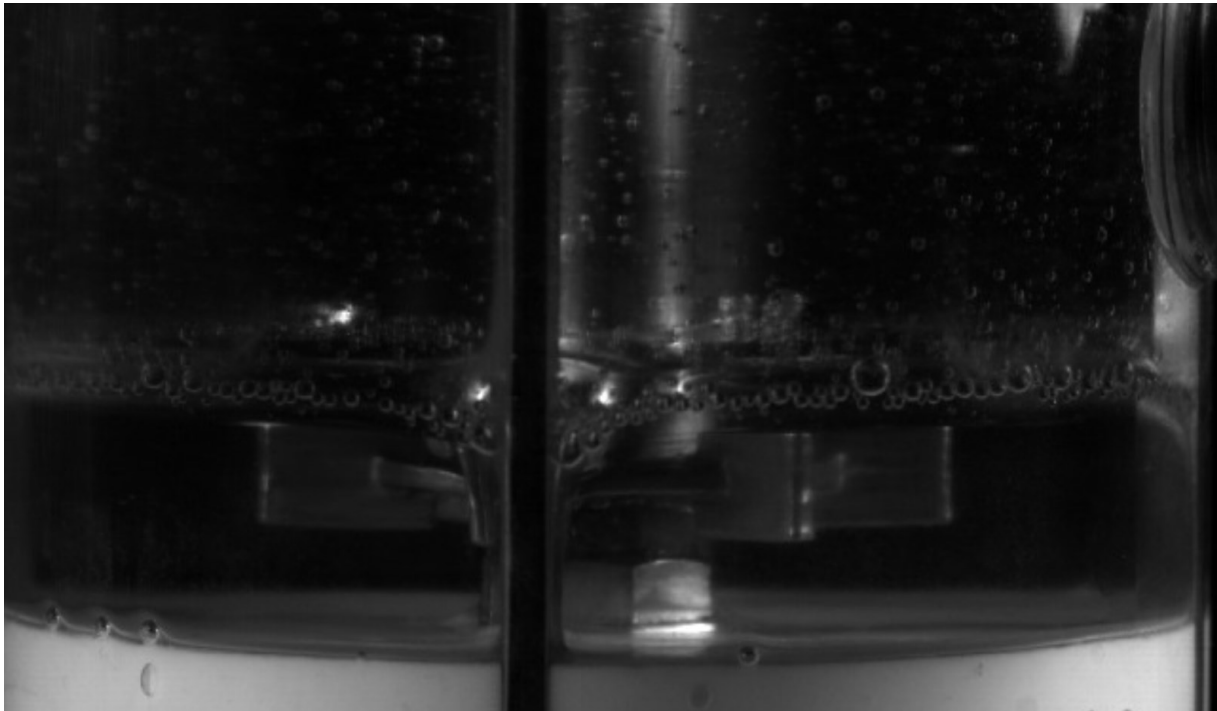
Table 6-13: Representative 10x microscope images of high-solids froth experiments with optimal mixing conditions: high bulk concentration (+) and high mixing energy (+).

Settling Time	Sampling Height Z1	Sampling Height Z2	Sampling Height Z3
5 minutes			
Occurrence (%)	100	74	93
10 minutes			
Occurrence (%)	100	92	64
15 minutes			
Occurrence (%)	66	80	100
20 minutes			
Occurrence (%)	100	71	100

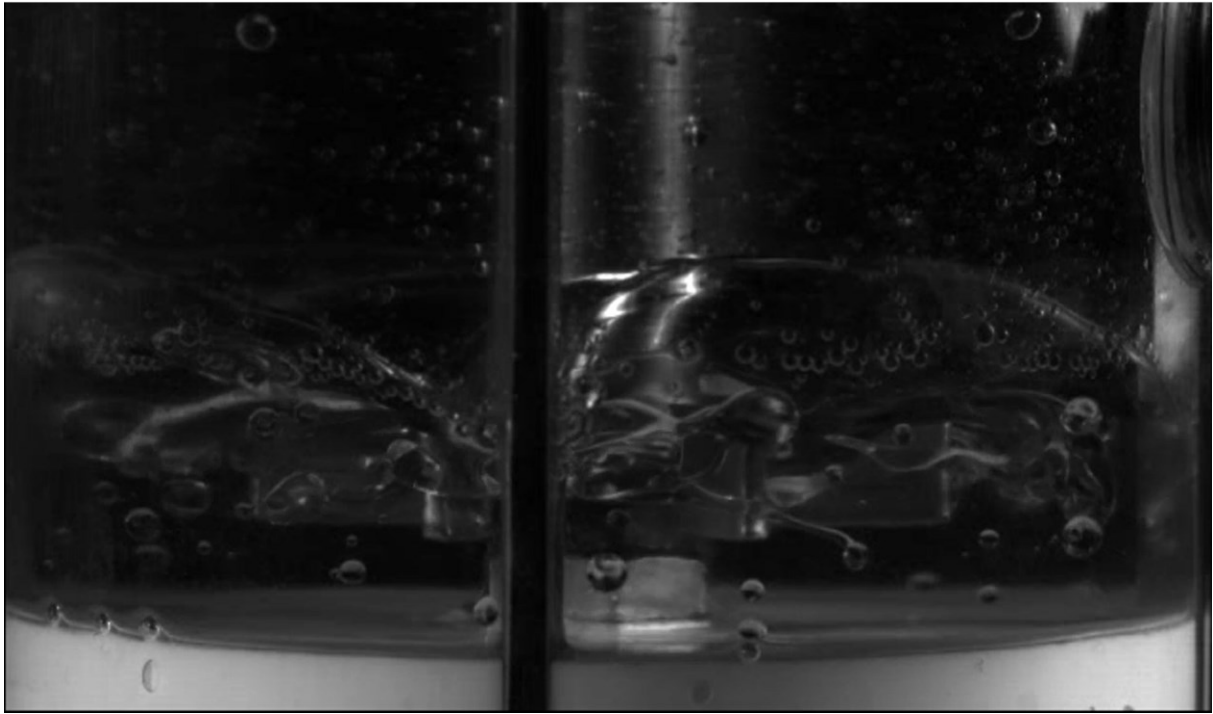
25 minutes			
Occurrence (%)	78	88	99
30 minutes			
Occurrence (%)	91	88	90
40 minutes			
Occurrence (%)	90	90	100
60 minutes			
Occurrence (%)	100	100	100

# Chapter 7: Formation of Small Water Drops during Turbulent Mixing and Future Research

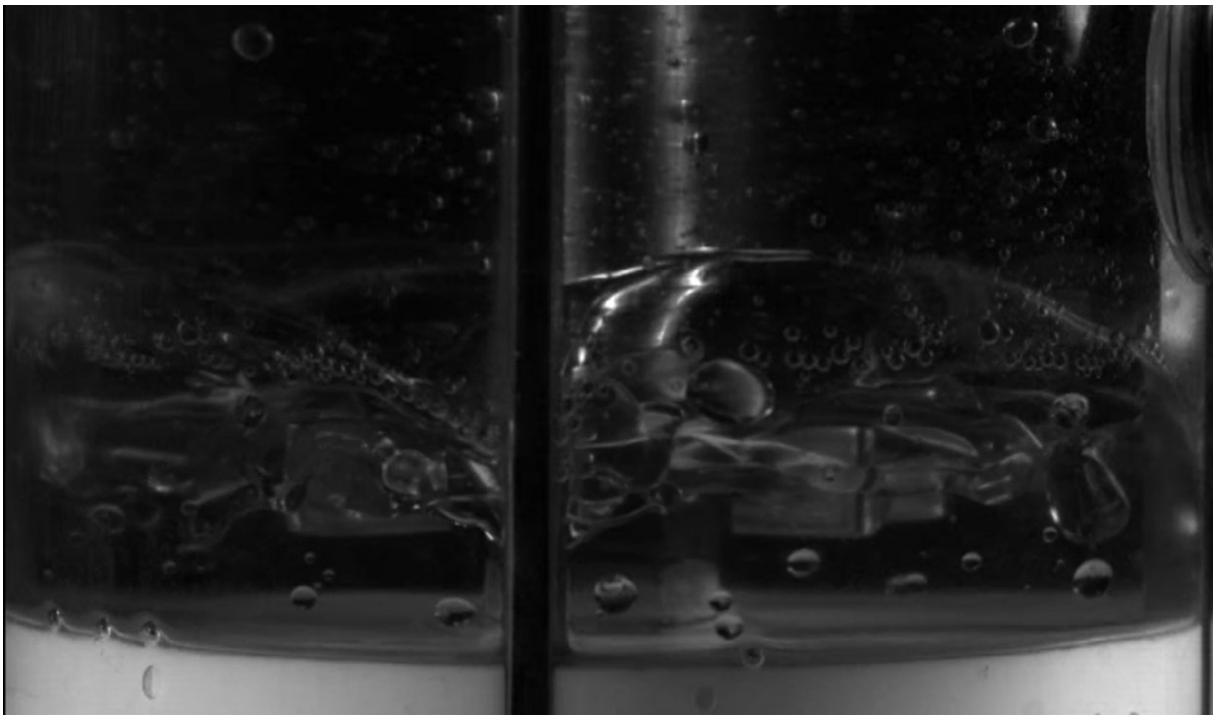
When studying the behavior of drops at the interface of a fluid system without demulsifier, which has 10wt% of water in canola oil, stretched water drops are first formed and small water drops are generated at turbulent mixing at the bench-scale. This observation can be tracked back to the breakup of water drops related to the formation of satellite drops, which has been discussed in Chapter 1.4.



(a)



(b)



(c)



Figure 7-1: Formation of small water drops at the interface of a fluid system which contains 10wt% of water in canola oil at the bench-scale of turbulent mixing in the CIST with a set of Rushton impellers at 655rpm: (a) oil-water interface before the impellers were turned on (b)  $t = 4$  s when a stretched water drop with a long tail is observed (c) and  $t = 10$  s when smaller drops are excluded from the stretched water drops.

Figure 7-1a shows that water drops were clearly present at the interface of canola oil and water system before impellers were turned on. Figure 7-1b shows that water drops were stretched with long tails behind after impellers at 655rpm went on at turbulent mixing. Figure 7-1c shows that smaller satellite water drops were formed after stretching was finished, but no obvious streams of water drops were observed.

As discussed in Chapter 1.4, surfactant-mediated tip streaming is the most likely drop breakup mode to form fine water drops compared to the formation of satellite water drops. It will be of great value to increase the rotating speed of impellers from laminar to turbulent mixing to study the formation of fine water drops in the future. Demulsifier can be also be added to see whether surfactant-mediated tip streaming can be replicated, and how mixing conditions, such as mixing energy, affect the formation of fine water drops via this mechanism.

# Chapter 8: Conclusion

There are different qualities of bitumen froths that the froth treatment plant can process in industry. The most important lesson is that a different bulk concentration of demulsifier is required to treat each quality of froth including average-quality, high-water, and high-solids froth. As provided by industry, the average-quality froth has 30wt% water, 60wt% bitumen and 10wt% solids; high-water froth has 37wt% water, 50wt% bitumen, and 13wt% solids; high-solids froth has 27wt% water, 54wt% bitumen, and 19wt% solids. If the effect of bitumen amount on the settling behavior is minimal, and the composition of water and the type of solids in each froth are also similar, the settling behavior of three froths can heavily depend on the amounts of water and solids respectively. Some important observations about settling behavior of three froths are summarized as follows:

Average-quality froth:

- Most of the settling finishes within the first 10 minutes. 60 minutes is required to reach the 1% criteria for the final water content. A little hindrance of settling was found at height Z2 (induction time of approximately 5 minutes) and Z3 (induction time of approximately 10 minutes) based on KF. Spherical water drops are dominant on the microscope images. Free water is coated with a thin layer of solids. Through investigating the mixing effects, high mixing energy and low injection concentration at suitable demulsifier dosage, which are considered as good mixing conditions, contribute to the lowest final water amount at the top height.

High-water froth:

- An induction time, which can be up to 40 minutes, is observed at height Z1 during settling. The settling time of 120 minutes is required to reach the 1% criteria for the final water content instead. The higher bulk concentration leads to a longer induction time, and longer induction time correlates to a lower final water content. There is also an

induction time, which can be up to 90 minutes, at height Z2. Height Z3 is at steady state, which plays a role of accepting and passing water drops from top to bottom. Compared to average-quality froth, there is lots of hindrance to make the overall settling sluggish. A great amount of large free water, not spherical water, is observed on the microscope images. The good mixing conditions, high mixing energy and low injection concentration at suitable demulsifier dosage, contribute to the lowest final water content at the top sampling height.

High-solids froth:

- An induction time, which can be up to 25 minutes, is observed at height Z1 during settling. The settling time of 60 minutes is enough to reach the 1% criteria for the final water content. Unlike high-water froth, it is hard to finalize the correlation between bulk concentration and final water content in high-solids froth due to limited data. Unlike high-water froth, there are many spherical water drops, which are associated with solids, observed on the microscope images. The effect of a higher end of bulk concentration between 75 ppm and 175 ppm under good mixing conditions is found to be insignificant since little difference in water removals is observed. For this froth, a lower level of bulk concentration between 35 ppm and 100 ppm instead of injection concentration of demulsifier is studied. The best operating condition, high bulk concentration at a low level and high mixing energy at the low injection concentration of demulsifier (12 wt%), contributes to the lowest final water content at the top sampling height. The microscope images for this system are difficult to interpret.

The FBRM probe was inserted into the test vessel to obtain chord length distributions of drops in mixing experiments of both high-water and high-solids froth. Although chord length distributions are obtained in both froths, they are hard to analyze and compare. The fouling index in bitumen froth, which is really a complex and dirty system, is much higher ( $\approx 20\%$ ) even after sapphire treatment compared to clean systems, such as canola in water fluid ( $\approx 2\%$ ) with no sapphire treatment required. High fouling index makes the FBRM data of bitumen froth hard

to interpret. More work should be done on how to take off the effect of fouling index to get the real dynamics of fluids in froth system.

To summarize, an induction time is observed in both high-water and high-solids froth. Both extra amounts of water and solids correlate to the appearance of an induction time. For future research, it is of great value to study the effects of extra amount of water vs. extra amount of solids on the separation of water and solids. In addition, the sufficient bulk concentration of demulsifier for average-quality froth is only based on hypothesis, so a complete experimental design is necessary to verify this chosen dosage. The mixing effects on the formation of small water drops as discussed in Chapter 7 are also useful to study in the future to further optimize mixing conditions.

# References

- Arora, N., 2016. Mechanisms of Aggregation and Separation of Water and Solids from Bitumen Froth using Cluster Size Distribution. Edmonton.
- Arora, N., Awosemo, A., Machado, M.B., 2015. Comparison of Sampling Orientation for Water/Solids Settling Experiments in a Diluted Bitumen System.
- BCG Engineering Inc., 2010. Oil Sands Tailings Technology Review.
- Chong, J.Y., 2013. Mixing Effects on Chemical Demulsifier Performance in Diluted Bitumen and Froth, Department of Chemical and Materials Engineering.
- Chong, J.Y., Machado, M.B., Bhattacharya, S., Ng, S., Kresta, S.M., 2016. Reduce Overdosing Effects in Chemical Demulsifier Applications by Increasing Mixing Energy and Decreasing Injection Concentration. <https://doi.org/10.1021/acs.energyfuels.6b00621>
- Czarnecki, J., Tchoukov, P., Dabros, T., 2012. Possible Role of Asphaltenes in the Stabilization of Water-in-Crude Oil Emulsions 5782–5786. <https://doi.org/10.1021/ef300904a>
- Gao, S., Moran, K., Xu, Z., Masliyah, J., 2010. Role of Naphthenic Acids in Stabilizing Water-in-Diluted Model Oil Emulsions 7710–7718.
- Gingras, J.P., Tanguy, P.A., Mariotti, S., Chaverot, P., 2005. Effect of process parameters on bitumen emulsions. *Chem. Eng. Process. Process Intensif.* 44, 979–986. <https://doi.org/10.1016/j.cep.2005.01.003>
- Gopalan, B., Katz, J., 2010. Turbulent Shearing of Crude Oil Mixed with Dispersants Generates Long Microthreads and Microdroplets 54501, 1–4. <https://doi.org/10.1103/PhysRevLett.104.054501>
- Gray, M., Xu, Z., Masliyah, J., 2009. Physics in the oil sands of Alberta. *Phys. Today* 62, 31–35. <https://doi.org/10.1063/1.3099577>
- Komrakova, A.E., Liu, Z., Machado, M.B., Kresta, S.M., 2017. Development of a zone flow model for the confined impeller stirred tank (CIST) based on mean velocity and turbulence measurements. *Chem. Eng. Res. Des.* 125, 511–522. <https://doi.org/10.1016/j.cherd.2017.07.025>
- Kukukova, A., Aubin, J., Kresta, S.M., 2009. Chemical Engineering Research and Design A new definition of mixing and segregation : Three dimensions of a key process variable 7. <https://doi.org/10.1016/j.cherd.2009.01.001>
- Laplante, G.P., 2011. On Mixing and Demulsifier Performance in Oil Sands Froth Treatment. *Dep. Chem. Mater. Eng. Master of*, 30–31.
- Leo, S., 2013. Measurement and Analysis of Changes in Drop Size Distribution during Bitumen Clarification using Image Analysis. *Dep. Chem. Mater. Eng. Master of*.

- Long, Y., Dabros, T., Hamza, H., 2004. Structure of water / solids / asphaltenes aggregates and effect of mixing temperature on settling rate in solvent-diluted bitumen 83, 823–832. <https://doi.org/10.1016/j.fuel.2003.10.026>
- Machado, M.B., Kresta, S.M., 2013. The confined impeller stirred tank (CIST): A bench scale testing device for specification of local mixing conditions required in large scale vessels. *Chem. Eng. Res. Des.* 91, 2209–2224. <https://doi.org/10.1016/j.cherd.2013.06.025>
- Maluta, F., Eaglesham, A., Jones, D., Komrakova, A., Kresta, S.M., 2017. A novel factorial design search to determine realizable constant sets for a multi-mechanism model of mixing sensitive precipitation. *Comput. Chem. Eng.* 106, 322–338. <https://doi.org/10.1016/j.compchemeng.2017.06.014>
- Mettler Toledo, 2011a. Inline Particle Measurement [WWW Document]. URL <http://www.mt.com/autochem>
- Mettler Toledo, 2011b. Inline Particle Measurement [WWW Document].
- Montgomery, D.C., Runger, G.C., 2011. *Applied Statistics and Probability for Engineers*, John Wiley & Sons, Inc.
- Quraishi, S., Acosta, E., Ng, S., 2015. The role of naphthenates and kaolinite in toluene and toluene – bitumen emulsions. *Fuel* 153, 336–345. <https://doi.org/10.1016/j.fuel.2015.03.016>
- Rao, F., Liu, Q., 2013. Froth Treatment in Athabasca Oil Sands Bitumen Recovery Process : A Review. <https://doi.org/10.1021/ef4016697>
- Rocha, J.A., Baydak, E.N., Yarranton, H.W., Sztukowski, D.M., Gong, L., Shi, C., Zeng, H., 2016. Role of Aqueous Phase Chemistry , Interfacial Film Properties , and Surface Coverage in Stabilizing Water-in-Bitumen Emulsions. <https://doi.org/10.1021/acs.energyfuels.6b00114>
- Saraka, C., 2017. Mixing and Settling Characterization in Low-Quality Bitumen Froth Treatment.
- Sonthalia, R., Ng, S., Ramachandran, A., 2016. Formation of extremely fine water droplets in sheared , concentrated bitumen solutions via surfactant-mediated tip streaming. *Fuel* 180, 538–550. <https://doi.org/10.1016/j.fuel.2016.04.053>
- Xu, A.R., Saraka, C., 2017. Re-assessment of Microscopic Images of Poor Quality Froth Settling Experiments Using a Mixed Approach: Qualitative and Quantitative Methods.
- Zhou, G., Kresta, S.M., 1998. Correlation of mean drop size and minimum drop size with the turbulence energy dissipation and the flow in an agitated tank 53.
- Zhou, G., Kresta, S.M., 1996. Distribution of energy between convective and turbulent flow for three frequently used impellers. *Chem. Eng. Res. Des.* 74, 379–389.

## Appendix A: Standardized Operational Procedures (SOP) for High-Solids Froth Mixing Experiments

### A.1 Experimental Procedures for High-solids Froth Mixing Experiments

The following procedures are developed based on previous studies on average-quality and high-water froth. There are several stages in this protocol including experiment preparation, naphtha blending, demulsifier dispersion and batch settling. The operating conditions of each mixing experiment is given out as well. It is important to follow the procedures strictly to get repeatable and consistent experimental data.

#### **Main Hazards:**

- Hot bitumen: skin irritant
- Hot hydrocarbon products: high vapour pressure and flammable gases. Should be handled under the fume hood at all times and respirator should be worn.

#### **Experiment Preparation:**

- Froth can:
  - Ensure froth can is more than 950 g (which will fill the vessel to approx. 1L). If not, heat a froth can, run premixing step, then pour into other froth cans.
  - Turn can upside down one or two days before experiment, with tissue underneath. Ensure lid is secure.
- Needles
  - Silanize
  - Chop pipette tips using the plate with a standard whole (1.5 mm diameter)
  - Mark needles for insertion depth (4.5 cm for  $r/R = 0.9$ )
  - Attach needles to pipette tips using duct tape
- Silanize and label microscope slides
- Label and weigh sample bottles (See Table 1)
- End-of-run OWS/CPA samples
  - Label bottles (See Table 1)

- Cut plastic tubing for various sampling depths (1 each @ 58, 150, 242 mm)
  - Attach tubing to 100ml glass syringe with duct tape
- CIST preparation
  - Install septa inside sampling ports, making sure they do not buckle
  - Screw in Teflon plugs over sampling ports
  - Put baffles and Teflon bearing at the bottom of CIST
- Prepare demulsifier at 12 wt%, which is constant throughout all high-solids settling experiments

### **On Experiment Day**

- Take the upside down can out of fridge and keep in fume hood in same orientation.
- Turn the Ethylene Glycol bath on.
- Install impellers (Rushton, Intermig or A310) in CIST with motor driver.
- Set CIST in fumehood and secure against back support plate using Velcro.
- Load demulsifier in syringe and prepare pump. Enter injection rate and volume. (ID = 32.43 mm)
- Mark insertion depth = 8.6cm on demulsifier injection tubing

### **Premixing**

- Heat Premixing Ethylene Glycol bath to 82°C for at least 1 hour.
- Measure the weight of froth can and based on  $N/B=0.7$  (by mass), and fill naphtha in another can.
- Heat froth can for 1.5 hours. Froth should heat up to 70°C.
- Install CIST in fumehood and start EG circulation and heating to 80°C.
- Once froth reaches 70°C, do premixing using PBT impeller at 1000 rpm for 15 minutes. Froth should heat up to 80°C at the end of premixing.
- Heat Naphtha can to 80°C for half an hour. Both froth premixing and naphtha should be ready for transferring to CIST at same time.

### **Naphtha Blending**

- Remove naphtha from bath, then dry and weigh
- Transfer heated Naphtha to CIST first using thermal glove, then weigh empty beaker



- Remove froth can from bath, then dry and weigh
- Transfer heated froth to CIST using thermal glove and weight empty can
- Check the liquid level in CIST in comparison to 1L mark.
- Set impeller speed (rpm) and time (min) as per Table 3.
- Set up FBRM to be above impeller/below feed pipe location.
- Blend for 2 min by hitting “Run” and take a sample at the end of naphtha blending (Table 1).

#### **Demulsifier dispersion**

- Set motor to appropriate time/speed and hit run
- Inject demulsifier using glass syringe by hand slowly (Table 3) after motor is running
- Take samples as per sampling schedule (Table 1)

#### **Batch settling**

- Once the impellers stop, start the timer
- Take samples accordingly to sampling schedule (Table B.1.1). For runs with 4 heights, each person takes 1 sample (e.g. Z1 and Z3) at 10 s before the nominal time, and one sample 10 s after the nominal time. This is to reduce the chance of an accident and to improve the quality of sampling.
- For Syncrude samples (OWS/CPA), start sampling from top and then move down

**Table A.1.1: Sampling schedule and labelling criteria**

<b>Label</b>	<b>Time</b>	<b>Location</b>	<b>Analysis</b>	<b>No of samples</b>
<b>P</b>	End of premixing	Just below the liquid surface	KF	0
<b>B</b>	End of Naphtha blending	Z1 mm below the liquid surface	KF, Microscope	1
<b>A</b>	30 s before demulsifier dispersion ends	Z1 and Z4	KF, Microscope	1

<b>5, 10, 15, 20,25 30, 40,50 60</b>	During settling	Z1, Z2, Z3, Z4	KF, Microscope	36
<b>DS_1, DS_5, DS_9</b>	End of settling	At z/H = 0.1, 0.5, 0.9	OWS (DS, CPA): 100 ml each	3

**Table A.1.2: Variable range for bitumen froth experiments**

	Regression Coefficient, X		
	-1	0	1
IC (wt%)	12		
J (J/kg)	425	12164	22778
BC (ppm)	35	67.5	100

**Table A.1.3: High-Solids Froth Trials Operating Conditions**

Run/Code	X <sub>BC</sub>	X <sub>J</sub>	Impeller	Naphtha Blending	Demulsifier Dispersion	Dem. Injection Rate (mL/hr), Volume (mL)	
HA-1	-1	-1	Intermig	1060 rpm/2 min	400 rpm/2 min	Injected manually	0.38
HB-1	+1	+1	Rushton	600 rpm/2 min	600 rpm/10 min	Injected manually	1
HC-1	+1	-1	Intermig	1060 rpm/2 min	400 rpm/2 min	Injected manually	1
HD-1	-1	+1	Rushton	600 rpm/2 min	600 rpm/10 min	Injected manually	0.38
CP-1	0	0	Rushton	600 rpm/2 min	600 rpm/5.25 min	Injected manually	0.72
HA-2	-1	-1	Intermig	1060 rpm/2 min	400 rpm/2 min	Injected manually	0.38
HB-2	+1	+1	Rushton	600 rpm/2 min	600 rpm/10 min	Injected manually	1

HC-2	+1	-1	Intermig	1060 rpm/2 min	400 rpm/2 min	Injected manually	1
HD-2	-1	+1	Rushton	600 rpm/2 min	600 rpm/10 min	Injected manually	0.38

## A.2 Receiving Test Material from Syncrude

Syncrude provides some of the test fluid: this includes naphtha for dilution, demulsifier chemical, diluted bitumen (dilbit), and bitumen froth. These must be sent safely and quickly: all except the bitumen froth are covered under Transportation of Dangerous Goods (TDG) requirements, and the bitumen froth and dilbit are known to experience aging effects, so should be warmed for as short a time as possible.

### **Lab (University) Procedure:**

- Send an email to Samson (ng.samson@syncrude.com) or Sujit (bhattacharya.sujit@syncrude.com) requesting material
- Bitumen Froth: two cans used per experiment (1 L cans)
- Diluted Bitumen: 1 4L can used for 2 experiments
- Once Samson or Sujit approve the request, another employee (such as Allan) will arrange for sampling
- Tell Kevin (Kevin.Heidebrecht@ualberta.ca) that he will be receiving a package soon and ask him to inform you as soon as he does.
- Once the material is prepared, order a pickup from Matt Express or a similar, same day service. You will need to tell them:
  - Contact info (at University and Syncrude)
  - Pickup point and instructions
  - Drop-off point and instructions (ICE Building Dock, back up to door and wait until it opens, 1-2 minutes, call University contact)
  - Unpack, store froth cans upside-down in fridge (dilbit cannot be stored upside-down; it will leak). Naphtha goes in flammable storage, demulsifier in fridge.
  - Add the received to the chemical receiving form in the lab safety binder.

### **Syncrude Procedure:**

- Note: Same-day shipment is critical as aging effects have been observed. Minimizing the time outside of refrigerated storage is important.

- Store froth at 5°C until courier pickup.
- Package and prepare for shipment per TDG requirements (TDG is not required for shipments of froth only, but is required for naphtha, demulsifier, and diluted bitumen).
- Request pickup from lab contact (Colin 306 280 0357, Anna, Marcio) to receive shipment. You will need to inform the student:
  - Your contact info
  - Address
  - Weight of shipment
  - Size of shipment

Send email when shipment is picked up so student knows to expect it

### A.3 Unisol Preparation

Unisol is used to dilute bitumen samples for use with the Karl Fischer titration cell. It is simply a 3:1 mixture of high grade toluene and isopropanol.

- Fill desired container with silica beads.
- Mix high-purity toluene and isopropanol in a graduated cylinder or beaker in approximately 3:1 proportions. Approximately 90 mL fills a 200 mL vessel with glass beads.
- Pour into vessel until full.

### Karl Fischer Titration

Karl Fischer titration tells you how many micrograms of water are in an injected sample. By carefully monitoring weights, you can back calculate water content in the sample taken from the vessel. Setting up an Excel sheet ahead of time with all the calculations is recommended. It is important to strictly follow the procedures to obtain repeatable and consistent Karl Fischer data.

#### Determine Unisol water content

- Shake Unisol bottle while closed, tap the lid to remove beads
- Remove a sample with a small needle, clearing 3-5 times depending on the last sample taken in this needle.
- Wipe the tip and weigh the needle.
- Press Run on KF and inject sample, ensuring tip is below liquid level.
- Wipe needle again and record empty syringe weight and KF reading.
- Calculate water content (it helps to set up an Excel sheet ahead of time to calculate this).

#### Determine Sample Water Content

- Measure weights of empty sample bottles.
- Take samples.

- *After* removing sample for microscope slides, weigh sample bottle.
- Dilute the sample by injecting approximately 5x (for dilbit) or 25-30x (for froth) the weight of the sample in Unisol.
- Weigh the sample bottle again and calculate actual dilution ratio.
- Ensuring lid is tight, agitate at 3000 rpm on the vortex mixer for 10s (for dilbit) or 20s (for froth).
- Remove sample with small needle. Clear 3-5 times.
- Wipe and weigh full needle.
- Press Run and inject sample, ensuring tip is below the liquid level in the cell.
- Wipe and weigh empty needle and record KF reading.
- Calculate actual water content.

#### Change KF Liquids

- Remove liquid cells, silica gel, injection port, electrode, and clean all connections with wipe and acetone if necessary. Be careful not to apply lots of pressure to glass ports (i.e. where the wire enters).
- Pour liquids into organic waste container.
- Fill large liquid cell first and place back in titrator along with silica gel and injection port connections.
- Snap small Karl Fischer liquid with bottle, using plastic safety cover or lab towel to protect hands from glass cuts.
- Use pipette to transfer most liquid from small bottle.
- Cover glass connections (about a pea-sized amount) with Apiezon M grease and insert.
- Press run, and increase speed, ensuring magnetic stirrer is working. Allow titration to run until completion. This can take half an hour to several hours, depending on how quickly the transfer was done.

#### A.4 Sending End-of-Run Samples to Syncrude

Syncrude performs a few tests at their facility to complement those done at the University. Dean Stark extraction gives the oil, water, and solids constant, and computerized particle analysis gives solids particle sizing. Hence it is important to follow the procedures below to make sure samples are properly stored and labelled.

##### **Procedure**

- Ensure samples are bottled correctly in 100 mL sample bottles with alternative cap (Qorpak Catalogue: CAP-00268).
- Fill out a sample tag for each sample ensuring separate series for CPA/OWS and EXM analysis. These are provided by Syncrude in the form of a booklet. Fill them out as follows:
  - Date and Time of sample taken
  - Submitter: U of A
  - Stream: Your identifier. Put a tag such as Run #-Sample A.
  - Work Order: Leave it empty. Syncrude will fill this part.
  - Wet/Dry/Pan: Leave it empty.
  - Check the desired tests: CPA and OWS
- Keep the left side of the sample tag for matching up with the data received later and for tracking. Affix the right sample tag to the sample with a rubber band and ensure it is secure. Copy the serial numbers and stream names into lab records.
- Put the samples into a box in numerical order, with consecutive tag numbers if possible, and write “start here” at the first sample.
- Tighten all the sample bottle lids to make sure that none of them leak.
- Pack small box into a larger box with absorbent material.
- Fulfill other TDG requirements (labelling, shipment documentation, etc). This should be done with a person trained in TDG or checked by one. Consult with the CME safety resource to clarify requirements.
- Store the sample box in the refrigerator until pick-up.



- Inform Allan ([yeung.allan@syncrude.com](mailto:yeung.allan@syncrude.com)) or other Syncrude resource in advance that he will be receiving samples.
- Fill out the shipping form located on the department website and get it signed by Marcio or Dr. Kresta. The signed shipping form, the TDG ground form, your TDG training record if applicable, and the applicable MSDS should be sent to SMS (780-492-4121; [shipping@ualberta.ca](mailto:shipping@ualberta.ca)) for review 2-3 days prior to shipping day. Wait for SMS approval before sending the samples.
- It is extremely important that the samples be delivered on the same day as shipping day. Matt Express (780-944-1582) provides same day shipping. Matt Express can pick up the samples from you directly (not through SMS) if you are certified in TDG (Transportation of Dangerous Goods) and you have complete paper work (MSDS, shipping form, TDG ground form).

Syncrude delivery address:

Allan Yeung

Syncrude Canada Ltd

Research and Development Centre

9421-17 Avenue NW

Edmonton, AB T6N 1H4

E: [yeung.allan@syncrude.com](mailto:yeung.allan@syncrude.com) T: 780-970-6942

## Appendix B: Experimental Data

### B.1 Karl Fischer Data of Two Simulating Experiments Using High-Solids Froth with Additional Process Water

BC (ppm)	N:B	Mixing	Settling Time (min) and Water Content (wt%)													
			0	5	10	15	20	25	30	35	40	45	50	60	90	120
<b>200</b>	0.69	good	26.38	26.18	34.54	31.46	24.21	26.88	27.83	23.49	24.10	25.97	14.03	4.01	NA	NA
<b>35</b>	0.70	good	37.41	39.49	31.49	34.28	29.07	29.03	30.84	30.64	21.53	19.54	16.04	12.76	11.75	18.11

### B.2 Karl Fischer Data for High-Solids Froth to Determine the Appropriate Bulk Concentration of Demulsifier to Study Mixing Effects

BC (ppm)	N:B	Mixing	Settling Time (min) and Water Content (wt%)													
			0	5	10	15	20	25	30	35	40	50	60	90	120	
<b>175</b>	0.72	good	16.33	16.41	15.35	16.87	14.33	14.26	10.70	1.19	0.60	0.56	0.39	0.00	0.21	
<b>150</b>	0.83	good	15.63	16.62	16.63	17.00	5.05	3.36	2.12	1.01	2.83	2.16	1.26	2.08	0.62	
<b>150</b>	0.67	good	14.37	13.35	13.11	14.08	14.67	13.94	10.89	1.52	1.03	0.91	0.68	0.56	0.54	
<b>125</b>	0.73	good	16.58	16.80	15.97	15.54	14.76	4.94	2.10	0.90	1.15	1.26	1.56	0.80	0.58	
<b>100</b>	0.79	good	14.14	13.51	16.08	16.01	2.17	2.45	1.63	1.31	1.43	1.77	1.32	1.48	0.88	
<b>100</b>	0.7	good	15.82	14.58	15.07	15.69	18.02	11.29	2.09	1.64	0.26	0.74	0.38	0.29	0.54	
<b>75</b>	0.7	good	16.86	16.88	16.29	15.89	15.82	13.80	13.14	13.18	11.69	11.23	8.89	6.50	6.02	
<b>75</b>	0.76	good	15.00	16.40	14.48	16.43	5.22	3.88	2.27	1.21	8.74	1.38	0.85	0.71	0.69	
<b>35</b>	0.69	good	13.22	13.36	11.96	12.20	11.67	5.93	4.92	4.10	4.09	3.12	2.69	2.31	1.71	
<b>0</b>	0.78	good	24.69	27.15	31.50	31.36	30.71	22.94	27.95	29.44	27.99	22.99	19.11	16.70	12.29	

### B.3 Karl Fischer Data for High-Solids Froth Mixing Experiments

		Settling Time (min) and Water Content (wt%)									
Run Code	Sample Height	0	5	10	15	20	25	30	40	50	60
<b>HA-1</b>	Z1	15.82	30.11	22.5	21.47	28.72	24.4	21.03	27.53	19.16	21.17
	Z2		24.65	22.9	28.6	32.39	24.2	25.68	31.11	19.58	26.04
	Z3		25.47	26.7	25.03	25.27	22.4	38.95	29.82	24.19	26.95
	Z4		31.3	31.3	30.79	27.45	26.3	9.247	29.96	31.37	29.09
<b>HB-1</b>	Z1	16.26	28.21	22	28.2	24.59	8.22	4.366	4.712	2.132	2.64
	Z2		25.95	27	26.79	24.88	24.7	24.56	24.77	15.7	5.733
	Z3		26.89	27.4	26.43	25.61	28.7	26.25	29.23	28.21	28.53
	Z4		27.27	28.6	27.33	28.27	28	30.14	32.32	30.57	29.9
<b>HC-1</b>	Z1	16.11	31.2	22.8	24.26	22.17	13.5	9.719	11.43	8.442	7.348
	Z2		27.29	25.7	30.74	26.82	28.7	26.01	27.06	21.92	16.15
	Z3		28.84	22.3	33.94	26.94	26.5	23.53	30.17	26.02	29.69
	Z4		23.92	26.2	27.18	27.13	30.3	33.1	28.03	33.45	27.81
<b>HD-1</b>	Z1	28.65	28.69	18.7	12.95	16.26	19.2	18.99	8.461	9.513	5.133
	Z2		27.9	24.5	22.2	26.38	25.1	24.15	13.04	12.31	11.81
	Z3		33.62	32.7	32.12	24.59	22.5	24.01	33.26	33.47	32.72
	Z4		32.52	31.2	25.28	24.93	28.9	30.73	28.95	41.03	31.81
<b>CP-1</b>	Z1	14.28	16.28	23.7	20.91	10.42	2.56	9.268	5.665	7.61	1.856
	Z2		20.49	9.51	21.03	22.26	19.8	20.73	19.05	13.42	13.15
	Z3		23.3	22.6	22.9	27.14	23	15.16	25.83	14.02	17.62
	Z4		23.36	22.9	22.14	20.28	27.9	24	27.48	15.05	24.72
<b>HA-2</b>	Z1	17.48	28.78	28.7	22.4	23.81	23.6	15.35	22.04	19.86	14.9
	Z2		24.21	24.3	24.17	23.09	25.8	19.28	23.19	23.16	21.2
	Z3		27.39	25.5	27.05	26.28	20.4	22.2	29.79	23.67	17.96
	Z4		29.65	29.2	27.91	23.92	23.7	29.09	121.7	29.51	32.51
<b>HB-2</b>	Z1	16.35	24.26	26.7	25.81	22.4	9.57	2.447	1.881	1.436	0.952

	Z2		27.98	25.1	23.32	24.93	25.3	27.29	28.01	21.53	9.355
	Z3		27.18	25.8	24.37	27.49	21.9	27.5	25.81	26.51	26.16
	Z4		NA	26.7	28.75	27.4	27.3	27.39	29.28	29.18	29.8
<b>HC-2</b>	Z1	17.74	44.17	19.9	28.5	23.66	16.2	11.17	6.599	6.738	3.465
	Z2		20.35	27.5	27.82	23.03	29.8	28.52	25.76	13.42	4.181
	Z3		29.91	28.8	25.24	26.95	26.4	28.33	22.89	26.28	25.31
	Z4		24.45	31	23.33	29.05	25.6	24.43	32.11	24.45	28.79
<b>HD-2</b>	Z1	24.21	18.42	19.5	18.31	20.85	20.8	17.52	15.04	8.402	9.637
	Z2		24.55	20.9	21.01	23.31	20.3	18.59	12.55	6.808	5.037
	Z3		26.69	28.4	26.96	27.69	25.5	22.53	23.01	31.02	30.56
	Z4		26.16	21.5	25.71	28.26	27.3	23.58	23.12	31.55	38.25

#### B.4 OWS Data for High-Solids Froth Settling Experiments

Technique	Sample Id	Sample	%_BITUMEN	%_WATER	%_SOLIDSS
UFX	E92651	HA-1,DS-1	55.03	7.38	3.39
UFX	E92652	HA-1,DS-2	51	11.2	4.74
UFX	E92653	HA-1,DS-3	33.31	27.67	18.27
UFX	E92654	HB-1,DS-1	57.3	1.85	1.17
UFX	E92656	HB-1,DS-2	49.16	11.4	6.84
UFX	E92657	HB-1,DS-3	32.72	26.56	18.31
UFX	E92658	HC-1,DS-1	58.76	3.43	2.42
UFX	E92659	HC-1,DS-2	48.3	13.31	7.99
UFX	E92660	HC-1,DS-3	34.54	26.89	17.12
UFX	E92661	HD-1,DS-1	56.53	4.15	2.68
UFX	E92662	HD-1,DS-2	49.81	10.55	5.57
UFX	E92663	HD-1,DS-3	33	27.96	17.21
UFX	E92664	HA-2,DS-1	55.61	7.46	4.24

<b>UFX</b>	E92665	HA-2,DS-2	53.59	9.79	4.77
<b>UFX</b>	E92666	HA-2, DS-3	34.9	27.67	15.85
<b>UFX</b>	E92667	HB-2,DS-1	59.71	1.43	1.09
<b>UFX</b>	E92668	HB-2,DS-2	49.85	10.28	6.19
<b>UFX</b>	E92669	HB-2,DS-3	32.63	26.63	18.41
<b>UFX</b>	E92670	HC-2,DS-1	56.53	5.35	3.52
<b>UFX</b>	E92671	HC-2,DS-2	50.13	12.16	7.69
<b>UFX</b>	E92672	HC-2,DS-3	35.99	26.58	14.56
<b>UFX</b>	E92673	HD-2,DS-1	53.9	5.84	3.2
<b>UFX</b>	E92674	HD-2,DS-2	53.41	6.08	3.48
<b>UFX</b>	E92675	HD-2,DS-3	35.84	24.3	14.34
<b>UFX</b>	E92676	CP-1,DS-1	56.83	2.71	1.86
<b>UFX</b>	E92677	CP-1,DS-2	54.18	6.4	4.13
<b>UFX</b>	E92678	CP-1,DS-3	34.05	25.88	15.99